Development of Nanobiosensors for Phenolic Endocrine Disrupting Compounds and Anti-Tuberculosis Drugs

By

Unathi Sidwaba

A thesis submitted in partial fulfilment of the requirements for the degree of

Magister Scientiae in Nanoscience

Faculty of Science

University of the Western Cape

Cape Town, South Africa

Supervisor: Prof. Emmanuel I. Iwuoha

November 2013

Abstract:

Tuberculosis still remains one of the world's killer diseases. Pyrazinamide (PZA) is one of the most commonly prescribed anti-tuberculosis (anti-TB) drugs due to its ability to significantly shorten the TB treatment period. However, excess PZA in the body caused hepatotoxicity and liver damage. This, together with the resistance of the bacteria to treatment drugs, poor medication and inappropriate dosing, contribute significantly to the high incidents of TB deaths and diseases (such as liver damage). This, therefore, calls for new methods for ensuring reliable dosing of the drug, which will differ from person to person due to inter-individual differences in drug metabolism. A novel biosensor system for monitoring the metabolism of PZA was prepared with a nanocomposite of multi-walled carbon nanotubes (MWCNTs), polyaniline (PANI) and cytochrome P450 2E1 (CYP2E1) electrochemically deposited on a glassy carbon electrode (GCE). The nanocomposite biosensor system exhibited enhanced electro-activity that is attributed to the catalytic effect of the incorporated MWCNTs. The biosensor had a sensitivity of 7.80 µA/ µg mL^{-1} PZA and a dynamic linear range (DLR) of 4.92 – 160 ng/mL PZA.

Bisphenol A (BPA) is a hormone-disrupting chemical used in production of epoxy resins and polycarbonates, which produce various products used on a daily basis. However, BPA can leach out of plastic during normal use and cause health effects such as cancer or disrupt the endocrine system. Moreover, BPA has also been proven to degrade from the containers in landfills and accumulate in groundwater and streams, thereby, polluting the environment while destroying aquatic organisms. Therefore, this also calls for new selective and sensitive methods for the monitoring of BPA. A novel biosensor system for monitoring the oxidation of BPA was prepared from a nanocomposite of polyaniline, polymethyl methacrylate and titanium dioxide nanoparticles, also electrochemically deposited on the GCE. Biosensor fabrication was conducted by immobilization of the enzyme manganese peroxidase (MnP)

onto the nanocomposite film. The nanobiosensor also revealed enhanced electro-activity, attributed to the incorporation of TiO_2 nanoparticles. The biosensor system had a sensitivity of 0.3 µA/nM and a detection limit of 0.12 nM. This detection limit falls within the range of the allowed daily intake of BPA as recommended by the Food and Drug Administration (FDA, USA) and other regulatory bodies.

UNIVERSITY *of the*
WESTERN CAPE

Keywords:

Tuberculosis

Bisphenol A

Mycobacterium tuberculosis

Polyaniline

Titanium dioxide nanoparticles

Pyrazinamide

Carbon nanotubes

Cytochrome P450-2E1

Manganese Peroxidase

Endocrine disrupting compounds

Declaration:

I declare that

'Development of nanobiosensors for phenolic endocrine disrupting compounds and anti-tuberculosis drugs'

is my own work, that it has not been submitted for any degree or examination in any other university and that all the resources I have used or quoted have been indicated and acknowledged by means of complete references.

Student: <u>Unathi Sidwaba</u>   Signed: _____

Supervisor: <u>Professor Emmanuel I. Iwuoha</u>   Signed: _____

Acknowledgements:

List of Publications:

(1) Unathi Sidwaba, Rachel Ajayi, Nicolette Hendricks, Samantha Douman, Usisipho Feleni, Priscilla Baker, Emmanuel Iwuoha. Electrosynthetic carbon nanotubes and CYP 2E1-derivatized polyanilino nanobiosensor for the detection of anti-TB drugs. (IET Nanotechnology, 2014, Submitted).

(2) Rachel F. Ajayi, Unathi Sidwaba, Usisipho Feleni, Samantha Douman, Subelia Botha, Priscilla G.L. Baker, Emmanuel I. Iwuoha (2013) 'Chemically amplified cytochrome P450-2E1 drug metabolism nanobiosensor for rifampicin antituberculosis drug (Electrochimica Acta, Accepted).

(3) Usisipho Feleni, Unathi Sidwaba, Samantha Douman, Ezo Nxusani, Rachel Ajayi, Priscilla Baker and Emmanuel Iwuoha. Selenide quantum dots electrochemical biotransducer for the determination of indinavir-a protease inhibitor anti-retroviral drug. (International Journal of Electrochemical Sciences, 2014, Submitted).

(4) Samantha Douman, Unathi Sidwaba, Rachel Ajayi, Nicolette Hendricks, Usisipho Feleni, Priscilla Baker, Emmanuel Iwuoha. Gallium Selenide quantum-dots genosensors for the determination of telomerase – a breast cancer biomarker. (Nano Hybrids, 2014, Accepted).

TABLE OF CONTENTS

Development of Nanobiosensors for Phenolic Endocrine Disrupting Compounds and Anti-Tuberculosis Drugs

CHAPTER 1

Introduction

Summary

Worldwide, there is an observable burden of diseases such as tuberculosis (TB) and HIV/AIDS. Drugs used during the therapy pose negative human health effects, induced by their metabolic routes. As a result, drug monitoring has been implemented so as to make sure that the levels of such drugs fall within the values recommended by various responsible regulatory organisations. The liver, being the main centre of metabolism, is very susceptible to the toxic damages induced by different species such as drugs, chemicals and their metabolites [1]. Hence, there are other health problems induced by chemicals used in the packaging of materials used in daily basis, whose monitoring has also been under consideration. This chapter gives a background on pyrazinamide (a drug used in the treatment of TB) and Bisphenol A (a chemical used in packaging material), covering aspects on their negative effects on human health and the environment. The motivation, main aim, objectives and delimitations of the study are postulated.

1.1 Background

1.1.1 (a) Pyrazinamide and Tuberculosis

Tuberculosis (TB) is ranked second to HIV/AIDS among the burden of diseases faced by South Africans and remains a highly infectious disease worldwide [2, 3]. The disease is caused by development of mycobacterium tuberculosis (MTB), a bacterium that affects the lungs, meninges, brain and spinal cord with the fully-developed diseases known as pulmonary-TB, TB meningitis, TB cerebritis and TB myelitis, respectively [4]. The bacterium has a dormant behaviour which makes it very difficult to detect at early stages and therefore has an impact on the incidences of multi-drug resistant TB (MDR-TB) and extensively drug-resistant TB (XDR-TB), which develop when the bacterium is resistant to one and two or more of the drugs, respectively. Due to such effects, tuberculosis treatment is a multi-drug regimen consisting of first-line and second-line TB drugs, categorized according to their effectiveness against the bacteria [5].
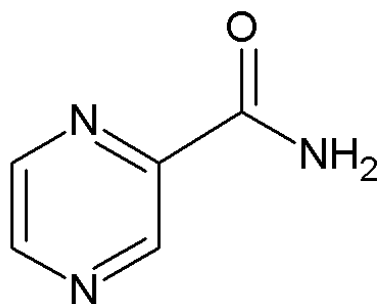
Figure 1.1: Structure of PZA.

Pyrazinamide (PZA) is a first-line pro-drug in the TB combination chemotherapy used in conjunction with rifampicin, ethambutol and isoniazid [6]. For effective bacterium destruction, PZA (**Figure 1.1**) has to be activated by enzymatic hydrolysis into pyrazinoic acid which possesses antibacterial activity against the old, slowly-replicating bacilli of

mycobacterium tuberculosis that cannot be attacked by the other drugs [6, 7]. PZA is considered the most fundamental element in the TB therapy due to its sterilizing activity, responsible for the shortening of the therapy from the former nine months to the current six months duration [6, 8-11].

1.1.1 (b) Problem statement

Despite the remarkable advantages of PZA introduction in the therapy, such as its activity against replicating bacilli and sterilizing activity, there is little understanding on the mode of action of pyrazinamide which requires acidic environment which, in turn, leads to loss of enzyme activity. This behaviour is associated with the diverse mutations in the pncA encoding of pyrazinamidase, and is the main cause of MTB resistance to PZA [12, 13]. Also, this gene variation is the main source for the different metabolic categories where there are slow and fast metabolizers. The latter refers to patients whose metabolic rates are fast while the former refers to those whose rates are slow. These differences, together with the fixed dose inferred irrespective of metabolic profile, lead to greater chances of liver damage and hepatotoxicity induced by the accumulation of the drug and/or its metabolite. To reduce toxic levels of therapeutic drugs, regulatory bodies have set minimal inhibitory concentrations (MICs) with an MIC of 50–100 mg/L for PZA [1, 9].

Although reports from bodies implemented to monitor TB (e.g. the DOTS, STOP-TB and TAC), have shown success in combating TB spread and recurrence, tuberculosis remains a major health problem in South Africa. This is enhanced by factors such as over-crowding (since TB is a respiratory disease spread easily through coughing and breathing), and poor health seeking behaviour (mainly in rural areas which constitute larger population percentages), leading to delayed detection of diseases. Above all, the TB-HIV correlation plays a vital part with 73% of TB patients being HIV positive [14]. Also, a recent report has

confirmed that PZA metabolites are responsible for hepatotoxicity [15]. Hence, there is an increased demand for onsite analytical devices that can quantitatively and qualitatively allow monitoring of PZA (and other therapeutic drugs) with high sensitivity, selectivity and faster response time and lower detection limits.

1.1.2 (a) Packaging and Bisphenol A

There is an observable strain on food-packaging industries, which is associated with the increasing demand of fresh and less-preserved safe foods of high quality by consumers. Such pressure is accelerated by the increased environmental awareness and knowledge about the information labelled on the packaging e.g. expiry dates, ingredients, dietary formulation, allergic caution and resin identification code. Bisphenol A (BPA) is one of the chemicals used in packaging, produced in high volumes of about 10-billion pounds per year [16, 17].

BPA (**Figure 1.2**) is the precursor monomer component for epoxy resins, polycarbonates, flame-retardants and in paper industries [18]. Polycarbonates are used in plastic-based ware and constitute 75% of BPA while epoxy resins are used in lining of metal cans (food and beverages) and lids for glass containers [19]. BPA has gained extensive interest due to its light-weight, transparency, durability and thermostability properties which have resultantly led to a wide range of applications for BPA.
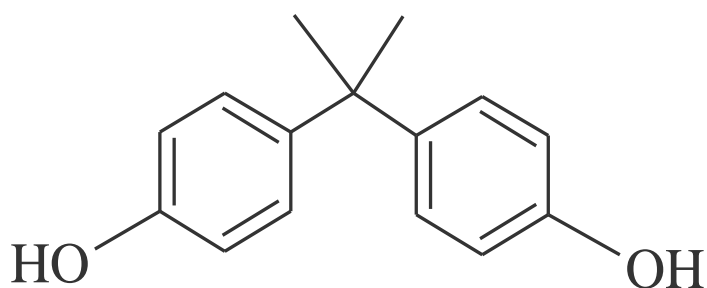
Figure 1.2: Structure of Bisphenol A.

1.1.2 (b) Problem statement

Although BPA has been applied in a wide range of products, it is categorized under endocrine disrupting compounds (EDCs). EDCs are defined as chemicals that interfere with the natural endocrine system responsible for development and reproduction in humans [20]. BPA has been proven to have an estrogenic effect by binding to α and β oestrogen receptors, thereby mimicking their functionality [21, 22]. Upon the endocrine disruption, BPA is associated with adverse health disorders such as cancer, recurrent miscarriages, ovarian dysfunction and altered female reproduction [23-30]. As a result, regulatory bodies such as EFSA, EPA and WHO have recommended a tolerable daily intake (TDI) of 0.05 mg/kg body weight [24, 31].

Avoiding human exposure to BPA is almost impossible since, as mentioned earlier, it is applied in a wide range of products such as baby feeding bottles, plastic toys, metal can linings and dental sealants which are all used on a daily basis. Moreover, BPA has been proven to leach out of the polycarbonates and epoxy resins during normal use, leading to the health problems mentioned earlier. The leaching or migration of BPA from the packaging into the contents is increased by factors such as temperature (mainly heating of plastic containers) and the alkalinity of the contents [34, 35]. The major concern is the existence of the adverse health problems caused by BPA at much lower concentrations than the allowable daily intake as recommended by the regulatory bodies [36-38] which has posed contradictory views about the stipulated TDI value. Therefore, there is still intensive research on the development of analytical methods for the detection and quantification of BPA [30, 32].

1.2 Rationale and motivation

Despite all efforts conducted to monitor TB treatment and combat its spread and recurrence, TB is still the world's most epidemic disease. In South Africa, there are incidents of

antituberculosis drug-induced hepatotoxicity (ADIH) reported in children [33]. On the other hand, although most countries have banished use of BPA in plastic ware (especially baby feeding bottles) , there are still reports on BPA being detected in various media such as fish, wines and waters that are consumed by humans. Therefore, considering the negative effects that therapeutic drugs, endocrine disrupting compounds and their metabolites have on human health and the environment, their quantitative monitoring is still of vital importance.

The most widely and extensively used analytical techniques for quantitative detection of therapeutic drugs and EDCs include chromatography linked to detectors (GC-MS, HPLC, LC-ESI-MS) etc.), ELISA (enzyme-linked immunosorbent assay), bioreactors and electrochemical methods (biosensors and electrochemical sensors) [39-43]. Amongst these techniques, electrochemical methods are the most preferred and advantageous due to lower detection limits, faster response speeds, low cost, lesser interferences, low energy consumption, high sensitivity and high selectivity which make them best candidates for real-time analysis [44]. This study was aimed at developing enzyme-based biosensors for monitoring the metabolism anti-TB drug, pyrazinamide and endocrine disrupting compound, BPA.

The other aspect of this study was the use of conductive polymers in the platforms of the biosensors proposed. Examples of these include polymers such as polyaniline and polypyrrole which have attracted interest as biosensor platforms. However, they have been reported in some cases to having chemical and physical limitations. As an alternative, polymer composites are now under extensive research due to their unique properties brought about by the individual moieties. The use of methacrylates in biosensors has vastly increased, due to their biocompatibility. Most composites employ nanomaterials, characterized by high

surface area and catalytic behaviour, thereby leading to composites with enhanced properties and performance [45-46].

Literature has revealed that incorporation of nanoparticles onto polymers results in nanocomposites of enhanced electrochemical activity, thereby yielding biosensors with high selectivity, sensitivity and faster response times. Based on this, this study combined the effects of conductive polyaniline, catalytic activity of carbon nanotubes and TiO_2 and the biocompatibility of polymethyl methacrylate to construct nanocomposites with enhanced properties that would give the biosensor high selectivity, sensitivity and enhanced electron transfer between the enzyme active sites and the electrodes. This study reports two nanobiosensors for PZA and BPA, respectively. For the former, polyaniline was doped with carbon nanotubes as a platform for CYP 2E1 (cytochrome P450 2E1), an isoenzyme from the Cytochrome P450 family of heme enzymes well-known for drug metabolism. The platform exploited the high surface area and catalytic behaviour of carbon nanotubes and the biocompatible polyaniline to host large enzyme loading for higher CYP2E1-PZA interactions. For BPA, the high surface area and catalytic properties of the transition metal oxide TiO_2, together with the biocompatible hydrogel polymethyl methacrylate (PMMA) are incorporated into conductive polyaniline as a receiving composite for manganese peroxidase (MnP). MnP is a bacterial enzyme capable of the oxidation of various phenolic substrates. The nanocomposites, therefore, are expected to have superior electrochemical properties which will enhance electron transfer between the enzymes active sites and the electrodes.

1.3 Objectives

The main aim of the study was to develop biosensors for detection of PZA and BPA, respectively. These sensors will be referred to as SENSOR 1 (PZA) and SENSOR 2 (BPA) for differentiation. The main objectives were:

1.3.1 SENSOR 1 (PZA)

(a) To electrochemically synthesize and characterize polyaniline-carbon nanotubes nanocomposite,

(b) To fabricate the biosensor by immobilization of CYP 2E1 onto the nanocomposite,

(b) To investigate the electrocatalytic properties of the CYP 2E1 based biosensor towards various concentrations of PZA.

1.3.2 SENSOR 2 (BPA)

(a) To synthesize and characterize TiO_2-doped polyaniline-polymethyl methacrylate (PANI-PMMA) composite,

(b) To fabricate a biosensor by immobilizing MnP,

(c) To characterize the biosensor,

(d) To detect various concentrations of BPA using the sensor.

1.4 Thesis outline
This thesis contains eight chapters.

Chapter 1 gives a detailed background, rationale and motivation towards the conductance of the study, covering the main aims and objectives.

Chapter 2 gives the literature reviewed.

Chapter 3 is based on the materials and methods conducted throughout the study. It covers all reagents and instruments used.

Chapter 4 provides the characterization results of the PANI/MWCNTs nanocomposite and the biosensor. Most importantly, it covers results and discussion for PZA detection.

Chapter 5 gives results obtained for the characterization of the PANI/PMMA/TiO_2 nanocomposite and its components.

Chapter 6 gives results for the characterization of the MnP based biosensor.

Chapter 7 discusses the detection of BPA using the MnP based nanobiosensor.

Chapter 8 gives conclusions and future recommendations

Chapter 9 gives references.

CHAPTER 2

Literature review

Summary

Biosensors are the most recently studied electro-analytical techniques for quantitative and qualitative detection of various species such as drugs and endocrine disrupting compounds, due to the negative impacts they pose on human health and the environment. They have drawn much attention due to their portability, low cost and lower detection limits, which have earned biosensors application in a wide range of fields. This study gives detailed background on the various aspects involved in this study. These include biosensors and components (transducers and biocomponents), Bisphenol A, tuberculosis and its treatment, nanomaterials, hydrogels and nanocomposites.

2.1. Electrochemical biosensors

Biosensors are electro-analytical devices comprising a transducer element which converts a biological response, induced by a biologically active component after recognition of the target analyte, into a measurable signal [47]. They are classified into amperometric, potentiometric and impedimetric biosensors, depending on the principle of transduction. The observed parameters would therefore be current, potential and impedance, respectively. The biological elements are the most important components of biosensors as they recognise and bind or interact with the substrates of interest. The biocomponents can be enzymes, DNA or antibodies while transducers can be electrodes modified with conductive polymers, for example. As such, biosensors fall under the third-generation of biosensors in which the biomolecule is directly bound to the transducer element and therefore becomes integral part of the biosensor [48]. Biosensors are characterized by low detection limits, high sensitivity, high selectivity, low cost, easy operation, high stability, portability and fast response times. As a result, biosensors are applied in in a wide range of fields such as environmental monitoring, disease screening, water treatment and therapeutic drug monitoring.

2.1.1. Transducers

With relevance to the working principle of amperometric biosensors, transducers are the electrode materials which act as receiving matrices for the biocomponents during biosensor fabrication. Modified electrodes have been proven as best transducers, compared to unmodified electrodes which are characterized by high formal potentials, that in turn, lead to electrode fouling hence limiting their applications. Polymers (conductive polymers and hydrogels) and nanomaterials have been under intensive recognition as electrode material due to their electroconductivity and biocompatibility properties. This study based its transducers on polymers (polyaniline and polymethyl methacrylate) and nanoparticles (carbon nanotubes

and titanium dioxide). The relevance of these components to our study is discussed in the following sessions.

2.1.1.1 Polymers in biosensors.

Conductive polymers (CPs) are organic material of metallic and semiconductive character, with conjugated sigma bonds (σ-electrons) and double bonds (π-electrons) along their backbones. This conjugation results in charge delocalization, causing electrons to move throughout the system, giving rise to the unique optical and electrical properties conductive polymers possess. CPs are often used as enzyme platforms for biosensors, mainly due to their capability to host different functionalities in their matrices during or after polymerization, in a process called modification [49]. CPs are also being used as biosensor platforms since they provide better transduction signal, sensitivity, flexibility and biocompatibility for enzyme immobilization. The mechanical and chemical properties of CPs can be improved through doping (electron addition) or de-doping (electron removal), depending on the nature (electron donating or electron withdrawing) of the dopant. Hence, nanocomposites and co-polymers have emerged as better support material for biosensors [49]. One of conductive polymers, under intensive investigation both industrially and academically, is polyaniline (PANI).

Hydrogels are three-dimensional polymeric networks capable of absorbing large amounts of water. Much attention has been drawn onto methacrylate-based hydrogels which are characterized by biocompatibility, bioadhesion, elasticity and high swellability [50]. Hydrogels have also been used as matrices for biomolecule immobilization in enzyme-based biosensors. Hence, they have been applied in biomedical fields such as biosensors, drug delivery systems, wound dressing, contact lenses, dental fillings and food technology [51]. As with conductive polymers, alternatives such as copolymerization, graft polymerization and formation of hydrogel blends, have been developed to improve properties of hydrogels.

Resulting hydrogels have better or improved physical and mechanical properties e.g. high degree of swelling, biocompatibility and thermal resistance [52, 53]. Some examples of methacrylate hydrogels are polymethyl methacrylate (PMMA), poly(hydroxylethyl methacrylate (pHEMA) and poly(glycidyl methacrylate) (PGMA) [54].

2.1.1.1. (a) Polyaniline

Along its backbone, PANI **(Figure 2.1)** has conjugated oxidized quinoid and reduced benzenoid units, which identify its oxidation states which are characterized by the ratio of amine to imine nitrogen atoms. PANI has three oxidation states; leucoemeraldine (fully reduced), emeraldine (partially oxidized) and pernigraniline (fully oxidized) forms. PANI is most conductive when it is in the emeraldine salt form (green conductive form), which can be obtained by the protonation of emeraldine base (blue insulative form) [55].
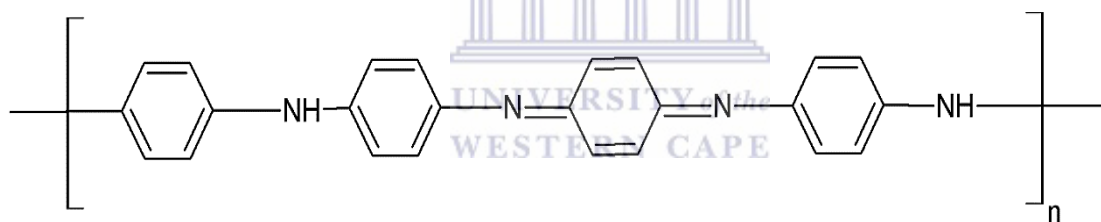
Figure 2.1: The structure of PANI.

PANI is characterized by easy synthesis which can be done electrochemically or chemically in an acidic environment. Amongst these synthetic routes, electrochemical synthesis is advantageous due to controllable growth and film thickness and formation of films stable in both aqueous and organic mediums. Besides its remarkable environmental stability and biocompatibility, PANI has drawbacks such as pH sensitivity and insolubility in some solvents [56]. The structure of PANI, and hence its conductivity, is affected by the synthetic conditions such as pH, monomer concentration, electrode potential and number of scans (for

the electrochemical synthesis). As a result, doping and de-doping means have been developed as attempts to improve its mechanical and electrical properties, leading to PANI being applied in a wide range of fields such as biosensors, energy storage, field effect transistors, photovoltaic cells, lithium-ion batteries and anti-corrosion coatings [57]. The most common doping materials include nanomaterials to form nanocomposites and electroconductive hydrogels with characteristic properties between those of PANI and the dopant [58].

2.1.1.1. (b) Poly(methyl methacrylate)

Poly(methyl methacrylate) (PMMA) is a transparent, low cost, polymeric thermoplastic which has drawn much interest due to its excellent biocompatibility and temperature resistance. PMMA (**Figure 2.2**) has therefore gained applications (both in composite form and on its own) in various fields such as bone implants, biosensors, electroluminescent devices and lithium-ion batteries [59, 60].
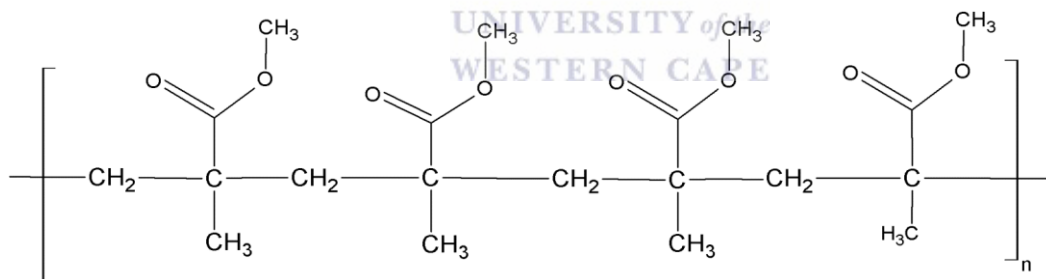
Figure 2.2: The chemical structure of PMMA.

In composite form, whether with nanoparticles such as TiO_2, conducting polymers such as PANI or with other methacrylates such as PGMA, physical, optical and chemical properties of PMMA are enhanced [61]. Recently, a grafted composite of PMMA and TiO_2 was incorporated into poly(vinylidene fluoride) (PVdF) to improve the ionic conductivity of the resultant electrolyte for use in lithium-ion batteries. The ionic conductivity and electrochemical stability of the electrolyte were both enhanced [62].

2.1.1.2 Nanomaterials

Since the emergence of nanoscience and nanotechnology, exploitation of nanomaterials towards development of nanocomposites with synergetic and enhanced performance has been on-going. Nanomaterials, defined as materials with dimensions in nanometer scale, have superior electronic, catalytic and optical properties resulting from their small size and quantum confinement effect [63]. With respect to biosensors, nanomaterials have been of great interest due to their high-surface-to-volume ratio and catalytic effect which ensure high biomolecule incorporation (which facilitates more enzyme-substrate interaction) and faster response times. Some major advantages of incorporating nanomaterials in biosensors include improved sensitivity, improved selectivity and enhanced electron transfer between the electrode and the immobilized biomolecule which yields biosensors of enhanced performance [64]. The most commonly used nanomaterials in biosensors include carbon nanotubes, quantum dots and metal nanoparticles.
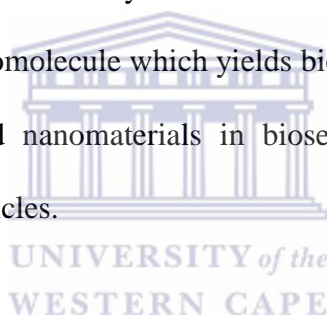
2.1.1. 2(a) Carbon nanotubes

Carbon nanotubes, first developed by Iijima in 1991, are one-dimensional (1D) cylindrical, sp^2-hybridized carbon material comprising graphene sheets. They are classified as single-walled carbon nanotubes (SWCNTs) and multi-walled carbon nanotubes (MWCNTs), depending on the number of graphene sheets contained in a tube wall. MWCNTs are made up of layers of SWCNTs held together by van de Waals forces. Due to quantum confinement effects, they possess size-dependant, unique mechanical properties (high surface-to-volume ratio, high Young's modulus and high tensile strength), electrical properties (high electrical conductivity), optical properties (small energy band-gaps) and thermal properties (high thermal stability). The properties of CNTs can be improved by introduction of different

functional groups, depending on the desired functionality. An example is their treatment with carboxylic acids to introduce or increase carboxylic groups on their walls.

An intensive research has been conducted on the introduction of MWCNTs into PANI to form PANI-MWCNT nanocomposites with improved electrical conductivity and mechanical properties. A PANI/SWCNTs composite was electrochemically prepared from a mixed solution of aniline and the SWCNTs [65]. It was reported that the intrusion of CNTs promoted the protonation of PANI, leading to increased electrical conductivity [65]. Another study [66] reported that their PANI-CNTs composite exhibited better anti-corrosion properties than PANI. Composites of PANI with carbon nanotubes (SWCNTs or MWCNTs) have been applied in photovoltaic devices, light-emitting diodes and supercapacitors [67, 68]. Several studies have also demonstrated that carbon nanotubes are biocompatible and enhance the electrochemical reactivity of immobilized biomolecules by promoting faster electron transfer reactions [69].
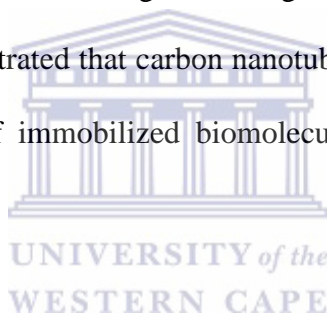
2.1.1.2 (b) TiO$_2$ nanoparticles

TiO$_2$ is an n-type semi-conductive transition metal oxide characterized by low cost, non-toxicity, environmental stability and biocompatibility [70]. TiO$_2$ exists in three forms which are rutile, anatase and brookite where rutile is the most stable form. TiO$_2$ has gained intensive investigation due to its photocalytic behaviour initiated by the generation of electron/hole pairs upon UV-light absorption at energies equal to or higher than the corresponding band gap. These electrons and holes recombine and produce highly reactive hydroxyl radicals and superoxide anions with electron donors or electron acceptors. The produced hydroxyl radicals and peroxide anions are responsible for oxidation of various organic and biological molecules [71]. Bulk TiO$_2$ is limited by its short life time, wide band gap and the narrow effective UV region of the electromagnetic spectrum. As an alternative, downscale to nanometer size and

doping with narrow band gap semiconductive material and non-metals have been investigated [72, 73].

Nano-TiO$_2$ possesses large surface-to-volume ratio due to the small size which gives it its excellent physical, chemical and optical properties than bulk counterparts. Hence, TiO$_2$ nanoparticles are applied in photocatalysis, sensors, pigments, coatings and solar cells [74]. Nanocomposites based on conductive polymers and metal oxide nanoparticles have been intensively developed and possess enhanced thermal, electrical and mechanical properties [75]. Hybrid materials or nanocomposites comprising PANI and TiO$_2$ nanoparticles are also under intensive investigation and can be processed via a variety of routes such as ultrasonic irradiation, electrochemical polymerization and chemical polymerization. These materials are being applied in anticorrosion coatings, electronics and optical devices. The enhanced properties result from the interactions at the interface between the conduction band of n-type TiO$_2$ and the lowest unoccupied molecular orbital of p-type PANI. A chemically prepared PANI-TiO$_2$ nanocomposite has been reported [76]. This nanocomposite was characterized to have high photocatalytic degradation behaviour. Another study [77], based on PANI and TiO2, investigated the anticorrosion properties of a PANI/TiO$_2$ nanocomposite that was also prepared chemically. The nanocomposites showed better corrosion resistance than PANI and TiO$_2$ individually.

2.1.2. Biocomponents

Biocomponents are the most important components of amperometric biosensors as they recognize the analytes or substrates of interest before they are biotransformed into their metabolites. Besides their intensive use in different assays (such as biosensors, immunosensors and aptasensors), biomolecules are susceptible to denaturation by various factors such as pH, temperature and the compatibility of the receiving matrix. For selective

biosensors, the electrochemical interaction between the enzyme active site and the electrode depends on the success in immobilization of the biomolecule as the receiving matrix plays a vital role in the activity of the biomolecule [78]. To overcome the inactivation of biomolecules through denaturation when immobilized directly onto bare electrodes, polymers, nanoparticles and their composites are extensively assayed as the best candidates. This is because of the biocompatibility of polymers and nanoparticles and, hence their composites, which increases their ability to effectively host biomolecules without activity loss. These receiving matrices yield biosensors of increased sensitivity which is of major importance for clinical diagnostics, drug monitoring and environmental monitoring as the analytes can be present in very small concentrations. The most commonly used immobilization techniques include physical adsorption, entrapment, electrochemical adsorption and covalent bonding [79].

Physical adsorption is the simplest immobilization which enzymes or proteins are deposited onto various support matrices through physical and chemical interaction between the enzyme and its receiving matrix. Binding forces involved in holding the enzyme onto the polymer surface include hydrogen bonds, van de Waals forces and hydrophobic interactions. The main advantage is that activity of enzymes immobilized using this technique is usually retained. However, these binding forces may not be strong and therefore affect the stability of the enzyme electrode film, in most cases the problem being enzyme leakage away from the matrix. Development of horse-radish peroxidase based biosensors for phenolic compounds using different enzyme immobilization techniques has been reported [80]. A copolymer film comprising polypyrrole, poly(glycidyly methacrylate) and poly(3-methylthienyl methacrylate) was dipped into a horse-radish peroxidase (HRP) solution. Interaction was based on chemical bonding between the epoxy groups of the copolymer and the amine groups

of HRP. Based on the results, it was concluded that the enzyme did not bind to the copolymer [80].

Entrapment provides better enzyme adhesion onto the matrix surface than physical adsorption. It refers to a process in which the enzyme is trapped or confined in the matrix during polymerization [81]. Besides the accurate control of the polymer thickness and precise modification, this technique is limited to polymeric materials which are synthesizable within the working pH of the hosted enzyme in order to avoid loss of enzyme activity [49]. With reference to polypyrrole and its derivatives, which are polymerized in neutral pH mediums this technique is most suitable since many biomolecules retain activity in neutral pH environments. As a result, many studies based on polypyrrole use this technique for enzyme immobilization [81].

Electrochemical adsorption provides better enzyme immobilization than entrapment since it can be also be done after polymerization in pH media suitable for the hosted enzyme. This is advantageous for many polymers such as polyaniline which requires highly acidic mediums for polymerization.

In *covalent binding*, the functional groups of the matrix bond covalently to the enzyme reactive groups which are mainly amino groups for enzymes. To ensure proper coupling or interaction between the targeted functional groups of the enzyme and those of the polymer matrix, cross-linkers are used. Cross-linkers have reactive ends specific to functional groups through which they link two or more molecules by a covalent bond. Some examples of cross-linking agents and their specific target groups are glutaric dialdehyde (amine/amine), 1-ethyl-3-(3-dimethylaminopropyl) carbodiimide (carboxylic acid/amine) and N-Hydroxysuccinimide ester (amine/amine). These cross-linkers not only link target groups but also act as adhesives and modifiers that improve stability and solvent sensitivity of

biosensors. A study on enzyme-based biosensors [82] showed that a biosensor prepared using NHS-modified horseradish peroxidase (HRP) exhibited stability in organic solvents than the biosensor prepared from native HRP which was only suitable for use in buffer medium [82].

Overall, to overcome all limitations associated with the activity, stability and bonding abilities of enzymes, membranes that act as protective barriers, stabilizers and modifiers are used. Examples of these include nafion, didodecyl dimethylammonium bromide (DDAB) and bovine serum albumin (BSA). BSA is used mainly as an enzyme modifier and also blocks unreactive groups in the enzyme, thereby ensuring effective coupling between the enzyme functional groups and the target groups of the receiving matrix. Nafion and DDAB provide biosensors with a membranous environment which reduces repulsion reactions, thereby facilitating electron transfer the electrode and the enzyme active site [83]. Choice and relevance of using enzymes CYP 2E1 and MnP as biorecognition elements in the proposed biosensors in this study are detailed in the following session.

2.1.2 (a). Cytochrome P450 2E1

Cytochrome P450 2E1 (CYP 2E1) is a member of the cytochrome P450 enzymes with diverse origins where they can be of bacterial, microsomal and mitochondrial origin. Cytochrome P450 enzymes are NADPH-dependent heme-containing monooxygenase enzymes which are well-known for metabolism of drugs and other different substrates in the body [84]. CYP 2E1 is one of the microsomal CYPs which play an important role in the biotransformation of drugs and was employed here for metabolism of pyrazinamide, an antituberculosis drug. CYPs are associated with different types of reactions such as hydroxylation, epoxidation, dehalogenation, dehydrogenation and N-dealkylation which, together with the monooxygenation capabilities of CYPs, has resulted in their application in biosensors and bioreactors [83].

19

2.1.2 (b). Manganese peroxidase

Manganese peroxidase (MnP) from *Nematoloma frowardii* belongs to manganese peroxidases [EC 1.11.1.13; Mn(II) oxidoreductases] which are heme-containing glycoproteins containing protoporphyrin IX as a prosthetic group. Manganese peroxidases are produced by various fungal strains such as *Phanerocaete chrysosporium, Irpex lacteus, Aspergillus terreus* and *Phlebia radiate* [85]. MnP catalyses the H_2O_2-dependant oxidation of Mn^{2+} ions to the highly reactive Mn^{3+} ions which are capable of attacking different phenolic substrates, non-phenolic compounds and other toxic pollutants such as polycyclic aromatic hydrocarbons. MnP enzymes are characterized by wide pH range and non-selectivity, with specificity differing for each species [86]. MnP has gained applications in decolourization of synthetic dyes, wastewater treatment, photobleaching and degradation of polychlorinated biphenyls [87-88]. Considering the wide pH range and broad specificity of MnP from *Nematoloma frowardii* towards phenolic compounds, this study took an opportunity to employ this enzyme to develop a biosensor for the phenolic endocrine disrupting compound, Bisphenol A.

2.2. Tuberculosis

Tuberculosis (TB) is a common infectious disease caused by infection by the bacterium *Mycobacterium tuberculosis.* TB affects one third of the world [89] at a rate of one new infection per second. The bacterium is easily spread through sneezing and coughing of infected individuals, leaving the bacterium suspended in air after which it is inhaled by others [90]. The bacterium lies dormant for a long time before the infected individual gets sick. This adds to the incidents of the bacteria being resistant to the treatment drugs. Hence, as a guideline, the WORLD Health Organisation made the therapy a multidrug regimen constituting pyrazinamide (PZA), ethambutol (ETH), rifampicin (RIF) and isoniazid (INH) as

the first line drugs due to their effectiveness against the bacteria. However, these drugs have adverse health effects, mainly liver damage, and this impacts negatively on the TB control [91]. Due to these effects, therapeutic drug monitoring is very crucial and the WHO implemented strategies such as the Directly Observed Treatment Short-course (DOTS) therapy, Stop-TB and the Treatment Action Campaign TAC) aimed at monitoring response and adherence to the treatment, promote public awareness on disease treatment and combat spread of the diseases [91].

2.2.1.Pyrazinamide (PZA)

PZA has possesses a sterile activity and has been proven to shorten the tuberculosis treatment from nine to the current six months duration [92]. However, the metabolic clearance of PZA varies from person to person due to the polymorphic behaviour of enzymes, leading to the different rates at which drugs are metabolized [93]. Such variations lead to the severe side effects caused by the accumulation of the drugs and their metabolites in the human system. The most common side effects of PZA include anti-TB drug-induced hepatotoxicity (ADIH), liver damage and gout. Besides enzyme polymorphism, other contributing factors to this phenomenon are enzyme inhibition and induction. Enzyme inhibition results from a competition over the enzyme active site by two substrates, leading to a decreased enzyme available, thereby decreasing the rate of metabolism and excretion. Induction greatly, on the other hand, occurs when the substrate increases the level of protein synthesis in the enzyme, leading to an increase in the rate of metabolism and excretion of drugs. These phenomena are common in microsomal CYP450 isoenzymes such as CYP2E1. Amongst the anti-TB drugs, the drugs with enzyme-inhibiting behaviour are isoniazid and pyrazinamide while rifampicin is an enzyme inducer. With respect to CYP2E1, polymorphism is common and results from mutations in the pncA gene encoding of the enzyme [94].

2.3. Endocrine disrupting compounds

EDCs are defined as chemicals which mimic the natural endocrine system responsible for reproduction, development, synthesis, secretion, transport, metabolism, binding action, or elimination of natural hormones in the body. These chemicals are known to possess estrogenic properties and are associated with negative environmental and human health problems such as cancer, miscarriages diabetes, breast and prostate cancers, reproductive problems, early puberty, obesity and reduced sperm count in males. As a result, regulatory bodies have set allowable or tolerated daily intake values for BPA such as the 0.1-0.4 µg/kg by the Food and Drug Administration (FDA) and 0.05 mg/kg by the European Food and Safety Authority (EFSA) [95].

2.3.1. Bisphenol A (BPA)

BPA, along with other phenolic compounds, is an endocrine disrupting compound (EDC). BPA has a wide range of applications such as in baby feeding bottles, water pipes, metal can linings and plastic storage containers and is associated with the negative health effects mentioned earlier even at very low concentrations [96]. The main exposure route to BPA is ingestion from various sources such as leaching of BPA from containers during normal use of degradation of BPA from dental sealants [95]. Environmentally, BPA is a pollutant which enters the environment from manufacturing institutes and degradation from landfills. BPA is therefore being detected in various environments and species such as fish [96]. BPA has been detected BPA from fish using liquid chromatography electrospray ionization tandem mass spectrometry (LC-ESI-MS/MS) and a detection limit of 0.5 ng/g was obtained [96].

22

CHAPTER 3

EXPERIMENTAL METHODS

Summary

This chapter outlines the synthesis of polyaniline nanocomposites, one comprising multiwalled carbon nanotubes and one with PMMA hydrogel and TiO$_2$ using appropriate reagents and routes as discussed below. The method of biosensor fabrication by immobilization of enzymes, CYP2E1 and MnP, onto the nanocomposite platforms is also stated. Finally, the composites and their respective individual components were characterized using electrochemical (CV, SWand DPV), spectroscopic (UV, FTIR and XRD) and microscopic (AFM and HR-SEM) techniques.

3.1 Reagents

All reagents were of analytical reagent grade and purchased from Sigma Aldrich. Aniline (99.13%) was purified by vacuum distillation and used in the electrochemical synthesis of polyaniline (PANI) in acidic media, hydrochloric acid (HCl: 37%) and sulphuric acid (H_2SO_4: 99.98%). Methyl methacrylate (MMA: 98%:) was purified by extraction with 25% sodium sulphate anhydrous (99%), followed by vacuum distillation at 40-50 ˚C. The following chemicals were used without further purification: Bisphenol A (BPA: 99%), carboxylic acid functionalized multi-walled carbon nanotubes (MWCNTs), Ti(IV) oxide rutile nanopowder (TiO_2: 99.5%), N-Ethyl-N′-(3-dimethylaminopropyl) carbodiimide hydrochloride (EDC: 99%), N-Hydroxysuccinimide (NHS: 98%) sodium phosphate monobasic dihydrate ($H_2NaPO_4·2H_2O$: 99%), disodium hydrogen phosphate dibasic ($Na_2PO_4·2H_2O$: 99.5%), polymethyl methacrylate, tetrahydrofuran (THF) and absolute ethanol. $Na_2PO_4·2H_2O$ and $Na_2PO_4·2H_2O$ were used in the preparation of 0.1 M phosphate buffer (PB) solution with pH=7.4. Pyrazinamide (PZA) was obtained from the University of the Western Cape Health Centre, courtesy of Kaaselsvlei Clinic in Bellville South, Cape Town, as a tablet with formulation containing 500 mg pyrazinamide. Stock enzyme solutions of 8.20 μM CYP 2E1 and 4.2 μM MnP were prepared from Cytochrome P450 (EC 1.14.14.1) and Manganese peroxidase from *Nematoloma Frowardii* (EC 1.11.1.13), respectively, supplied by Sigma Aldrich. De-ionized water, used throughout the experiments, was prepared with a Milli-Q water purification system. Analytical grade argon obtained from Afrox South Africa, was used for degassing the cell solutions.

3.2. Instrumentation

3.2.1 Electrochemical techniques

The electrochemical techniques (discussed below) were used to study the redox properties of the biosensors and their prospective platform components at the electrode surface which occur when a potential is applied. From the redox behaviour of different materials under different conditions, various parameters such as rate constant, diffusion coefficient, formal potential, film thickness, sensitivity, detection limits, surface concentration, solution resistance, charge transfer resistance and process reversibility can be determined. The most commonly used techniques are cyclic voltammetry (CV), square wave voltammetry (SWV) and differential pulse voltammetry (DPV). However, the main limitation of voltammetric techniques is that the species under investigation must be either reducible or oxidizable in the range where both the electrode and the electrolyte are electrochemically inert.

3.2.1.1 Cyclic voltammetry

Cyclic voltammetry is one of the versatile electrochemical techniques which are used to investigate kinetics and mechanisms of various reactions at electrode surfaces, with much attention towards peak currents and applied potentials at which the reactions occur. Such reactions can either be reduction or oxidation depending on the scan direction. The magnitude of the peak current is related to the analyte concentration, using the Randles-Sevčik equation. Besides, from the gradient or slope of the Randles-Sevčik plot, the diffusion coefficient and the number of electrons transferred during the reaction can also be determined. However, CV has a major drawback, which is the reduced sensitivity at very low levels of analyte concentration, brought about by currents caused by double-layer effects and other sources.

Cyclic voltammograms, from this study, showed increased peak currents and potential shifts for doped PANI (PANI-TiO_2, PANI-PMMA and PANI-PMMA-TiO_2) than pure PANI. This behaviour is attributed to the intrusion of PMMA and TiO_2 into the polymer backbone of PANI which alters its electronic properties by increasing charge, thereby leading to enhanced

electrochemically activity of the composites. Similar behaviour has been observed after an introduction of carbon nanotubes into PANI [66].

3.2.1.2 Differential pulse voltammetry

Differential pulse is a technique, designed to overcome the sensitivity limitations of CV. The DPV monitors current changes against the applied potential. According to the Osteryoung-Parry the peak current is proportional to the analyte concentration and voltage. Despite the major drawback associated with large potential separation, DPV is more sensitive than CV.

3.2.1.3 Square wave voltammetry

The square wave voltammetry is a more sensitive pulse technique than DPV and CV since it gives the net peak current higher than both the forward and reverse peak currents. The most notable advantages of SW over DPV and CV include higher sensitivity and background current rejection which allows determination of different species at trace levels. This advantage is brought about by the net current of the SW being higher than either the forward or reverse currents, resulting in very small charging current contributions.

3.2.2 Spectroscopic techniques

Spectroscopic techniques are the most highly sensitive and nod-destructible techniques used to study different materials, including human cells and tissues. The most advantageous features of these techniques are the small sample volumes and that no complex sample preparations of biological samples is required.

3.2.2.1 Ultra-Violet Visible spectroscopy (UV-Vis)

UV-Vis spectroscopy is used for the quantitative determination of different analytes, such as highly conjugated organic compounds, transition metal ions and biological molecules, with

respect to their electronic and optical properties. The most fundamental process of absorption spectroscopy is the absorption of a discrete amount of energy. The energy required for the transition from a lower energy state (E_1) to a higher energy state (E_2) is equivalent to the energy of electromagnetic radiation that causes transition (electronic band gap). A typical UV-Vis spectrum shows absorption peaks or bands corresponding to electronic transitions of different structural groups within a molecule (chromophores). The electronic band gaps can be determined using **Equation 1**. Literally, band gaps are 0 eV for conductors, 0.1-1.3 eV for semiconductors and >3 eV for insulators. With respect to biosensors, platforms with band gaps characteristic of semiconductors are biocompatible.

$$E_2 - E_1 = E = h\nu = \frac{hc}{\lambda}$$
<div align="right">Equation 1</div>

Where E is energy absorbed, h is the universal Planck's constant, ν is the frequency of incident light, c is velocity of light and λ is the wavelength.

In a study on electronic properties of PANI [72], UV-Vis results showed bands at 335 nm, 430 nm and 840 nm corresponding to π-π*, π-polaron and polaron-π* transitions of polyaniline, respectively. Our study also revealed bands at 335 nm, 461 nm and 840 nm which were also attributed to the π-π*, π-polaron and polaron-π* transitions of polyaniline, respectively. Also, our nanocomposite had a band gap of 2.2 eV which shows that it is biocompatible.

3.2.2.2. Fourier Transform Infra-Red spectroscopy (FTIR)

FTIR is a technique universally used to investigate chemical bonding or molecular structure of materials due to the presence or absence of different functional groups. In this study, FTIR was used for structural characterization of PANI and its composites. The FTIR spectrum exhibited peaks at 1455 cm^{-1} and 1633 cm^{-1} which, respectively, correspond to stretching

modes of C=C (benzenoid ring) and C=N (quinoid ring) of PANI. Also, the spectrum for PANI showed a peak at 3857 cm^{-1} corresponding to N-H vibrations. For the PANI-TiO$_2$ this peak shifted to a higher wavenumber (3920 cm^{-1}) which is attributed to the covalent bonding between nitrogen (from PANI) and oxygen (from TiO$_2$). This behaviour has been confirmed [97] and attributed to the electron-withdrawing nature of TiO$_2$ which affects the delocalization of electrons around the nitrogen atoms of PANI [97].

### 3.2.2.3 X-Ray Diffraction spectroscopy (XRD).

X-Ray diffraction is a versatile non-destructive technique used to investigate crystallinity, crystal size, orientation and composition of materials. Diffraction patterns show the diffraction peak intensities against the angle of diffraction and are unique for different types of materials. The intensities of these diffraction peaks are proportional to the abundance of the corresponding crystal facets in the material lattice while sharp and broad peaks correspond to the crystalline and amorphous nature of the material being studied. Relative to this study, XRD was used to investigate the crystallinity of PANI before and after doping with carbon nanotubes. The XRD patterns exhibited sharp peaks at $2\theta = 26.5°$ and $2\theta = 25.8°$ corresponding to the (200) crystal plane of PANI and the graphite-like structure of MWCNTs, respectively. The introduction of CNTs did not alter with the crystallinity of PANI which is shown by the retained sharp peak of the nanocomposite. A similar finding for PANI-MWCNTs composite has been demonstrated [97].

3.2.3. Microscopic techniques

3.2.3.1. Atomic Force microscopy (AFM)

The AFM is one of non-destructive techniques used to study topographic properties of different materials, such as plastics, metals, glasses and biological samples by measuring the

deflections resulting from repulsive or attractive forces between the cantilever tip and the material under investigation, giving out three-dimensional images of high resolution. The AFM is advantageous over other techniques since it does not require conductive samples for analysis and can use different modes such as tapping mode, contact mode and non-contact mode for determination of different parameters such as pore size, pore density and pore size distribution of material. However, the choice of sampling mode is very crucial. For this study, AFM was used to investigate morphology and roughness of different materials at different stages towards biosensor fabrication. The incorporation of MWCNTs into PANI resulted in a different form of material exhibiting structures present in both PANI and MWCNTs individually. Furthermore, the immobilization of CYP 2E1 resulted in a surface of increased roughness with appearance completely different from the composite platform and its individual components. This behaviour was observed when a surface of reduced roughness was obtained after immobilization of DNA onto a film of nanostructured ZnO (zinc oxide) [98].
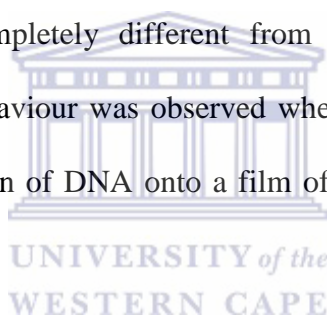
3.2.3.2. High-resolution Scanning Electron Microscopy (HR-SEM)

HR-SEM is one of the versatile techniques used to study morphologies of all types of materials, based on interactions between a highly accelerated electron beam and the atoms in the material of interest. However, like any other technique, HR-SEM has a major limitation where it only analyses conductive materials [99]. In this study, surface morphologies of the PANI-PMMA-TiO$_2$/MnP biosensor, its composite platform (PANI-PMMA-TiO$_2$) and the respective individual components were studied using HR-SEM.

3.3 Measurements

All voltammetric experiments were carried out with a BioAnalytical Systems (BAS) 100W electrochemical workstation (BioAnalytical Systems: BAS, West Lafayette, IN) and a

Princeton Applied Research Potentiostat Model 273 A. both workstations were interfaced to a three-electrode system with a BAS glassy carbon electrode (GCE with diameter 0.071 cm^2), a Sigma Aldrich platinum wire and a BAS Ag/AgCl (3M NaCl) type electrode as the working electrode, counter and reference electrodes, respectively. Prior to use, the GCE was polished with 1.0, 0.3 and 0.05 µm alumina slurries (Buehler, IL, USA), followed by ultrasonication in absolute ethanol and deionized water, respectively.

Ultraviolet-Visible (UV-Vis) spectra of PANI, PANI/TiO$_2$, TiO$_2$, PMMA, PANI/PMMA, PANI/PMMA/TiO$_2$ (dissolved in DMSO), MnP and PANI/PMMA/TiO$_2$/MnP (dissolved in buffer) were recorded on a Nicolet Evolution 100 (Thermo Electron Cooperation, UK).

SEM images were taken with a Hitachi S3000N scanning electron microscope at an acceleration voltage of 20 kV at various magnifications. Small amounts of TiO$_2$ and PMMA (in powder form) were placed on copper grids. PANI, PANI/TiO$_2$, PANI/PMMA, PANI/PMMA/TiO$_2$ and PANI/PMMA/TiO$_2$/MnP were dissolved in DMF after electrodeposition and dropcoating of MnP. An aliquot of 2 µL of each sample were drop coated on the copper grids and dried for two days at room temperature. The samples on the grids were coated with gold using a SC7640 Auto/ Manual high resolution super coater (Quorum Technology Ltd., England) at a voltage of 2 kV and plasma current of 25 mA for one minute.

FTIR spectra were recorded in the range 4000-300 cm^{-1} using a Perkin Elmer model Spectrum 100 series.

X-ray diffraction (XRD) spectra of MWCNTs, PANI and PANI/MWCNTs were recorded using a Bruker AXS D8 Advance diffractometer (voltage 40 KV; current 40 mA). The XRD spectra were recorded in the range 15-85˚.

AFM scanned with a silicon tip at a spring constant of 1-5 N/m and resonance frequency of 60-100 kHz. The scanned AFM images were taken using a Veeco NanoMan V model (Cambridge, USA).

3.4. Preparation of GC/PANI/MWCNT/CYP2E1 nanobiosensor

A polymerization monomer was prepared by refluxing a 0.1 M aniline solution containing 0.2 %wt MWCNTs at 130 ˚C for 3 h and followed by vacuum filtration. The PANI/MWCNT film was deposited on the GCE by oxidative electropolymerization of the aniline-MWCNT solution by scanning the electrode at 40 mV/s from -250 mV to +950 mV for 10 cycles. An argon blanket was maintained throughout the polymerization process.

The PANI/MWCNT polymer film was reduced at -500 mV for 1200 s. The reduced polymer film was then immersed in a 3 mL PB cell solution containing 20 μL of CYP2E1. The modified electrode was then oxidized +400 mV for 1800 s, during which CYP2E1 was deposited on the PANI/MWCNT film by chemical and electrostatic interactions as depicted in **Scheme 1**. The biosensor (denoted as GC/PANI/MWCNT/CYP2E1) was carefully rinsed with water and stored at 4 ˚C when not in use.
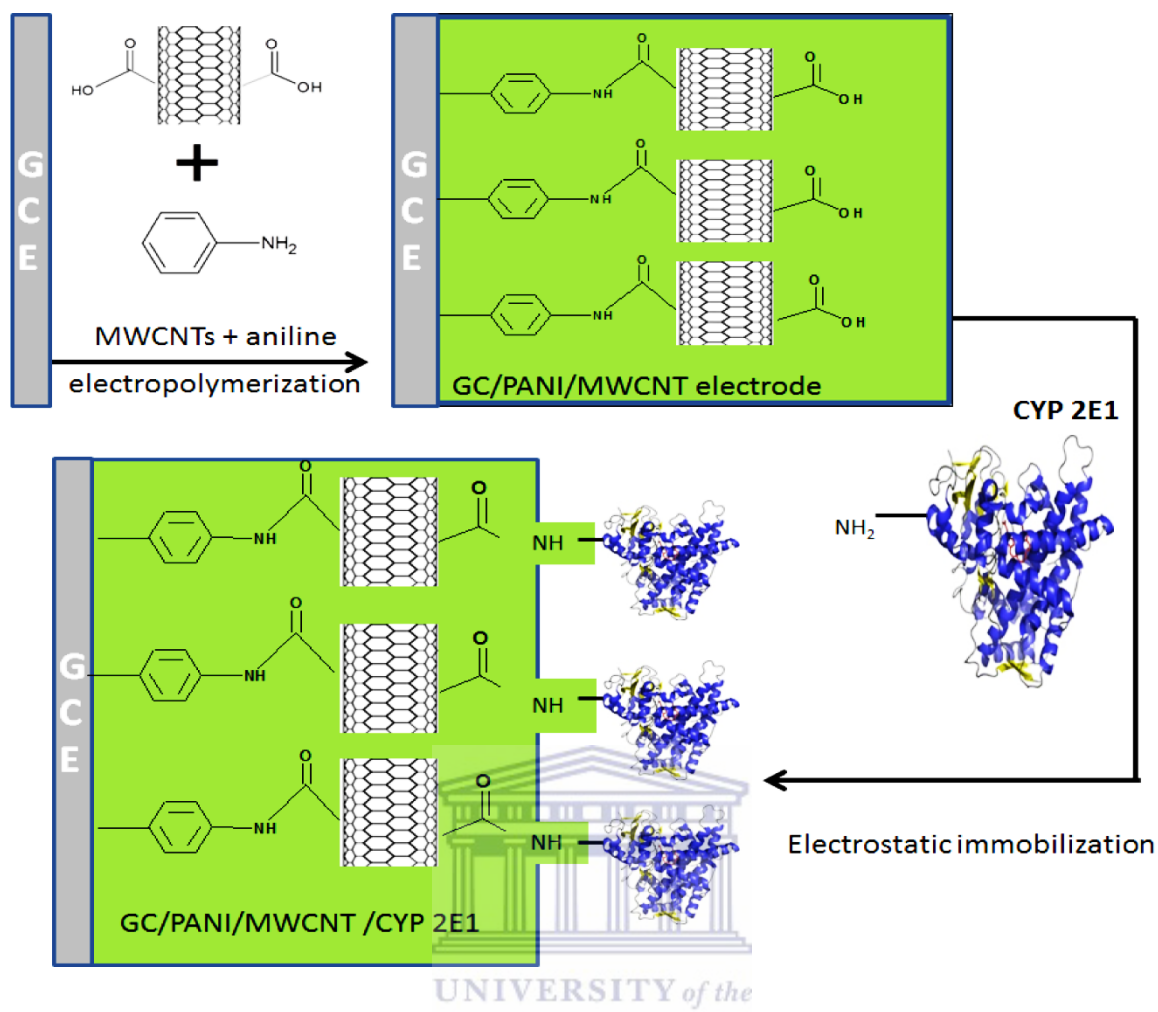
Scheme 1: Schematic presentation of the preparation of the CYP2E1 nanobiosensor.

3.5. Preparation of the GC/PANI/PMMA/TiO₂/MnP nanobiosensor.

A solution of poly(methyl methacrylate) (PMMA) was prepared by dissolving 2 mg of PMMA in 10 mL of tetrahydrofuran (THF), followed by ultrasonication until PMMA dissolved completely. An aniline-TiO₂ monomer solution was prepared by refluxing 5 mL of distilled aniline with 0.02 % wt TiO₂ at 130 ˚C for 3 h ˚C. A MnP:BSA solution was prepared by mixing a 5 µL solution of BSA (from 2 mg BSA dissolved in 50 µL PB) and 5µL of 4.2 µM MnP. All the polymerization processes were conducted in a 10 mL solution in 1 M H_2SO_4 and an argon blanket was maintained throughout.

A 10 mL monomer solution was prepared from 92 µL of aniline-TiO$_2$, 0.1 g TiO$_2$, 108 µL MMA and 1 mL PMMA solution in H$_2$SO$_4$. The PANI/PMMA/TiO$_2$ nanocomposite film was deposited on the GCE by oxidative electropolymerization of the monomer solution by scanning the electrode at 30 mV/s from -200 mV to +1200 mV for 10 cycles. A 1:1 solution (3 µL) of EDC:NHS was drop-coated onto the nanocomposite and was left to dry for 30 min at room temperature. This was followed by drop-casting of 3 µL of MnP:BSA solution. The biosensor, denoted as GC/PANI-PMMA-TiO$_2$-MnP, was immersed in 3 mL PB solution and was kept at 4 ˚C for 4 h before use. The biosensor system was kept at 4 ˚C when not in use.

For comparison, individual effects of TiO$_2$ and PMMA on PANI were also investigated from PANI/PMMA and PANI/TiO$_2$ films prepared under the same conditions using the following monomer solutions:

(a) 92 µL of distilled aniline for the PANI film

(b) 92 µL of 0.1 M aniline-TiO$_2$ solution and 0.05 M TiO$_2$ for the PANI/TiO$_2$ film and

(c) 0.1 M distilled aniline, 0.1 M MMA (108 µL) and 1 mL of the PMMA solution for the PANI/PMMA film.
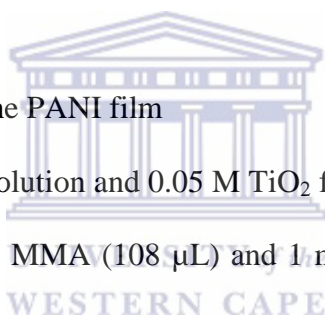
3.6. Biosensor measurements

The CYP2E1 based biosensor was tested for the sensing of different PZA concentrations in 10 mL phosphate buffer (pH 7.4) from a standard solution (0.08 M) of PZA prepared by dissolving PZA capsule in 50 mL of PBS.

The MnP based biosensor and its components were tested for sensing of Bisphenol A. A 0.1 M stock solution of BPA was prepared in absolute ethanol and was kept at 4 °C. The stock solution was used to prepare 1 mM and 1 µM solutions in an ethanol:water mixture (2:3) and distilled water, respectively. Then, 40 nM working solutions were prepared in PBS (from the 1 µM solution).

CHAPTER

CHARACTERIZATION OF THE PANI/MWCNT and PANI/PMMA/TiO$_2$ NANOCOMPOSITES

Summary

This chapter outlines and discusses the results obtained for the study based on developing the nanocomposite platforms, PANI/MWCNT and PANI/PMMA/TiO$_2$. The chapter deals specifically with the characterization of the structural, morphological, optical and electrochemical properties of the nanocomposites which were investigated using XRD, AFM, HR-SEM, UV-Vis, CV, SW and DPV techniques. Therefore, this section illustrates the importance and potential of the nanocomposites towards the development of the nanobiosensors.

4.1 Structural characterization of PANI/MWCNT and PANI/PMMA/TiO$_2$ nanocomposites.

4.1.1. X-Ray Diffraction analysis.

(a) PANI/MWCNT nanocomposite.

The XRD is a versatile technique used to investigate the crysallinity, orientation and composition of the material. The diffraction peak intensies are proportional to the abundance of the corresponding crystalline facets of the material. The sharpness and broadness of the peaks determines the crystallinity and amorphousity of the material. In this study, the XRD was used to study the crystallinity of polyaniline (PANI) and the effects of incorporating multiwalled carbon nanotubes into PANI. **Figure 4.1** shows the RXD patterns of the nanocomposite and its individual components, PANI and MWCNTs.
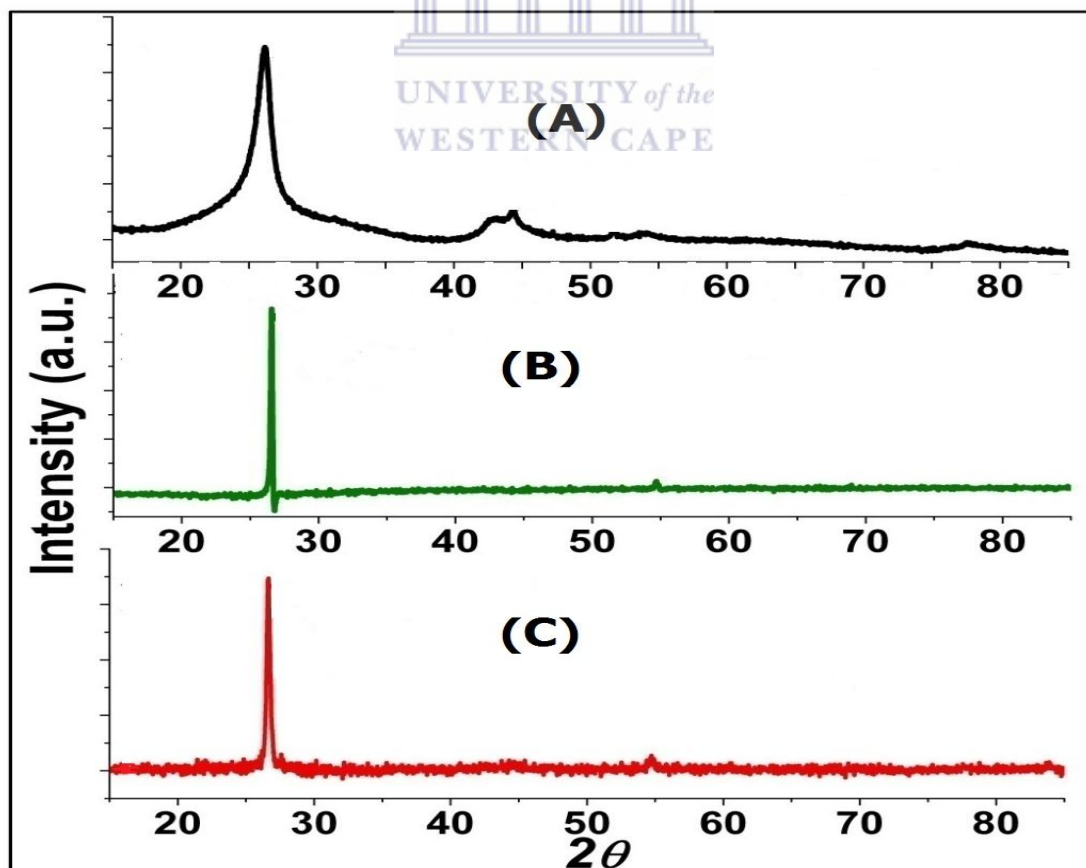

Figure 4.1: *XRD patterns of MWCNTs (A), PANI (B) and PANI/MWCNT composite (C)*

The XRD pattern consists of sharp, well-resolved peaks at 26.0˚ and 26.5 ˚. These peaks are associated with carbon (002) of MWCNTs [100] and the periodicity perpendicular to polymer chain i.e. (200) crystal plane of PANI [101]. However, in the nanocomposite (PANI/MWCNT), the sharp and strong diffraction peak of PANI at 26.5˚ was observed to overlap with the peak of MWCNTs resulting in a sharp and intense peak at 25.8˚ due to the bonding between PANI and MWCNTs. This peak shift (from 26.5˚ to 25.8˚) is attributed to a decrease in the sp^2 C=C layer spacing of the carbon nanotubes due to its interactions with PANI [102].

There is no additional peak observed for the composite which indicates that no additional crystalline order has been introduced into the composite. Also, there is no new effect brought up by the MWCNTs on the crystal nature of PANI as it retains the sharp peak in the composite. However, the shift in the diffraction angle can be ascribed to the formation of the new crystal appearing at 25.8˚. From this result, it was concluded that the MWCNTs were well dispersed in polymer matrix. Similar behaviour of a PANI/MWCNT nanocomposite was observed [103].

4.1.2. FTIR analysis.

(a) PANI

The FTIR was used to investigate the structural composition of the nanocomposites by identifying the functional groups present. The FTIR spectrum of the electrochemically synthesized PANI, taken in the 4000-500 cm^{-1}, is shown in **Figure 4.2**. The spectrum shows a peak at 3776 cm^{-1} which is attributed to the N-H stretching mode of the amine and imine groups of PANI. The band at 1668 cm^{-1} corresponds to the C=N stretching vibration of the quinoid unit while the peaks assigned at 1433 cm^{-1} and 1270 cm^{-1} respectively correspond to the C=C and C-N stretching vibrations of the benzenoid unit of PANI. The peaks at 1132 cm$^-$

[1] and 889 cm^{-1} are respectively assigned to the C-H in plane and out-of-plane deformations indicating the presence of the emeraldine form of PANI which is formed during protonation.
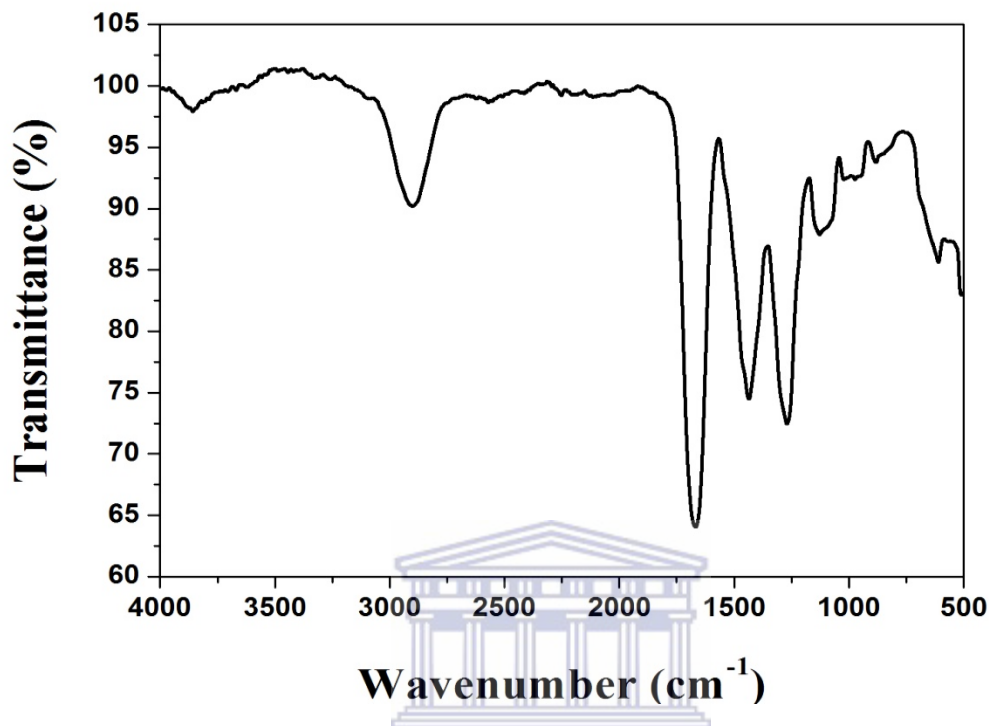

Figure 4.2: FTIR spectrum of PANI.

(b) PANI/MWCNT nanocomposite.

The spectrum of PANI/MWCNT nanocomposite also shows the main characteristic peaks of PANI. The peaks at 1414 cm^{-1}, 1308 cm^{-1} and 811 cm^{-1} are respectively attributed to the C=C, C-N and C-C stretching vibrations of the benzenoid ring while the peak at 1524 cm^{-1} is assigned to the C=N stretching mode of the quinoid ring [104]. The peaks obtained at 3360 cm^{-1} and 1112 cm^{-1} are ascribed to the N-H stretching vibration and C-H out-of-plane bending vibration, respectively. The broad peak at 1770 cm^{-1} is ascribed to the C=O stretching vibration which reflects presence of the carboxylic acid group from the functionalized MWCNTs. Therefore, this peak arose from the interactions between PANI and MWCNTs and assures successful intrusion of MWCNTs onto the backbone of PANI.
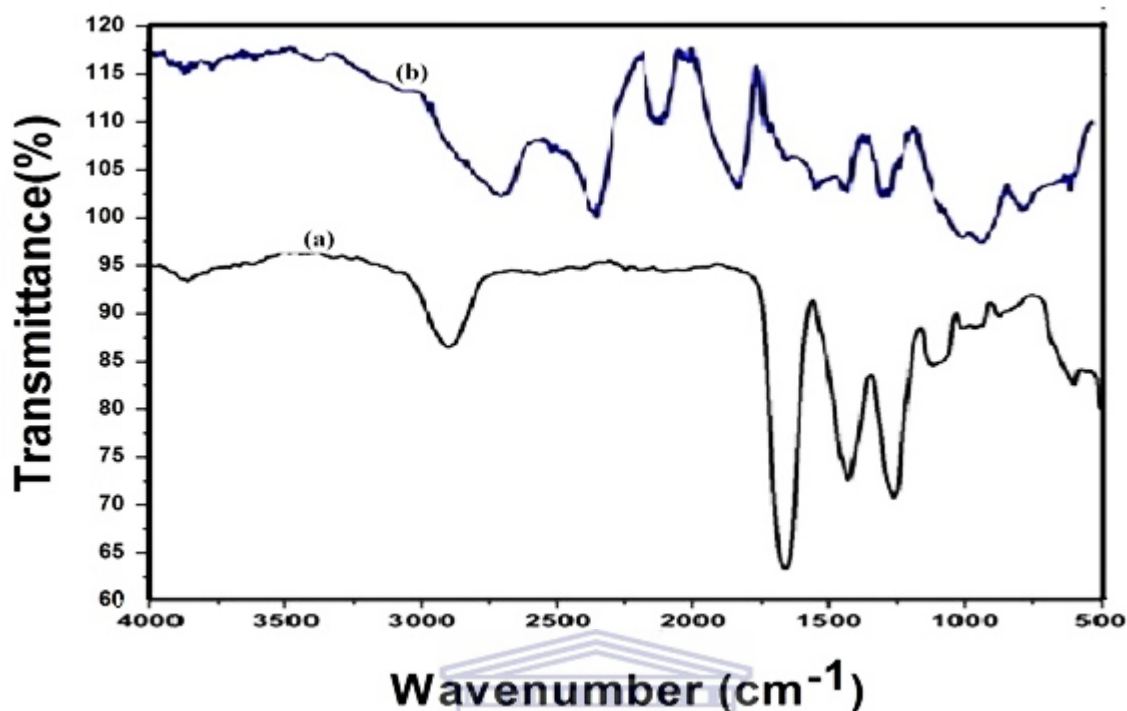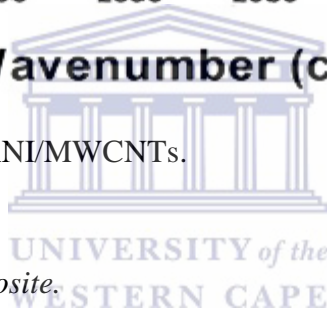
Figure 4.3: FTIR spectrum of PANI/MWCNTs.

(c) PANI/PMMA/TiO₂ nanocomposite.

The effects of TiO_2 and PMMA on the structural composition of PANI were also investigated using FTIR. The spectrum of the PANI/TiO_2 composite **(Figure 4.4)** also exhibits the characteristic peaks of PANI. When compared to the spectrum of PANI, the peaks assigned to the N-H stretching mode of the amine and imine groups and the C=N stretching vibration of the quinoid unit of PANI show shifts to higher wavenumbers at 3787 cm^{-1} and 1676 cm^{-1} respectively. The characteristic peak assigned to the C=C stretching vibration at 1433 cm^{-1} is retained at the same wavenumber while the peaks assigned to the C-N stretching vibration of the benzenoid unit and the C-H in-plane deformation of PANI have shifted to lower wavenumbers at 1268 cm^{-1} and 1118 cm^{-1}, respectively. This means that the bond strengths of C-N and C-H have become weaker in PANI TiO_2 composite while those of N-H and C=N

became stronger. The composite also shows new peaks at 3588 cm^{-1} and 2342 cm^{-1} which are attributed to the incorporation of TiO_2 into PANI. This means that there is a strong interaction between PANI molecule and TiO_2 nanoparticles. Because titanium is a transition metal, TiO_2 has intense tendency to form a coordination compound resulting from interactions between the oxygen atom of TiO_2 and the nitrogen atom of PANI. These interactions strengthen or weaken the bond strengths in the PANI molecule, hence the peaks shifts to higher and lower wavenumbers, respectively. Also, the hydrogen bonding between TiO_2 nanoparticles and the PANI molecule also contributes to the shift of peaks [72].
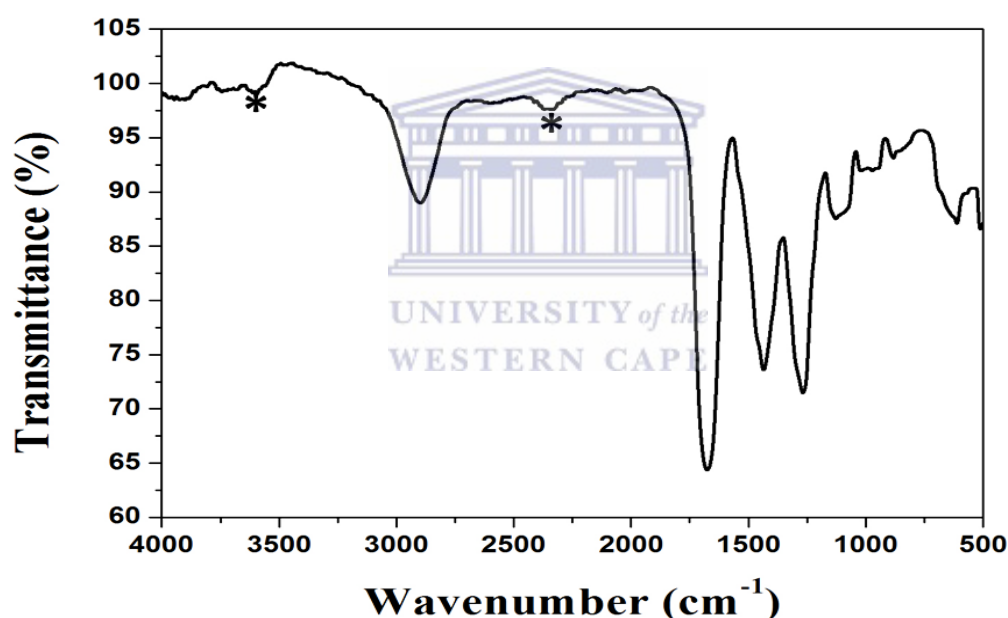
Figure 4.4: FTIR spectrum of PANI/TiO_2. The new peaks are marked with a star (✱).

As with TiO_2, the doping of PANI with PMMA is expected to yield a composite with properties exhibiting those of PANI and PMMA. The introduction of PMMA into PANI has led to the formation of a new peak at 2256 cm^{-1} attributed to the interaction between the TiO_2 and PANI. The absence of the N-H peak in the region 3600-3800 cm^{-1} in this composite is attributed to the interactions between the O groups of PMMA and the N groups of PANI

which leads to a conclusion that the PMMA completely altered the structure of PANI. The composite **(Figure 4.5)** also exhibits a shift to a higher wavenumber (1677 cm^{-1}) for the C=N stretching vibration of the quinoid unit while showing a shift to lower wavenumbers (1266 cm^{-1} and 1118 cm^{-1}) for the C-N stretching vibration of the benzenoid unit and the C-H in-plane deformation of PANI, respectively. This means that the PANI/PMMA interaction strengthens C=N bond strength while weakening the C-H and C-N bond strength.
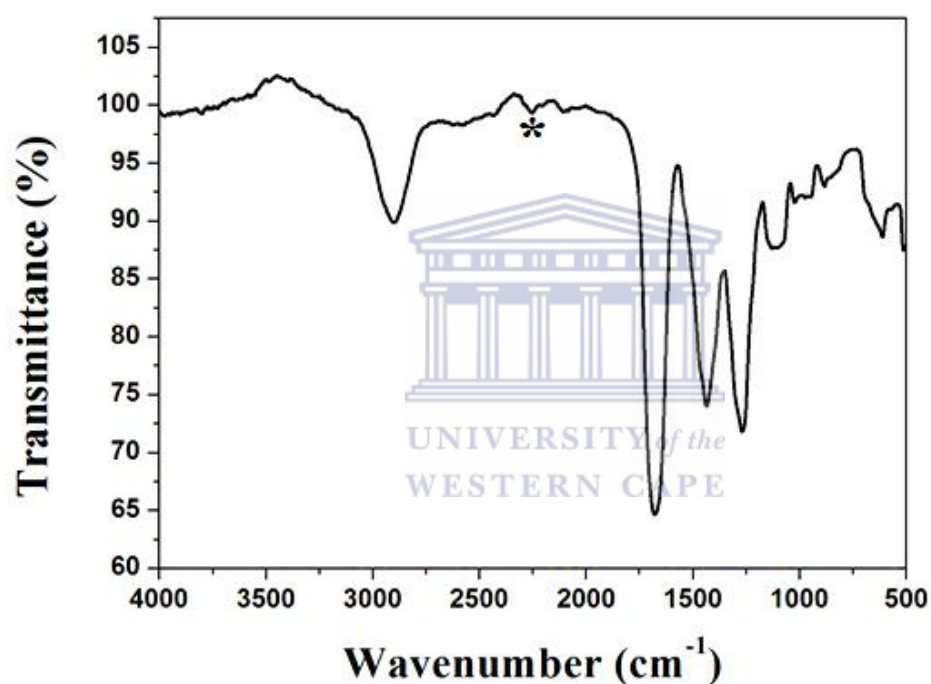
Figure 4.5: FTIR spectrum of PANI/PMMA. The mark (✱) shows the location of the new peak resulting from the incorporation PMMA into PANI.

The nanocomposite **(Figure 4.6)** comprising PANI, PMMA and TiO$_2$ exhibits the characteristic peaks of PANI at 1676 cm^{-1} and 1433 cm^{-1} assigned to the C=N stretching vibration of the quinoid unit and the C=C stretching vibration of the benzenoid unit. The broad peak at 3796 cm^{-1} is assigned to the N-H stretching vibration of PANI but has shifted to an even higher wavenumber as compared to PANI. This shift is associated with the

combined effect of incorporation of TiO_2 and PMMA into PANI. It is concluded that interactions between the oxygen atoms from both TiO_2 and PMMA strengthen the N-H bond strength of PANI.
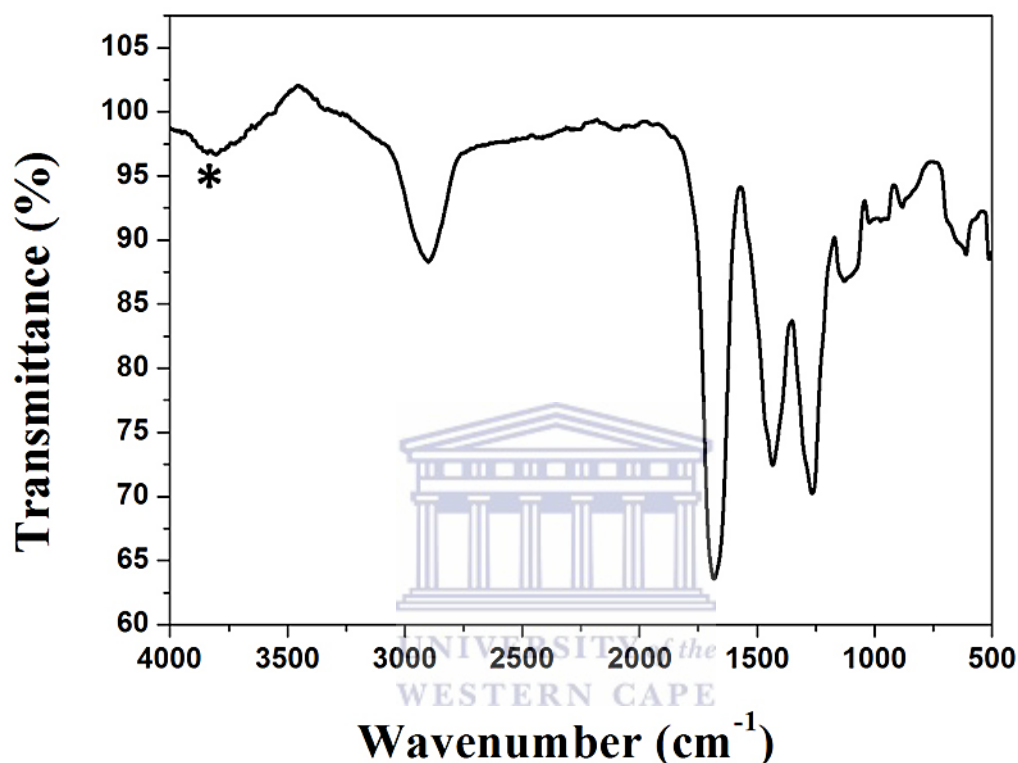
Figure 4.6: FTIR spectrum of PANI/PMMA/TiO_2 nanocomposite. The * marks the broad peak assigned to N-H.

4.2 Morphology characterization of PANI/MWCNT and PANI/PMMA/TiO_2 nanocomposites.

(a) AFM analysis of PANI/MWCNT.

The AFM was used to interrogate morphology of the material through the steps of nanocomposite synthesis. For comparison, the AFM images of the bare electrode and the individual components (PANI and MWCNTs) are also included. **Figure 4.7** shows AFM

41

images of the bare screen printed glassy carbon electrode (SPGCE) **(Figure 4.7A)** and the SPGCE modified with PANI and PANI/MWCNT nanocomposite, respectively.
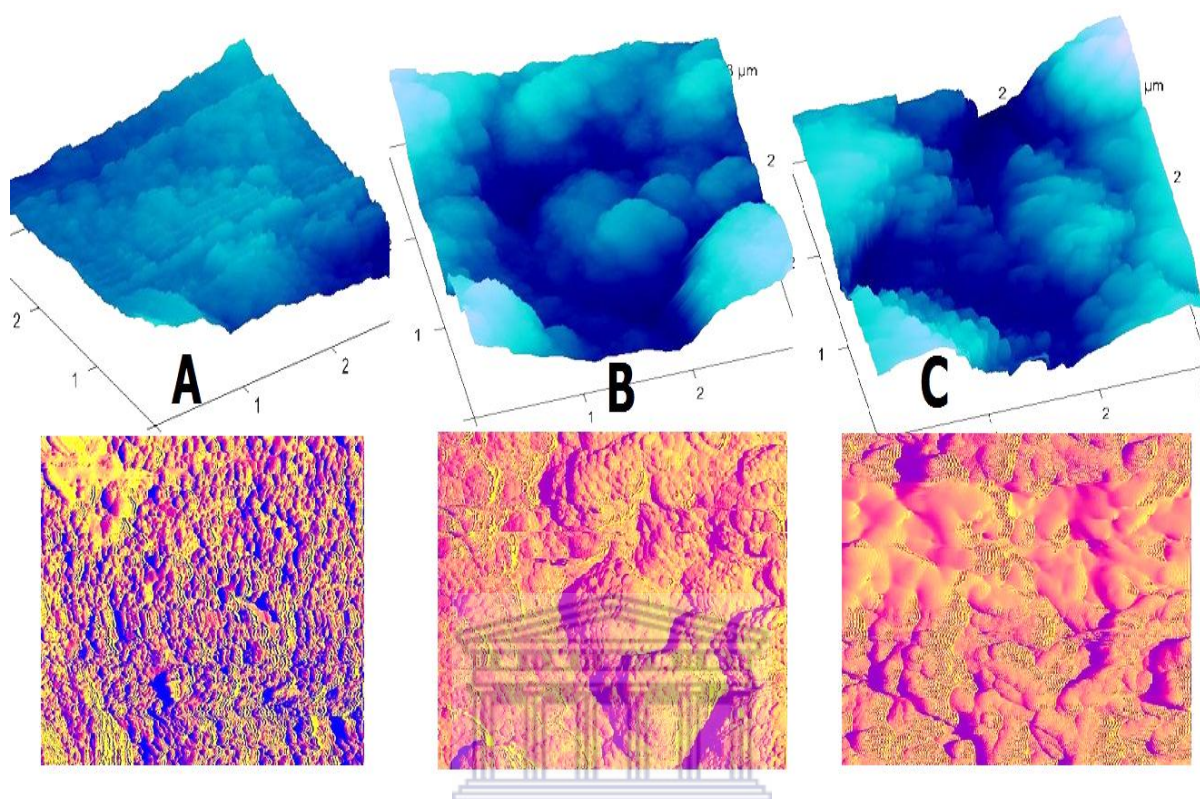
Figure 4.7: AFM images of bare electrode (A), PANI (B) and PANI/MWCNT nanocomposite (C).

The PANI/MWCNT nanocomposite exhibits tubular structures **(Figure 4.7 (C))** while PANI **(Figure 4.7 (B))** film displays spherical particles of uniform size. When the MWCNTs were incorporated into PANI, the resultant PANI/MWCNT nanocomposite reveals the distribution of MWCNTs (of 115 nm average diameter) within the nanocomposite.

(b) HR-SEM characterization of PANI/PMMA/TiO$_2$ nanocomposite

After electropolymerization in sulphuric acid, the PANI film was dissolved in tetrahydrofuran and its morphology was studied using SEM. As shown by the micrograph, PANI **(Figure 4 8 (i))** exhibits spherical nanoparticles with sizes approximately 200 nm which are closely packed, resulting in tubular structures of different lengths and diameters.

42

The effect of TiO$_2$ on PANI was evaluated using the HR-SEM. The resultant PANI/TiO$_2$ composite, synthesized electrochemically from the mixture of aniline and TiO$_2$ nanoparticles, is shown in **Figure 4.8 (ii)**. The composite exhibits structures for both PANI and TiO$_2$. The TiO$_2$ particles show agglomerated spherical nanoparticles of sizes ranging between 30 nm and 100 nm distributed evenly in the PANI network.

The effect of PMMA on PANI was also investigated. The SEM image of the PANI/PMMA composite is shown in **Figure 4.8 (iii)**. From the image, the prominent tubular structural characteristics of PANI are exhibited by the composite. However, the composite shows a rigid, compact morphology when compared to PANI alone. It is then concluded that the introduction of PMMA into PANI did not alter the lattice of PANI but only stabilized the morphology of the composite.

UNIVERSITY of the
WESTERN CAPE
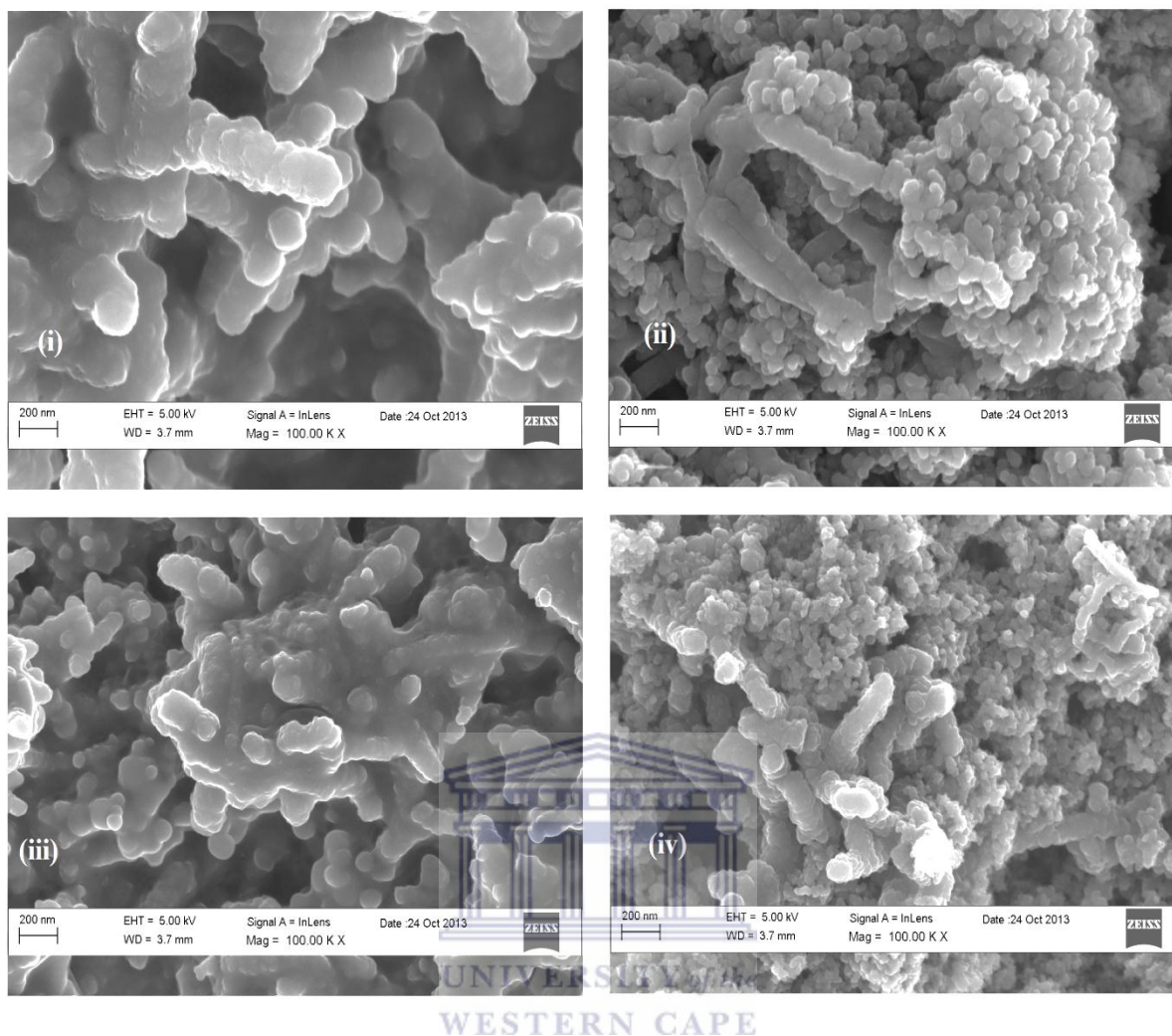
Figure 4.8: HR-SEM images of PANI (i), PANI/TiO$_2$ (ii), PANI/PMMA (iii) and PANI/PMMA/TiO$_2$ nanocomposite (iv).

The morphology of the nanocomposite **(Figure 4.8 (iv))** comprising PANI, PMMA and TiO$_2$ shows all structures revealed by the individual components. As compared to the PANI/PMMA composite, the nanocomposite does show a morphological structure assigned to the PMMA. The PANI tubular structures are embedded in between the TiO$_2$ and PMMA. Therefore, a nanocomposite to exhibit combined characteristics of PANI, PMMA and TiO$_2$ has been successfully synthesized.

4.3 Optical properties of PANI/PMMA/TiO$_2$ nanocomposite using UV-Vis.

(a) PANI

The UV-Vis spectrum showing the optical properties of PANI is shown in **Figure 4.9**. The spectrum shows three peaks at 335 nm, 460 nm and 823 nm which are characteristic of the emeraldine base form of PANI. These peaks are respectively attributed to the π-π^* transitions of the benzenoid ring, π-polaron band transitions and polaron- π^* transitions of the quinoid ring and are characteristic of protonated polyaniline [103]. PANI has a band gap of 2.70 eV which is characteristic of a biocompatible platform.

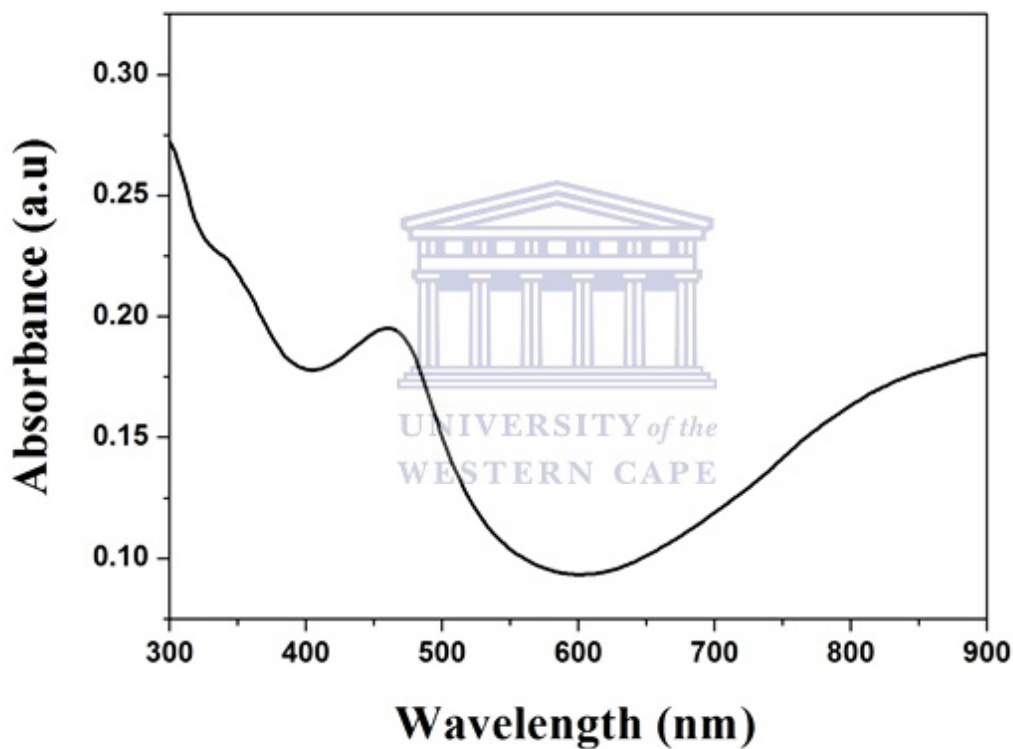

Figure 4.9: UV-Vis spectrum of PANI.

(b) PANI/TiO$_2$

The effect of TiO$_2$ nanoparticles introduced in the PANI was investigated. For comparison, the UV-Vis spectrum of TiO$_2$ is also shown in **Figure 4.10**.Compared to the spectrum of

PANI alone, the composite shows a peak at 305 nm which is also attributed to the π-π*
transitions of the benzenoid ring. However, this peak has shifted to a lower wavelength which
is attributed to the interactions between the TiO_2 and PANI. As discussed in the literature
review, the semiconductive transition metal TiO_2 is characterized by hole-electron
recombinations in which an electron from its conduction band is injected into the LUMO of
PANI. Comparatively to PANI, the composite shows a new peak at 610 nm which reveals the
strong interactions between PANI and TiO_2. This peak is assigned to the charge transfer
excitons of the quinoid ring of PANI. Moreover, the shifts in peaks to higher wavenumbers
attributed to the electron withdrawing nature of TiO_2 which effectively increases the degree
of electron delocalization around the nitrogen atom of PANI.
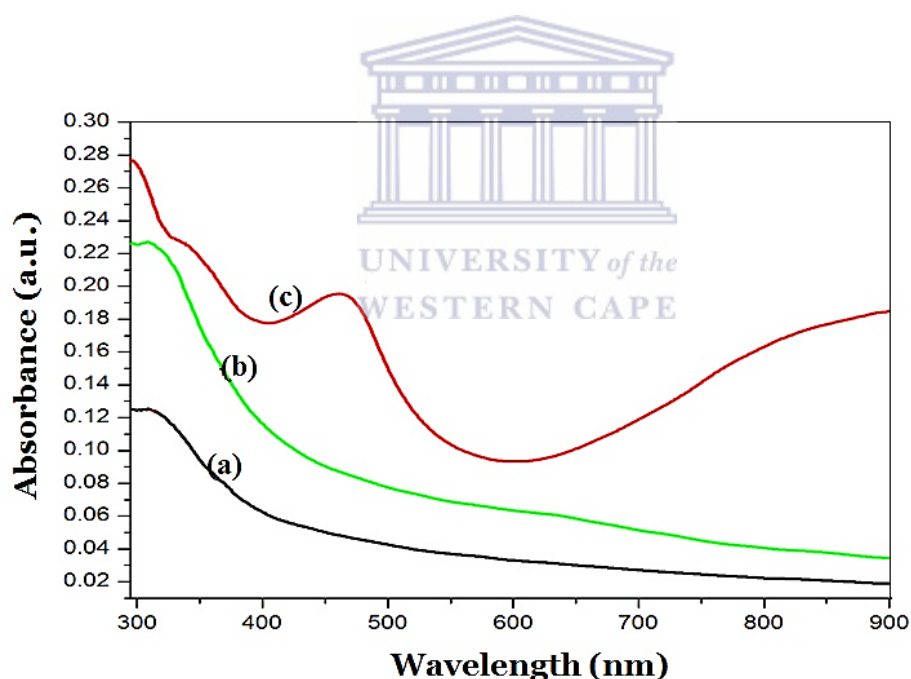

Figure 4.10: UV-Vis spectrum of (a) TiO_2, (b) PANI/TiO_2 and (c) PANI.

(c) PANI/PMMA.

The photoactivity properties of PMMA were also studied using UV-Vis so that their effect on
PANI can be clearly understood. However, PMMA did not exhibit any absorption peaks and

its spectrum is not included. The composite **(Figure 4.11)** comprising PANI and PMMA shows the characteristic peak of PANI assigned to the π-π* transitions of the benzenoid ring at 330 nm. Similarly to the PANI/TiO$_2$ composite, this peak shows a shift to a lower wavelength when compared to PANI alone. This means that there is also a strong interaction between the oxygen of the PMMA and the nitrogen of PANI which alters the bonds of PANI. This is corroborated more by the formation of the peak at 621 nm attributed to the charge transfer excitons of the quinoid ring of PANI.
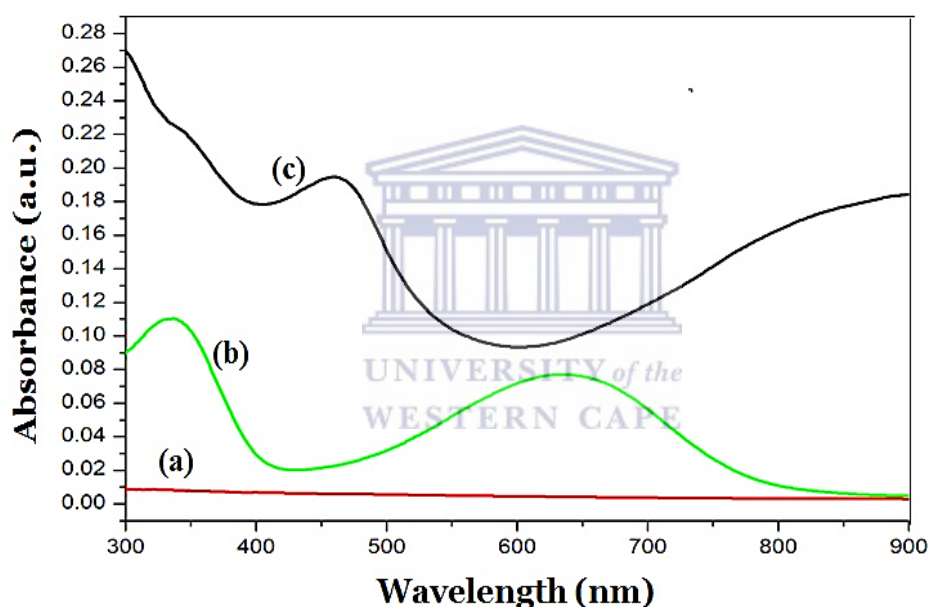
Figure 4.11: UV-Vis spectrum of (a) PMMA, (b) PANI/PMMA and (c) PANI.

(d) PANI/PMMA/TiO$_2$ nanocomposite

The UV-Vis spectrum of the nanocomposite is shown in **Figure 4.12**. The combined effect of introducing PMMA and TiO$_2$ into PANI was investigated. The nanocomposite shows two absorption peaks as shown by the PANI/PMMA and PANI/TiO$_2$ composites. These peaks are allocated at 311 nm and 615 nm and are assigned to the π-π* transitions of the benzenoid ring

and the charge transfer excitons of the quinoid ring of PANI, respectively. These peaks are allocated at wavelengths in between those of PANI/PMMA and PANI/TiO$_2$. Therefore, it is concluded that both TiO$_2$ and PMMA increase the electron charge localization along the backbone of PANI. According to literature, the nature of the interaction between the conduction and valence bands and the size of the band gap determines the optical properties of semiconducting materials. The calculated band gap of the nanocomposite is 2.02 eV which characterizes biocompatible semiconductive materials. Therefore, this nanocomposite will serve a good receiving matrix for MnP.
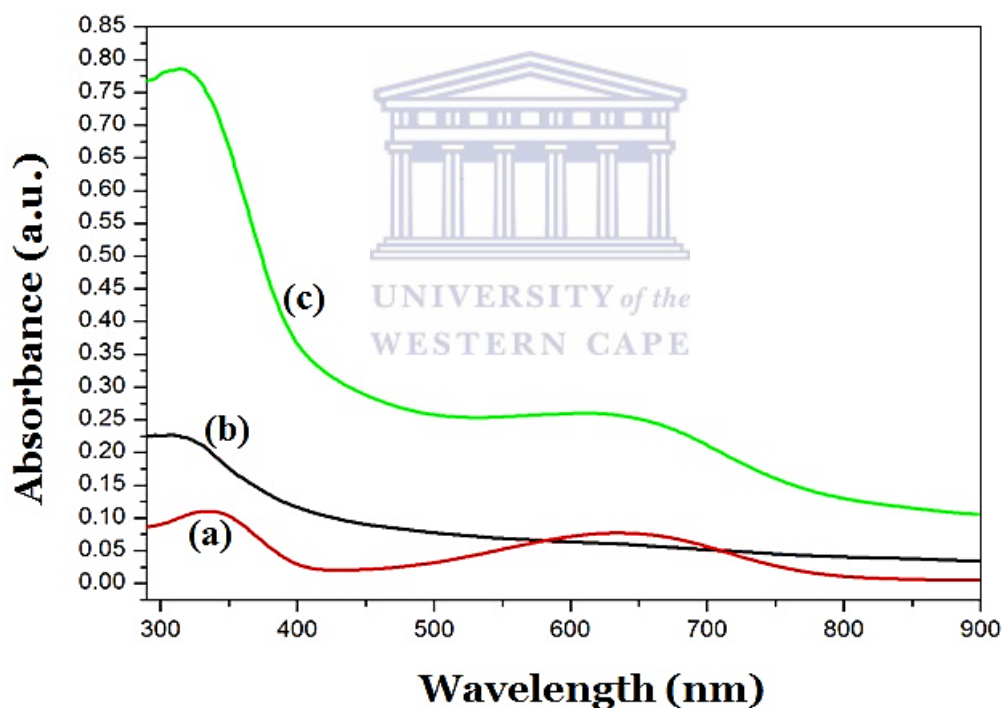
Figure 4.12: UV-Vis spectrum of (a) PANI/PMMA, (b) PANI/TiO$_2$ and (c) PANI/PMMA/TiO$_2$ nanocomposite.

4.4 Electrochemical characterization of PANI, PANI/MWCNT and PANI/PMMA/TiO$_2$

(a) PANI.

The electrochemical behaviour of the electrochemically prepared PANI was evaluated using cyclic voltammetry. The cyclic voltammogram of PANI in **Figure 4.13** shows three redox peaks labelled A/A′ (+150/+90 mV), B/B′ (+460/+420 mV) and C/C′ (+630/+530 mV) (vs Ag/AgCl) at lower scan rates. The redox processes to A/A′, to B/B′ and to C/C′ can be attributed to the leucoemeraldine/leucoemeraldine radical cation, emeraldine radical cation/emeraldine and pernigraniline radical cation/pernigraniline states of PANI, respectively [105].
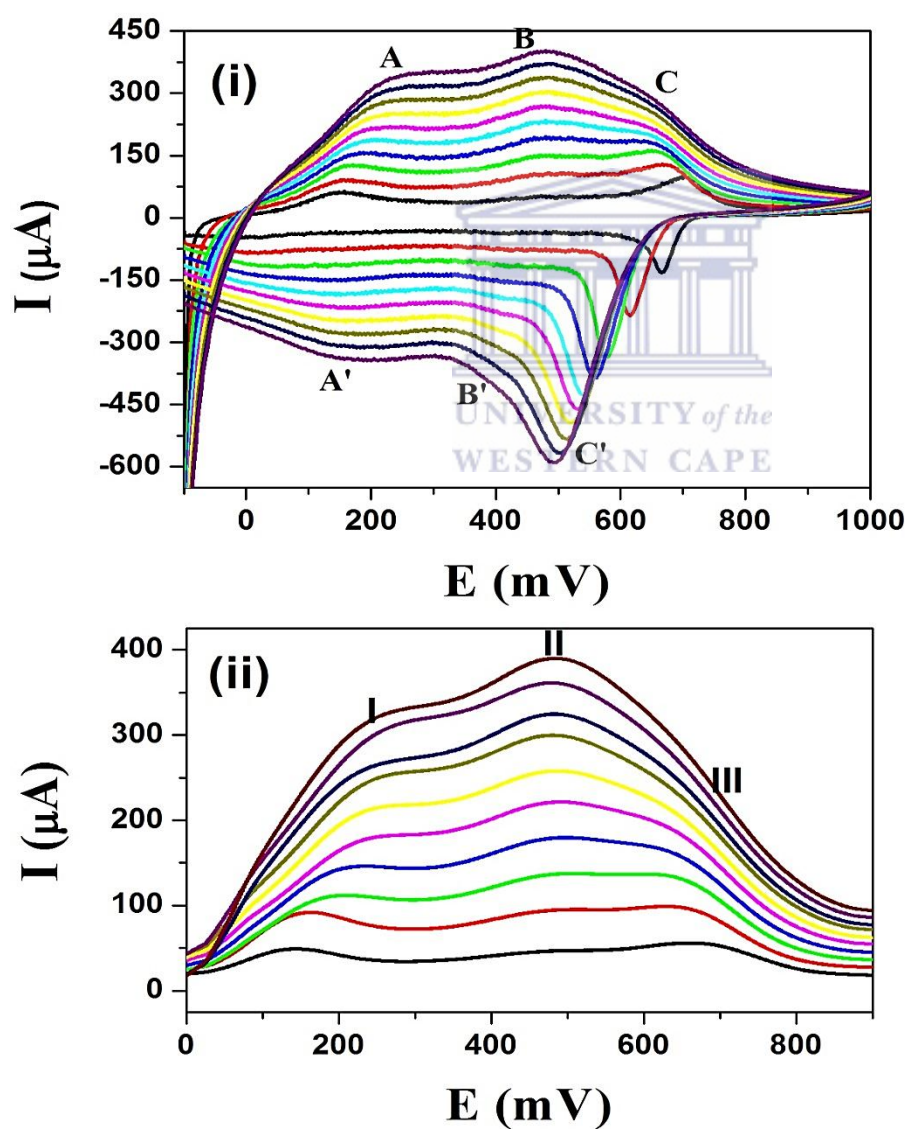
Figure 4.13: CV (i) and oxidative SW (ii) graphs of GC/PANI in 1M HCl at scan rates from 1-10 mV/s at 1 mV/s increments.

PANI shows an observable increase in peak current density with increasing scan rates. However, at higher scan rates, the peak assigned to the pernigraniline shifts cathodically and broadens until it is not observed. This means that the rate at which it gains an electron is very slow. The voltammograms correspond to a reversible system with $I_{p,a}$(peak A)/$I_{p,c}$(peak A′) value of 1.01 and $\Delta E_p = E_{p,a}$(peak A) $- E_{p,c}$(peak A′) $< 57/n$ mV which characterizes a reversible reaction. Comparable to other peaks, the peak assigned to the emeraldine state of PANI does not shift with increasing scan rates. This behaviour is characteristic of a conductive surface bound species. Therefore, the polyaniline film is a surface adsorbed species undergoing fast reversible electron transfer reaction. Of particular interest, it is observed that anodic peak currents for the emeraldine state show higher peak currents than other states which leads to a conclusion that the emeraldine state is highly oxidizable than other states.

Due to its sensitivity, SW was used to further investigate the electrochemical behaviour of PANI. The SW graph, scanned oxidatively, also reveals the three oxidation peaks. These oxidation peaks (I, II and III) are assigned to the leucoemeraldine, emeraldine and pernigraniline forms of PANI. The SW also shows higher peak currents for emeraldine as observed from the CV.

(b) PANI/MWCNT

The electrochemical properties of the nanocomposite were investigated using cyclic voltammetry (CV) and differential pulse voltammetry (DPV). The CV graph of the nanocomposite (**Figure 4.14 (I)**) also shows three redox processes corresponding to A/A′ (+260/+210 mV), B/B′ (+480/+560 mV) and C/C′ (+590/+620 mV) (vs Ag/AgCl) at lower scan rates. The redox processes to A/A′, to B/B′ and to C/C′ can be attributed to the

leucoemeraldine/leucoemeraldine radical cation, emeraldine radical cation/emeraldine and pernigraniline radical cation/pernigraniline states of PANI, respectively [105].
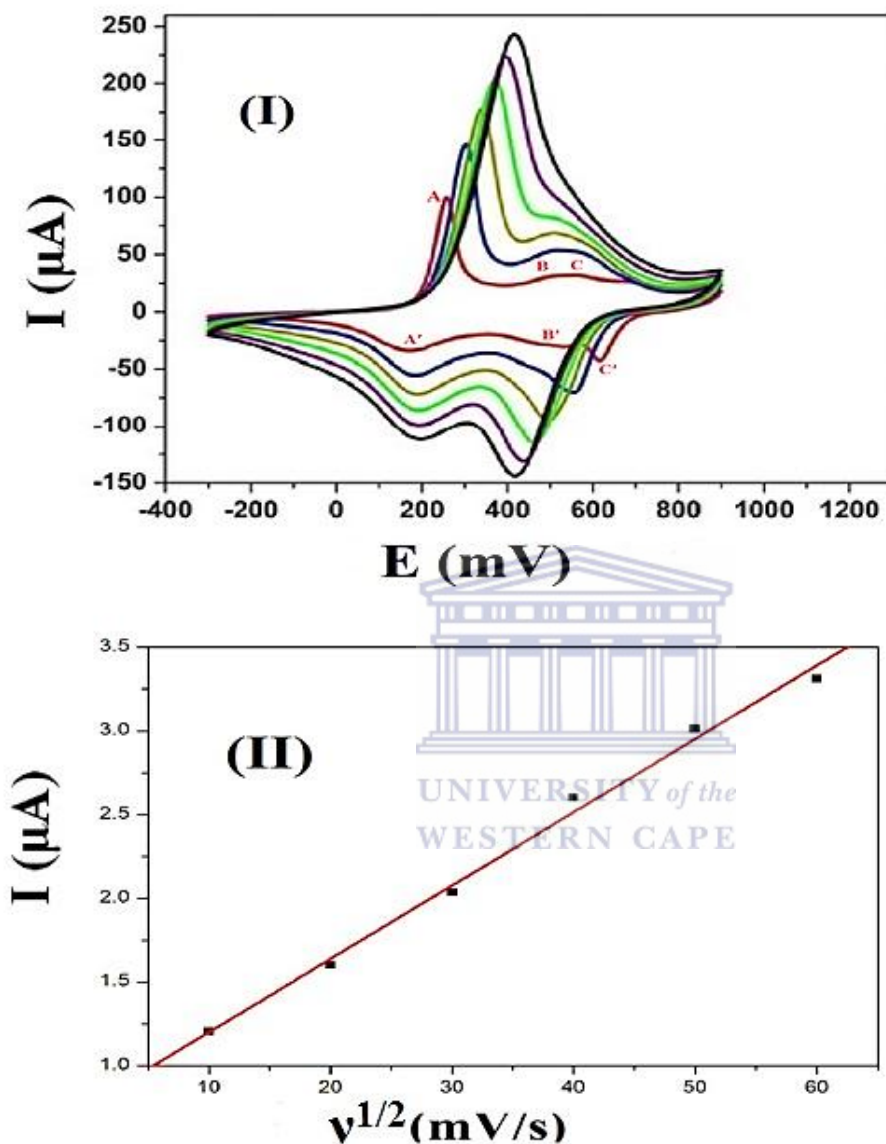

Figure 4.14: CV and Randles-Sevčik plot of PANI/MWCNT nanocomposite performed in 1 M HCl at different scan rates between 10 mV/s and 60 mV/s.

At higher scan rates, there are two redox pairs with peak C broadening out and disappearing at scan rates of 50 mV/s and 60 mV/s. It can therefore be concluded that the rate at which the pernigraniline radical cation gains an electron is very slow. The voltammograms correspond to a reversible system with $I_{p,a}$(peak A)/$I_{p,c}$(peak A′) value of 1.2 and ΔE_p =

$E_{p,a}$(peak A) – $E_{p,c}$(peak A′) < 57/n mV. These are characteristic of a surface adsorbed species undergoing fast reversible electron transfer reaction [105]. There is a distinct increase in the current density with increasing scan rates between the scan rtates of 10 mV/s and 60 mV/s. There is also an observed shift in the peak potential for redox pairs A/A′ and C/C′ which is indicative of electron hopping along the polymer chain [106]. The curve in **Figure 4.14 (II)** shows the effect of scan rate on the behaviour of the nanocomposite and the curve was used to calculate the diffusion coefficient (D_o) of the polymer nanocomposite using Randles-Sevčik equation **(Equation 2)**. The calculated value was 2.86 x 10^{-7} cm^2/s which is much higher than the diffusion coefficients of un-doped PANI [107]. This value indicated the faster movement of electrons along the polymeric platform.

$$I_p = 0.4463 \, n \, FA \left({nF}/{RT} \right)^{1/2} D^{1/2} \, v^{1/2} \, c \qquad \text{Equation 2}$$

(c) TiO₂ effect on PANI

The effect of introducing TiO$_2$ nanoparticles into PANI was evaluated using CV (**Figure 4.15**). From the graph, the TiO$_2$-doped PANI shows the three characteristic redox peaks of PANI. When compared to PANI only, the composite shows increased peak currents and a decrease in the separation between reduction and oxidation peaks. This behaviour is demonstrative of a better reversibility of the PANI composite doping with TiO$_2$ nanoparticles.
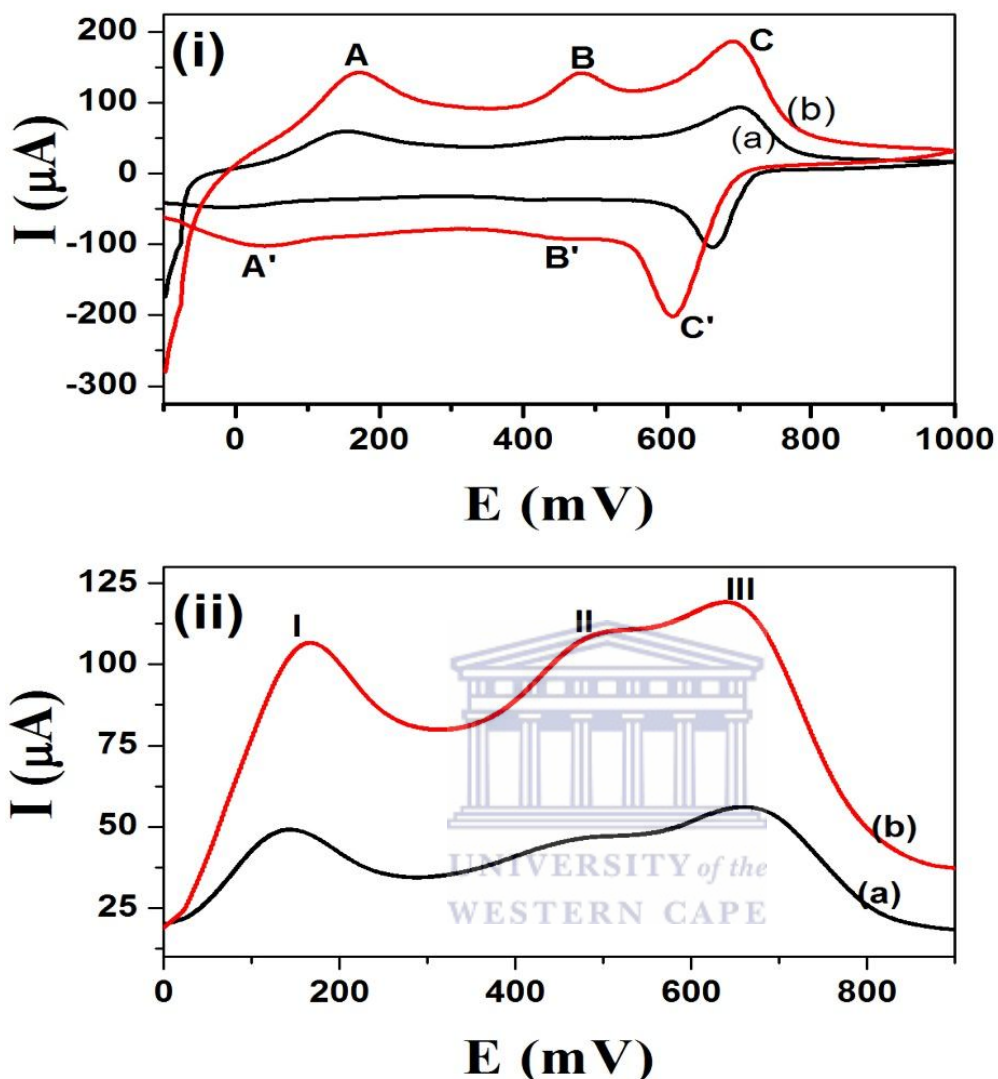
Figure 4.15: CV (i) and oxidative SW (ii) of different electrodes in 1 M HCl at 1 mV/s: (a) GC/PANI and (b) GC/PANI/TiO$_2$.

At different scan rates **(Figure 4.16),** the PANI/TiO$_2$ composite shows an increase in peaks currents with increasing scan rates at a two-fold magnitude when compared to pure PANI. Unlike PANI, the PANI/TiO$_2$ composite shows higher anodic peak currents for the leucoemeraldine state of PANI, as also observed from the SW graph. However, there is an observable potential shift as with PANI which indicates an electron hopping along the

polymer chain [108-110]. Also, the peak assigned to the emeraldine state of PANI (peak (II) in the SW graph) does not shift with increasing scan rates which is indicative of a surface bound species. Overall, it is worth notable that TiO_2 interacts well with PANI by contributing charge to its polymer backbone hence increasing its eletroactivity.
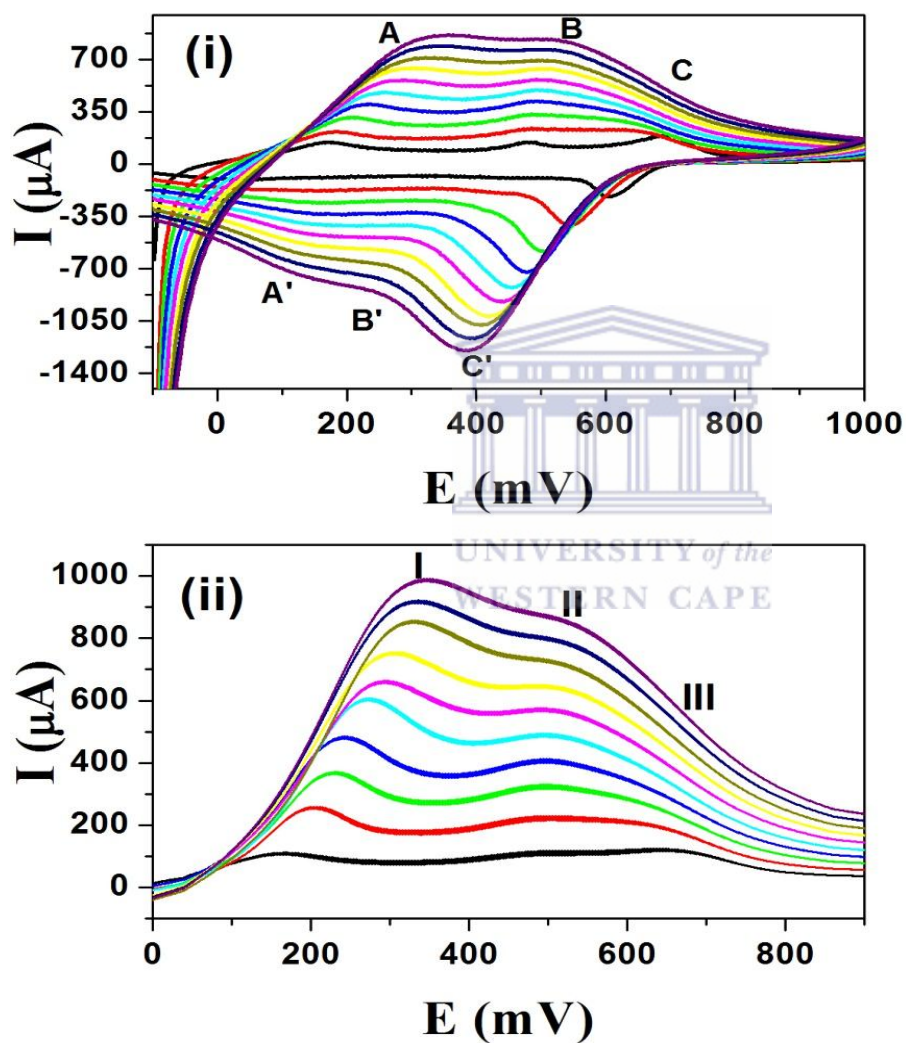
Figure 4.16: CV (i) and oxidative SW (ii) graphs of GC/PANI/TiO_2 in 1 M HCl at scan rates from 1 mV/s to 10 mV/s.

(d) PMMA effects on PANI

To clearly understand the effects of PMMA in the electroactivity, a composite comprising the two polymers was studied and compared to PANI. **Figure 4.17** shows CV and SW voltammograms comparing the PANI/PMMA composite with pure PANI. The PANI/PMMA composite also exhibits the three characteristic redox peaks of PANI with increased peak current and smaller peak separations than the pure PANI indicating higher electroactivity and faster electron hopping along the polymer backbone.
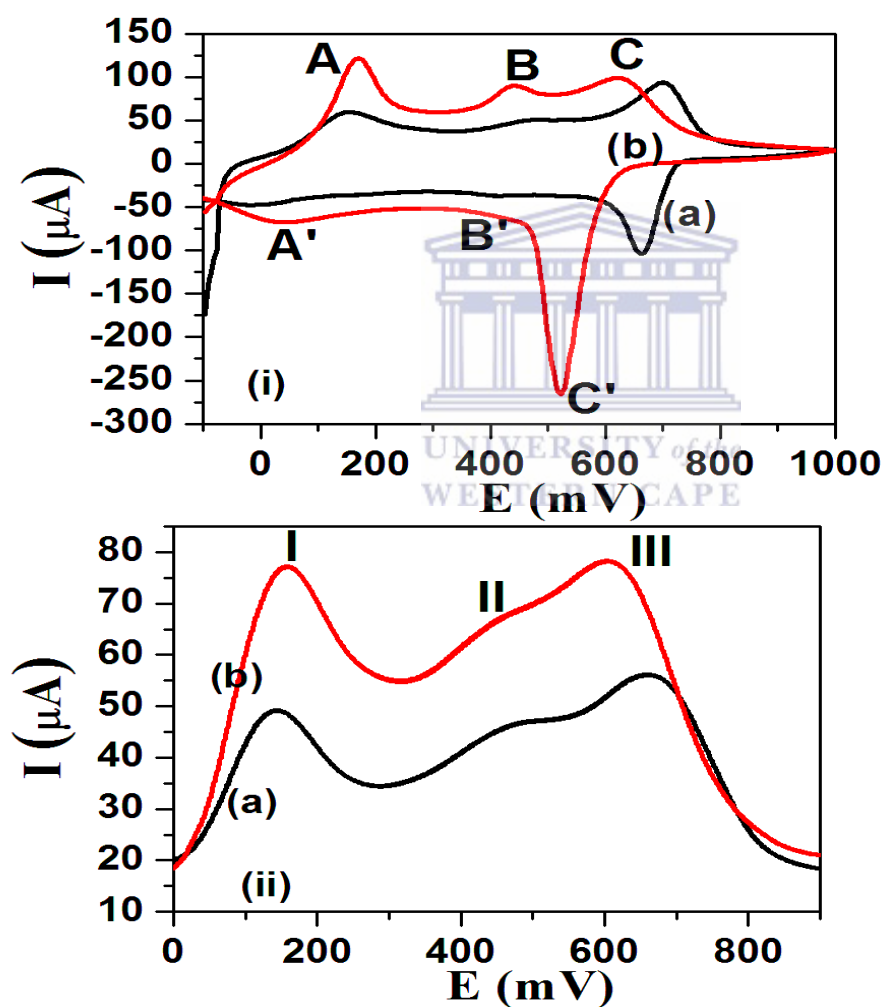
Figure 4.17: CV (i) and oxidative SW (ii) of (a) GC/PANI and (b) GC/PANI/PMMA in 1 M HCl at 1 mV/s.

As observed with PANI and the PANI/TiO$_2$ composite, the PANI/PMMA composite shows increasing peak currents with increasing scan rates (see **Figure 4.18).** This indicates that the polymeric composite is surface bound to the electrode surface [111]. The exhibited stability (no potential shift) of the peak assigned to the emeraldine form of PANI, irrespective of scan rate, indicates the surface bound polymer composite.
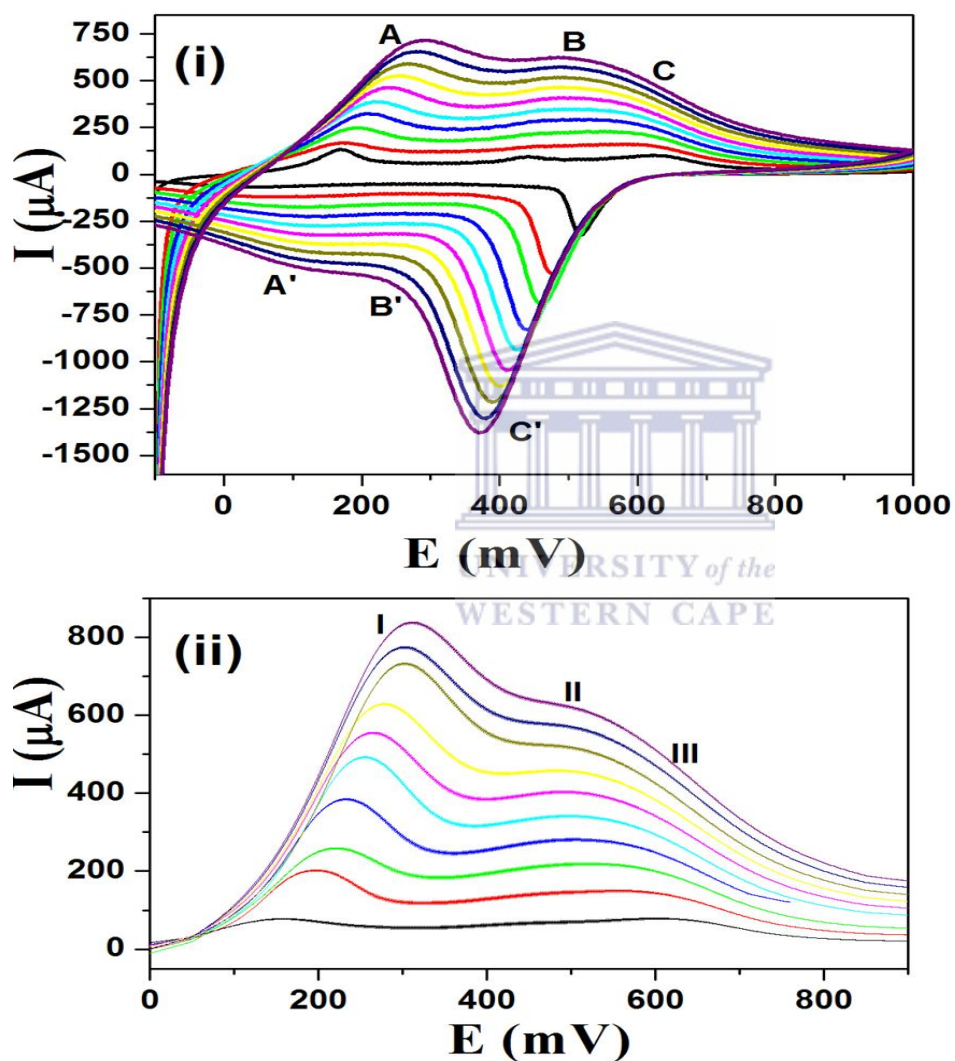
Figure 4.18: CV (i) and oxidative SW (ii) graphs of GC/PANI/PMMA composite in 1 M HCl at different scan rates between 1 mV/s and 10 mV/s at increments of 1 mV/s.

With reference to the PANI/PMMA and PANI/TiO$_2$, it is noteworthy that the TiO$_2$ and PMMA have similar effect on the structural backbone of PANI. When compared to PANI,

both the PANI/TiO$_2$ and PANI/PMMA composites show higher peak currents for the leucoemeraldine form with a two-fold magnitude. This behaviour has also been observed during UV-Vis analysis where both the PANI/PMMA and PANI/TiO$_2$ composites exhibited similar absorption bands but at different wavelengths from PANI. This suggests that there are strong interactions between these dopants and PANI.

(e) PANI/PMMA/TiO$_2$ nanocomposite

The main component of the transducer element in this study is the nanocomposite fabricated onto a glassy carbon electrode. Its electrochemical behaviour was evaluated using CV and SW and was compared to the composites discussed earlier. **Figure 4.19** shows the CV and SW voltammograms of the nanocomposite compared to PANI/TiO$_2$ and PANI/PMMA.
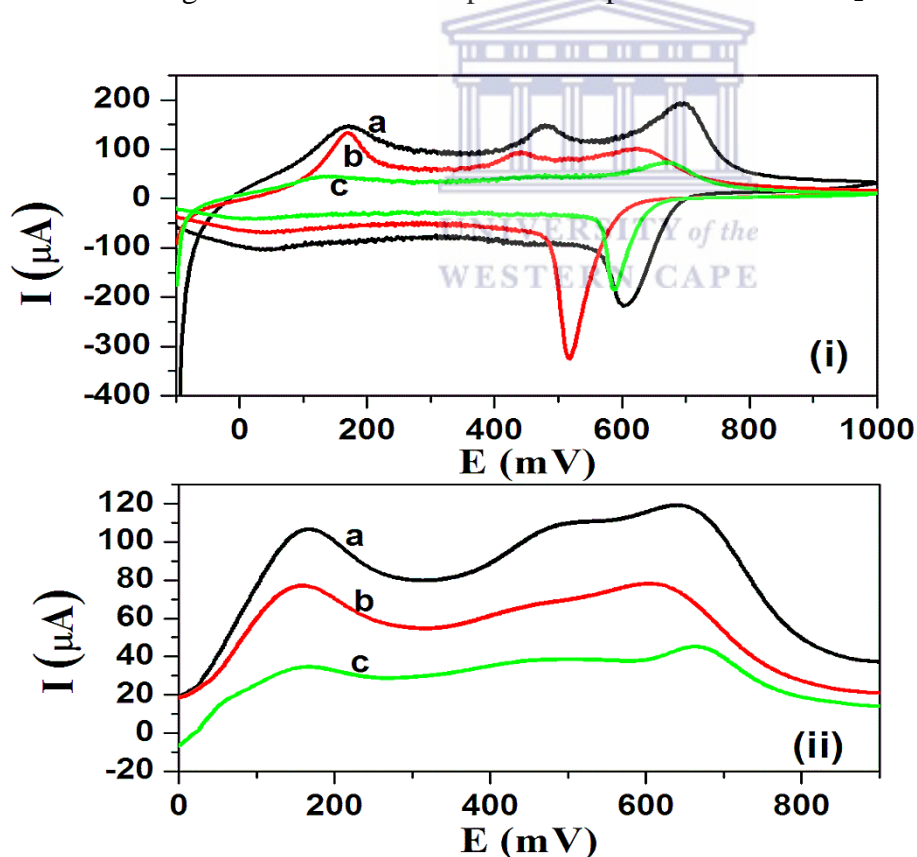
Figure 4.19: CV (i) and oxidative SW (ii) voltammograms different composites. Experiments were run in 1 M HCl at 1 mV/s: (a) GC/PANI/TiO$_2$ (b) GC/PANI/PMMA and (c) GC/PANI/PMMA/TiO$_2$.

From both the CV and SW graphs, the nanocomposite shows lower peak currents than both the PANI/PMMA and PANI/TiO$_2$ composites. This is attributed to the increased distance for an electron to travel between the electrode surface and the polymeric platform. However, the peak separations for the nanocomposite are smaller than for pure PANI, which means better reversibility attributed to the introduction of PMMA and TiO$_2$ into the PANI backbone. Also, of interesting behaviour, the oxidation peaks assigned to the leucoemeraldine and emeraldine forms of PANI show peak currents at almost the same magnitude as opposed to the PANI/PMMA and PANI/TiO$_2$ which show enhanced peak currents for leucoemeraldine than other peaks.
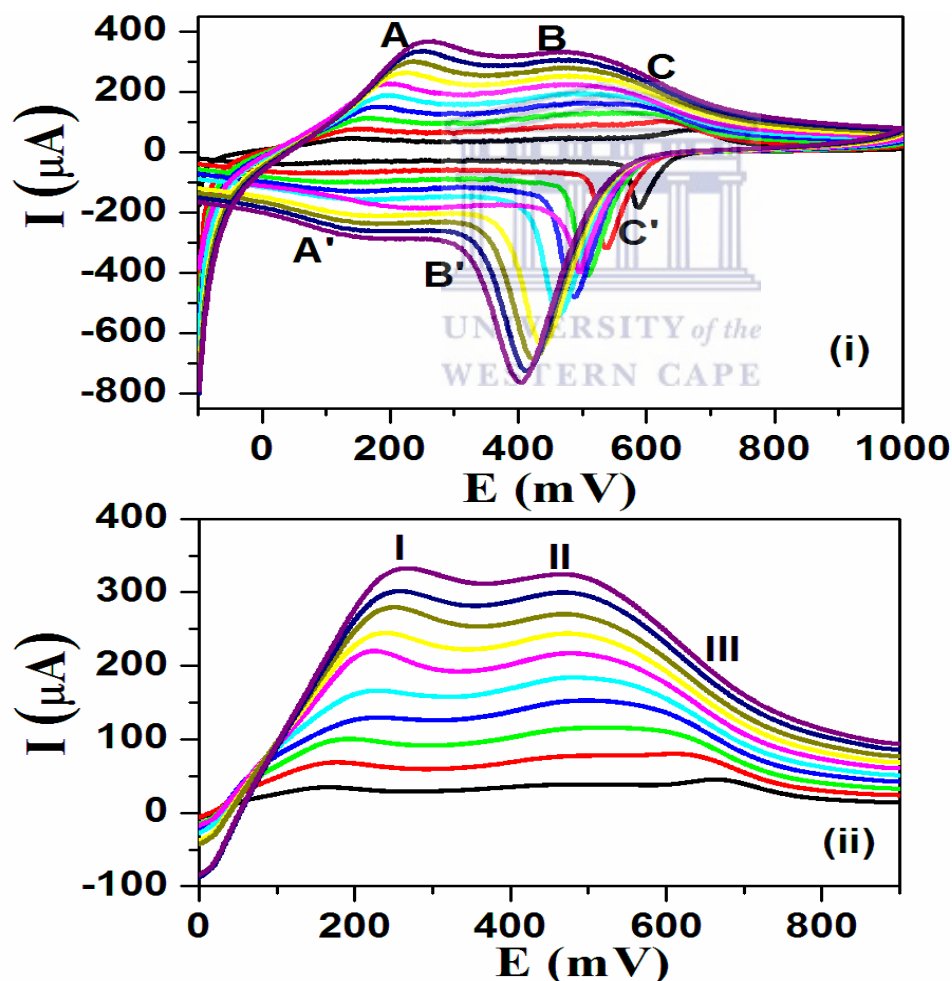
Figure 4.20: CV (i) and oxidative SW (ii) voltammograms of GC/PANI/PMMA/TiO$_2$ in 1 M HCl at scan rates from 1 mV/s to 10 mV/s in increments of 1 mV/s.

The multiscan CV and SW results of the nanocomposite modified glassy carbon electrode are shown in **Figure 4.20**. The nanocomposite behaves in a similar way as the individual PANI composites by showing anodic and cathodic potential shifts which indicate electron hopping along the backbone of the polymeric nanocomposite [106]. The dependence of current on the scan rate is shown in **Figure 4.21**. It is notable from the graphs that the nanocomposite also showed an increase in the magnitudes of the peak currents upon increases in scan rate suggesting that the peak currents are diffusion controlled. However, the nanocomposite shows reversible electrode reactions at lower scan rates (1-5 mV/s) characterized by unity values of cathodic to anodic peak ratios (I_{pc}/I_{pa}), while it shows quasi-reversible behaviour at higher scan rates (1-10 mV/s). The diffusion coefficient (D_o) of the nanocomposite was calculated to be 2.156 x 10^{-7} cm^2/s.
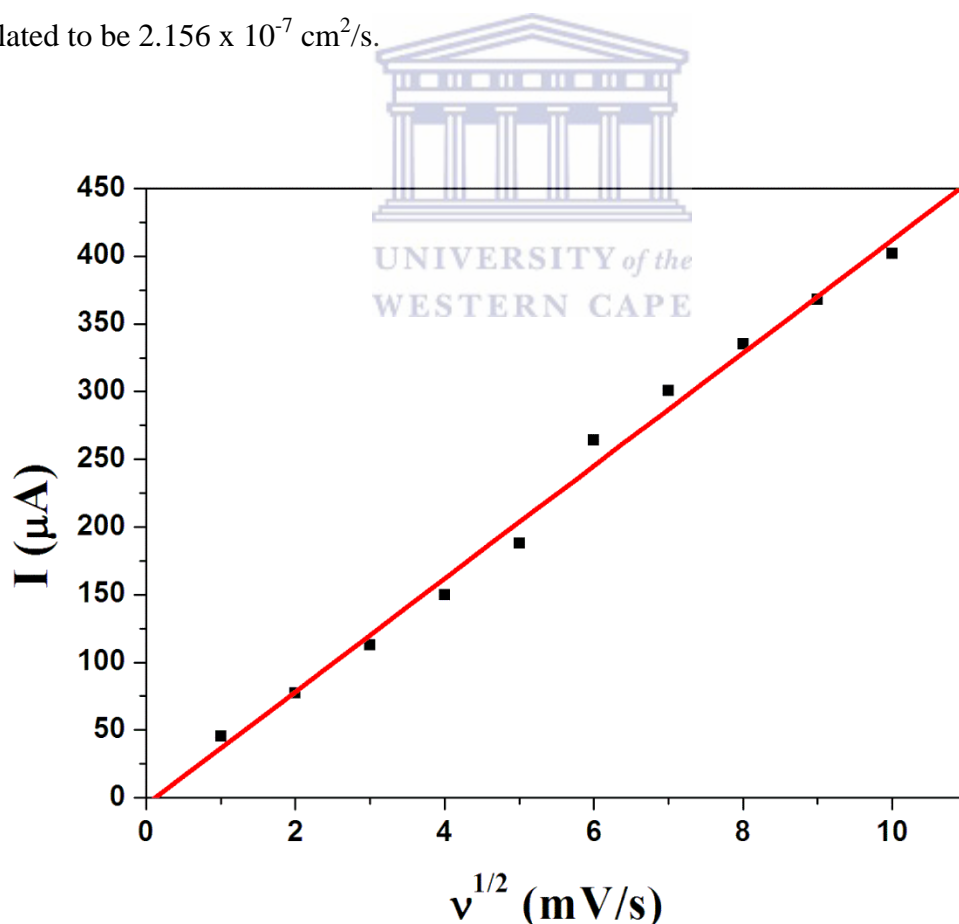
Figure 4.21: The Randles-Sevčik plot of the PANI/PMMA/TiO$_2$ nanocomposite.

Comparable to the individual PANI composites, the nanocomposite shows higher peak currents with increasing scan rates for both the leucoemeraldine and emeraldine forms of PANI. This means that the TiO_2 and PMMA increase the charge on PANI and therefore the nanocomposite shows smaller peak separations and better electroactivity than pure PANI.

UNIVERSITY *of the*
WESTERN CAPE

CHARACTERIZATION OF THE CYP2E1 NANOBIOSENSOR AND DETECTION OF PZA

Summary

This chapter outlines and discusses the results obtained for the study based on developing the nanobiosensor for detection of pyrazinamide. The chapter deals specifically with the characterization of the structural, morphological, optical and electrochemical properties of the nanobiosensor and the detection of PZA using the biosensor.

5.1. Characterization of the biosensor.

5.1.1. AFM analysis.

The surface of the biosensor exhibits a morphology which exhibits forms from both PANI and PANI/MWCNTs. This is indicative of the fact that the chemical modification of CYP2E1 did not drastically alter the morphology of the polymeric platform.
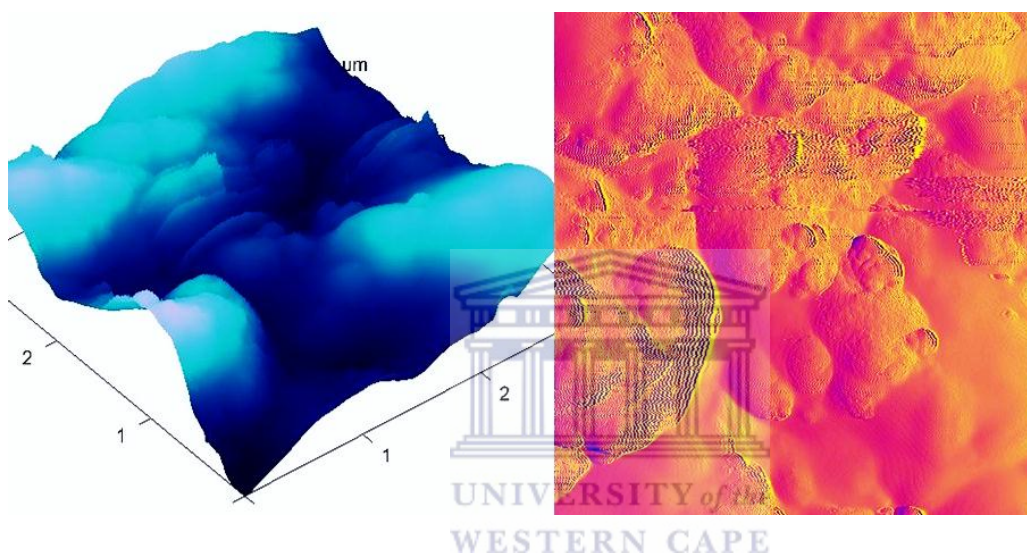
Figure 5.1: AFM image of PANI/MWCNTs/CYP2E1.

However, there is an observable increase in the roughness of the surface, which is attributed to the bulkiness of the enzyme. This is an indication that the enzyme has been successfully attached onto the composite material.

5.1.2. Electrochemical properties

The electrochemical activity of the CYP2E1 nanobiosensor was evaluated using CV and DPV which are represented in figure. From the CV, the nanobiosensor exhibits one redox pair centred at +50 mV and -82 mV (vs Ag/AgCl). This pair was attributed to the Fe^{3+}/Fe^{2+} transitions of the CYP2E1 active site. Heme proteins exhibit different formal potentials which are attributed to the effect of different system configurations and different

microenvironments on the direct electron transfer [107]. For the CYP2E1-based biosensor, the calculated formal potential was 66 mV (vs Ag/AgCl). The symmetry shown by the DPV confirms the surface confined species on the electrode.
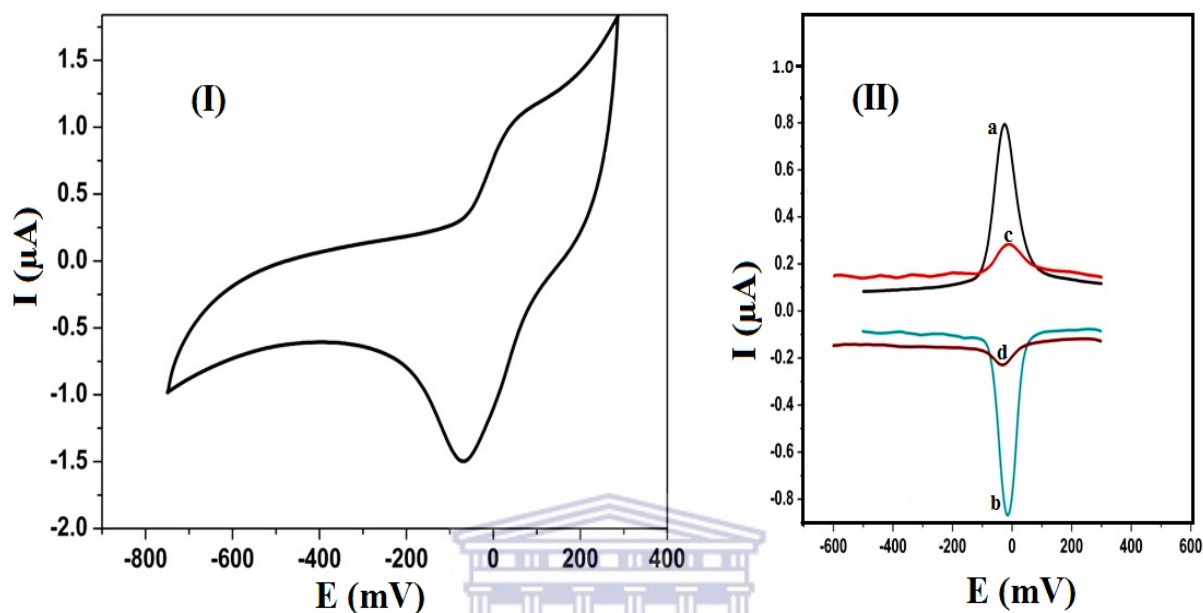
Figure 5.2: (I) CV of PANI/MWCNTs/CYP2E1 at 20 mV/s and (II) DPV of the PANI/MWCNTs (a and b) and PANI/MWCNTs/CYP2E1 (c and d) in PB pH 7.5.

5.2. Electrocatalytic detection of PZA

The most important aspect of the study, detection of PZA, was interrogated using SW. The necessity of oxygen during the enzymatic reaction was also investigated using CV. **Figure 5.3** illustrates the cyclic voltammetric responses of the PANI/MWCNTs/CYP2E1 nanobiosensor in the absence and presence of PZA at a potential scan rate of 20 mV/s.

63
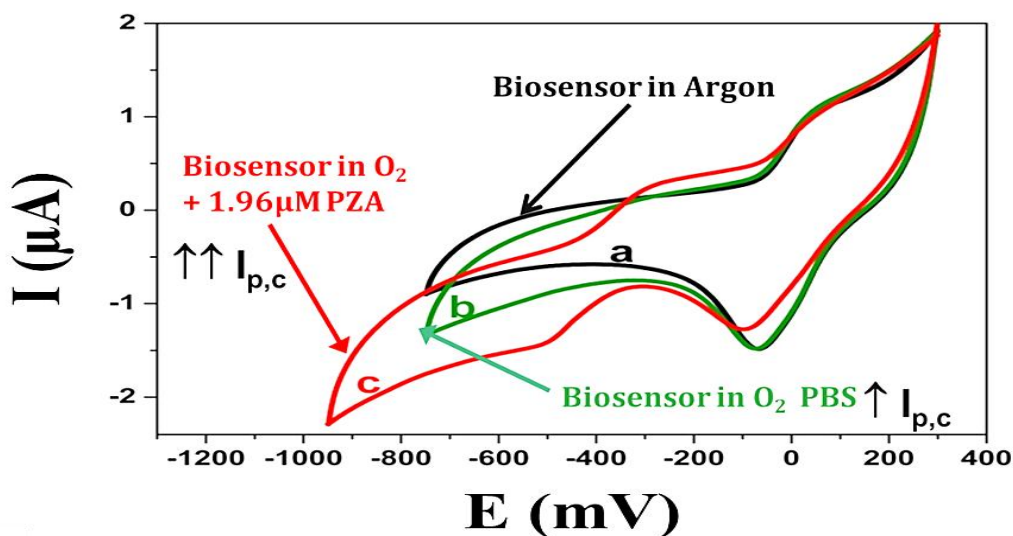
Figure 5.3: CV graphs of GC/PANI/MWCNT/CYP2E1 nanobiosensor for different systems.

The cyclic voltammograms obtained in the absence of PYR were performed in anaerobic and aerobic solutions. In the presence of oxygen, the biosensor showed an increase in the cathodic peak current with an onset potential of -160 mV (vs Ag/AgCl) which is indicative of the oxygenation of CYP2E1 heme Fe atom being coupled to the electron transfer reaction that occurs in argon degassed medium represented by the voltammogram á'. Then, in the presence of 1.96 μM PZA, there was development of a large cathodic catalytic wave with a peak at -490 mV (vs Ag/AgCl). This behaviour was only observed for the biosensor in the presence of PZA. Voltammogram 'c' consists of a shift of the electron transfer cathodic peak potential from ($E_{p,c}$) from -25 mV (vs A/AgCl) in argon medium to -50 mV(vs Ag/AgCl) in oxygenated PZA solution. This implies that the electron transfer at the GCE/PANI/MWCNT/CYP2E1 electrode that occurred at -25 mV (vs Ag/Ag/Cl) was followed by

(i) the binding of PZA to CYP2E1 that shifts the $E_{p,c}$ to -50 mV (vs Ag/AgCl),

(ii) the oxygenation (binding of O_2) of PZA-CYP2E1 at -160 mV (vs Ag/AgCl) and

(iii) the reduction of PZA-CYP2E1-O_2 starting at an onset potential of -300 mV reaching a peak at -490 mV (vs Ag/AgCl). This result is in agreement with the mechanism for metabolic reaction of cytochrome P450 (haemolytic) enzymes [110].

Figure 5.4 is the plot of the square wave voltammograms (SWVs) of the biosensor response to PZA. After the first addition, a catalytic current response resulting from the reduction peak of PZA was observed at -460 mV (vs Ag/AgCl). The reduction peak current was observed to increase with increasing concentrations of PZA**.** This behaviour is attributed to the coupling of the fast electron transfer at the electrode surface with the reduction of PZA on or within the biosensor film [111]. The increase in current is proportional to the amount of the analyte. There was also an observed anodic shift in the peak potential which is attributed [111] to the ease of reduction of the CYP2E1 heme Fe from Fe^{3+} to $Fe^{2+,}$ brought about by the PZA-induced conversion of low spin Fe^{3+} to high spin $Fe3^{+}$ (the latter being easier to reduce to Fe^{2+} that preferentially binds O_2).
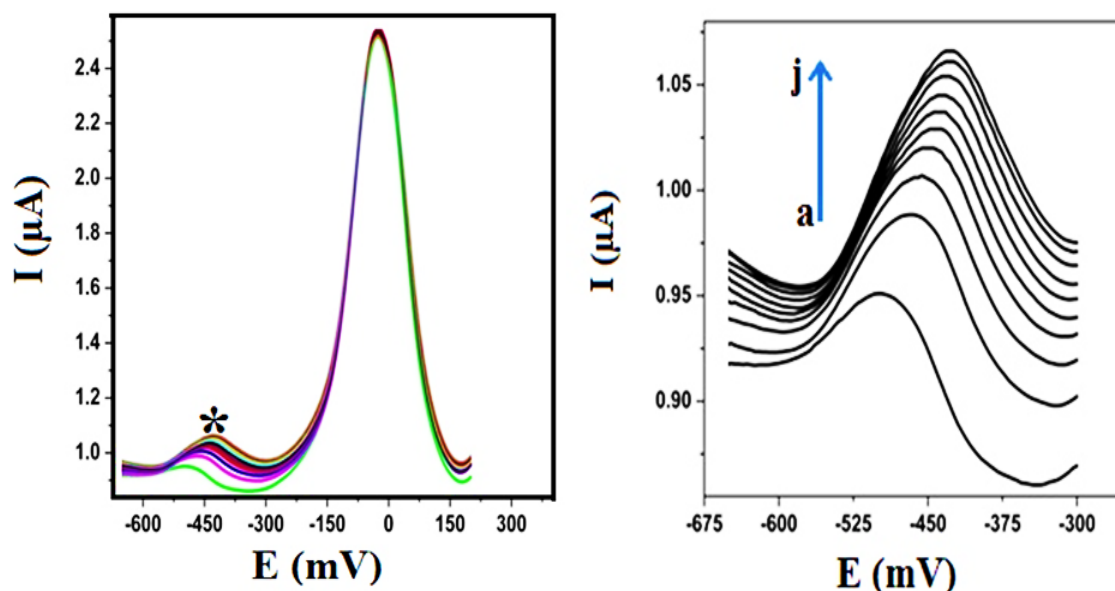
Figure 5.4*:* SW response of the GC/PANI/MWCNTs/CYP2E1 nanobiosensor to PZA concentrations (left), with the reduction peak of PZA shown by a star. SW graph on the right is a magnified view of the reduction process.

The peak currents calculated from the SWVs of **Figure 5.4** zoomed area (right) have a linear relationship with PZA concentrations, as shown in **Figure 4.9,** with a dynamic linear range (DLR) of 0.04 – 1.30 mM PZA (i.e. 4.92 – 160 ng/mL PZA). The sensitivity of the nanobiosensor is 0.96 µA/µM (i.e. 7.80 µA/µg mL^{-1} PZA). The limit of detection (LOD) of 500 mg formulation of PZA analysed by liquid chromatography (LC) is 40 ng/mL [112].
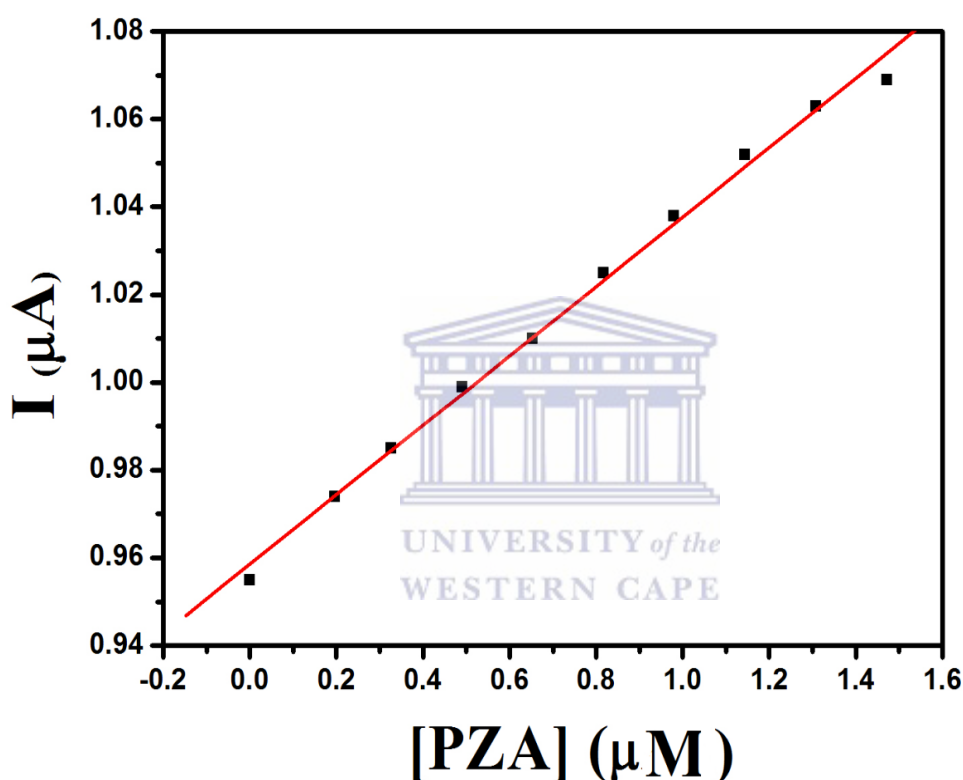
Figure 5.4: Calibration plot for the PZA nanobiosensor.

5.3. Mechanism of PZA metabolism

The mechanism through which the biosensor catalytically reduces PZA is shown in **Scheme 2.** The first step is the binding of PZA into the active site of CYP2E1 which is in the ferric resting state. An electron from the nanocomposite modified electrode reduces the enzyme to the ferrous state which then binds to molecular oxygen. During this stage, PZA is hydroxylated to 5-hydroxypyrazinamide. This is followed by the O-O bond cleavage by the

introduction of the second electron resulting in a highly active iron-oxoferryl intermediate CYP2E1 (Fe^{4+}) with 5-hydroxypyrazinoic acid as the product which is released. From the graph, the compounds $RONH_2$, R-O-OH-HN_2 and R-OH-O-OH respectively refer to pyrazinamide, 5-hydroxypyrazinamide and 5-hydroxypyrazinoic acid whose structures are shown in **Figure 5.5.**
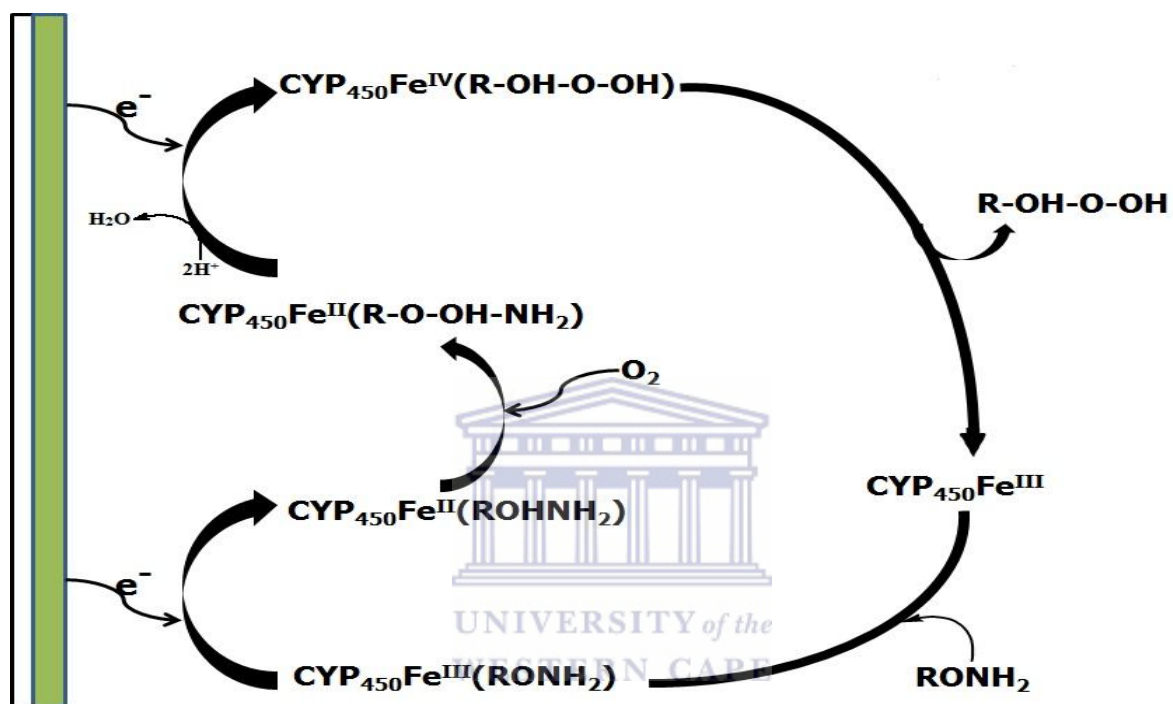
Scheme 2: The proposed mechanism for PZA reduction using the CYP2E1 based nanobiosensor.

Figure 5.5: The structures of PZA and its metabolites.

The detection limit of the nanobiosensor falls within the DLR of the GC/PANI/MWCNT/CYP2E1 nanobiosensor. However, from the LC analysis of human blood [112], the peak concentration (C_{max}) of PZA determined 2 h after drug intake is 3.44 – 4.09 mg/mL, which is very detectable with the nanobiosensor due to its high sensitivity (current).

CHAPTER 6

CHARACTERIZATION OF MnP NANOBIOSENSOR AND DETECTION OF BPA

Summary

This chapter is focussed on the characterization of the MnP-based nanobiosensor. The electrochemical behaviour of the nanobiosensor is compared to that of the nanocomposite and MnP at the GC electrode. Most importantly, the response of the nanobiosensor to different systems (presence and absence of BPA) is evaluated. . For comparison, the detection limit obtained for the nanobiosensor is compared to other results postulated in other studies in literature.

6.1 Electrochemical characterization of the biosensor.

The electrochemical behaviour of the biosensor was evaluated using CV and SW. For comparison, the nanocomposite was also characterized in the 0.1 M PB, pH = 7.4 solution. The main aspect was to observe electroactivity changes before and after enzyme immobilization onto the polymeric platform and therefore the behaviour of the nanobiosensor was compared to that of the nanocomposite and the pure enzyme alone. From **Figure 6.1(II),** the bare glassy carbon electrode does not show any peak while the enzyme modified electrode (denoted as GC/MnP) shows two reduction peaks (I and II) and one oxidation peak (II′). These redox pair (II/II′) is attributed to the Fe^{3+}/Fe^{2+} electron transitions of the enzyme active site while peak I is assigned to the reduction of manganese. The nanobiosensor (denoted by GC/PANI/PMMA/TiO$_2$/MnP) shows the redox pair of peaks (III′/III′) and peak III assigned to the Fe^{3+}/Fe^{2+} electron transitions of the enzyme active site while peak I is assigned to the reduction of manganese. The nanobiosensor system shows peaks with enhanced current density when compared to the enzyme modified electrode.
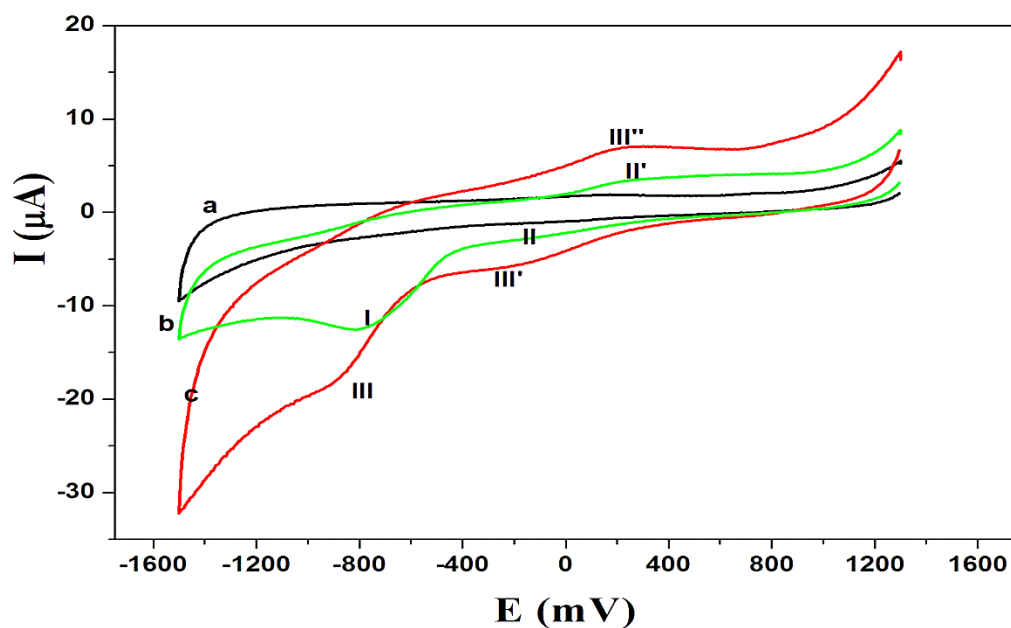
Figure 6.1: Cyclic voltammograms of different electrode systems in 0.1 M PB solution, pH 7.4 at 50 mV/s. (a) bare electrode, (b) GC/MnP and (c) MnP nanobiosensor (II c).

As seen from the voltammograms in **Figure 6.2**, as the scan rates increased the peak amplitudes also increased, indicating that the electrochemical behaviour of the MnP-based nanobiosensor is a surface controlled process. On the other hand, a slight shift in the potential is observed illustrating that the PANI/PMMA/TiO_2 nanocomposite has not lost its conductivity and electro-activity upon enzyme immobilization [103, 104]. Most importantly the potential shifts with varying scan rates indicate that the presence of the enzyme enhances the electron transfer transportation between its active site and the electrode.
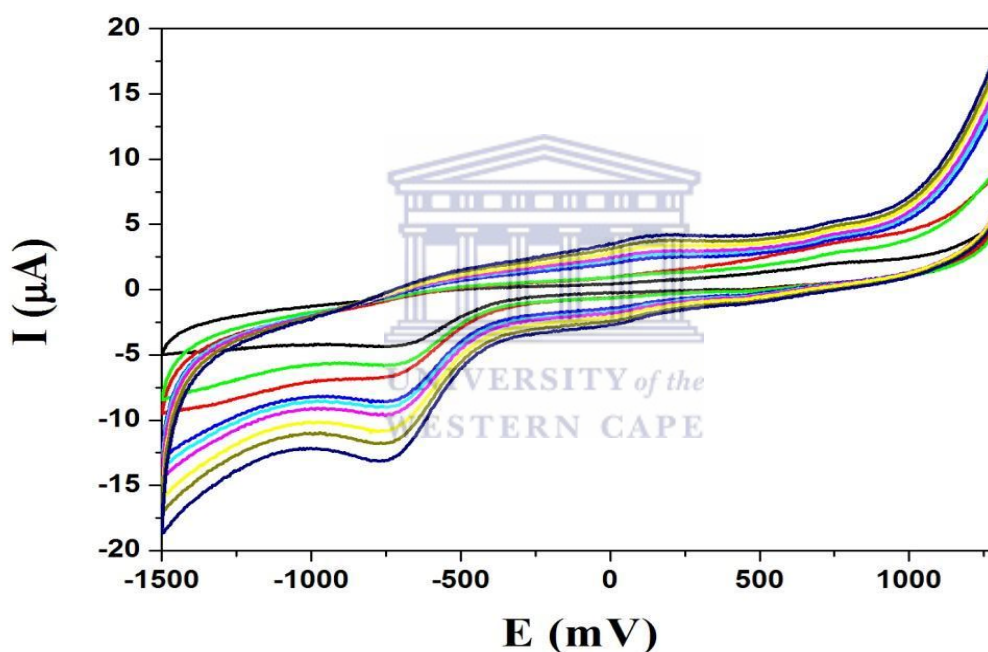
Figure 6.2: CV of the nanobiosensor at different scan rates between 20 mV/s and 100 mV/s in 0.1 M PB solution, pH 7.4.

The surface coverage concentration of the nanobiosensor was also found to be 1.36 x 10^{-5} mol cm^{-2}. The high surface concentration is attributed to the presence of TiO_2 nanoparticles in the nanocomposite and the combined effects of the individual components which led to a nanometer sized composite [105]. The diffusion coefficient was calculated to be 1.97 x 10^{-6} cm^2/s which is indicative of a faster electron transfer.

6.2. The catalytic response of the MnP nanobiosensor to BPA

To clearly observe if the nanobiosensor detected BPA, it was characterized in the presence and absence of BPA. **Figure 6.3** shows cyclic voltammograms of the nanobiosensor in the presence and absence of BPA. It is clearly observed that after addition of 0.04 nM BPA into the cell solution, there appeared a peak around 750 mV (peak III) (vs Ag/AgCl). This peak is assigned to the oxidation of BPA into its metabolites. The peaks I and II/II′ are assigned as before, to the reduction of manganese and the electronic transitions of Fe^{3+}/Fe^{2+} of the heme.
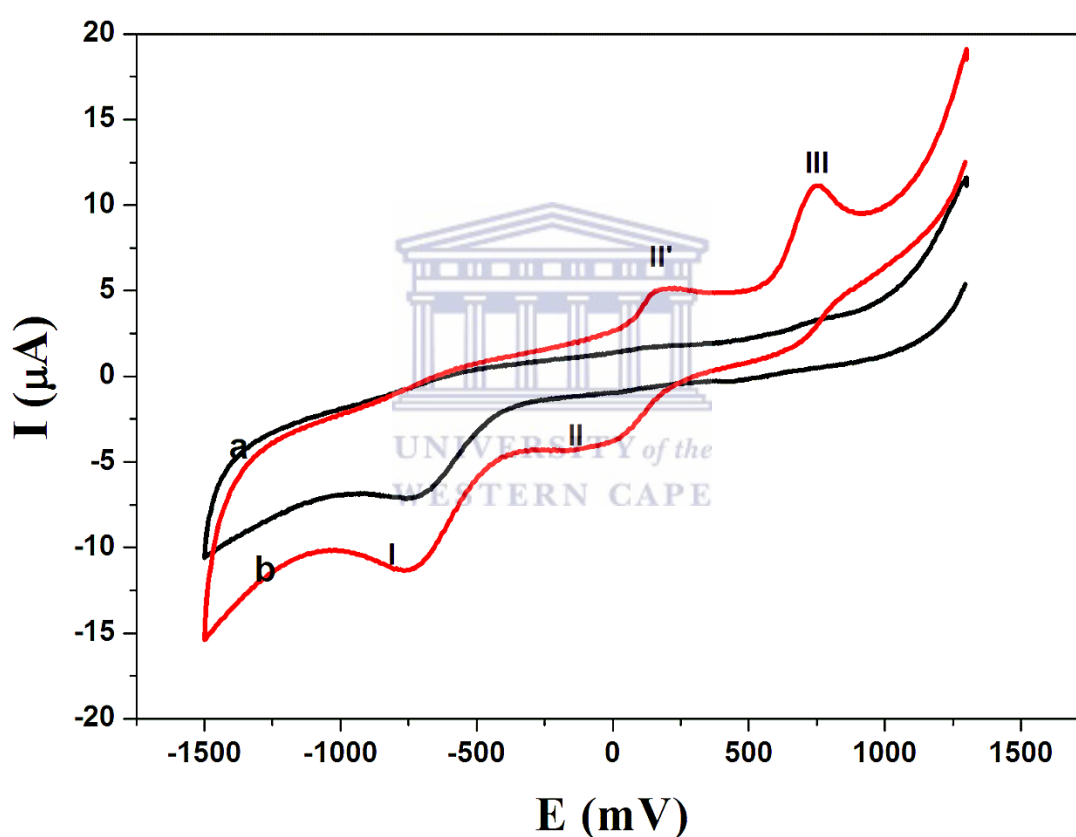
Figure 6.3: cyclic voltammogram of the nanobiosensor for different systems at 50 mV/s. Experiments were performed in the absence (a) and presence (b) of 0.04 nM PZA.

This behaviour was further corroborated using SW which was run both oxidatively and reductively. The SW graphs **(Figure 6.4)** show symmetry with the oxidation peak of BPA around 750 mV (vs Ag/AgCl) still evident.
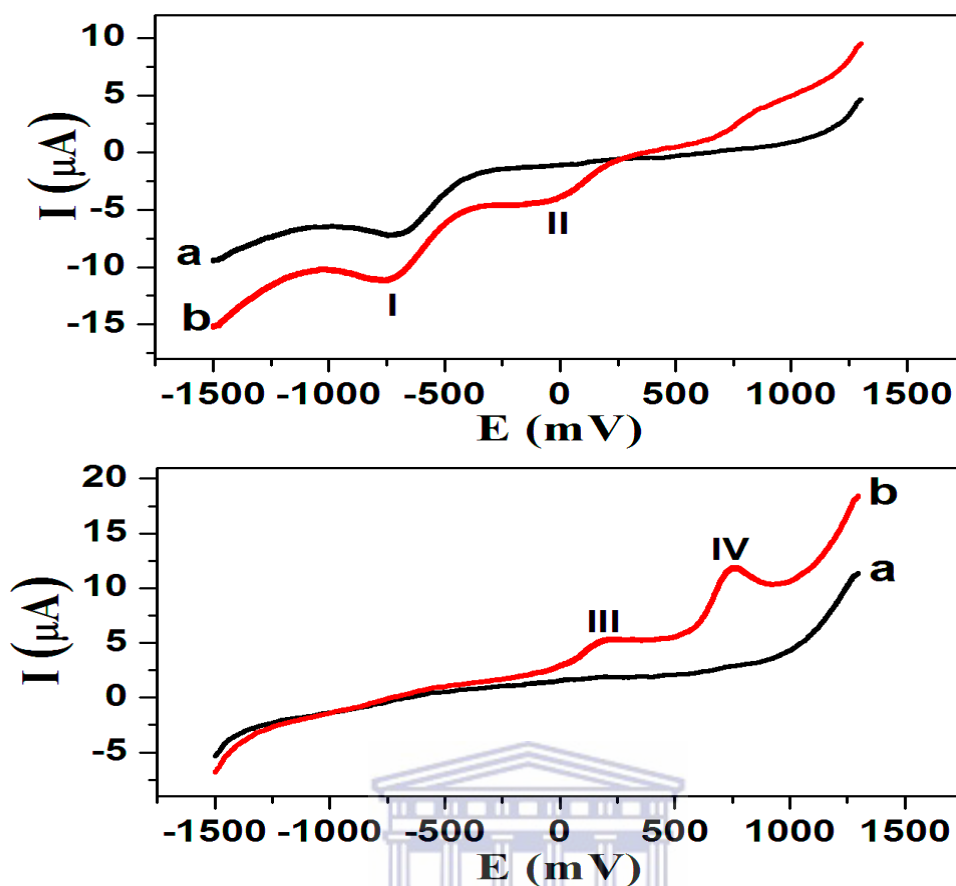
Figure 6.4: Reductive (top) and oxidative (bottom) SW graphs of the nanobiosensor for different systems at 50 mV/s: (a) 0 nM BPA and (b) 0.04 nM PZA. Experiments were scanned reductively (left) and oxidatively (right). Peak IV is assigned to the oxidation of BPA.

After introduction of BPA into the system, it was observed that the biosensor can oxidize BPA. The electrocatalytic response of the biosensor was then evaluated against increasing concentrations of BPA **(see Figure 6.5)**. With reference to the peak assigned to BPA oxidation, the CV graph shows an increase in peak currents with increasing BPA concentrations.
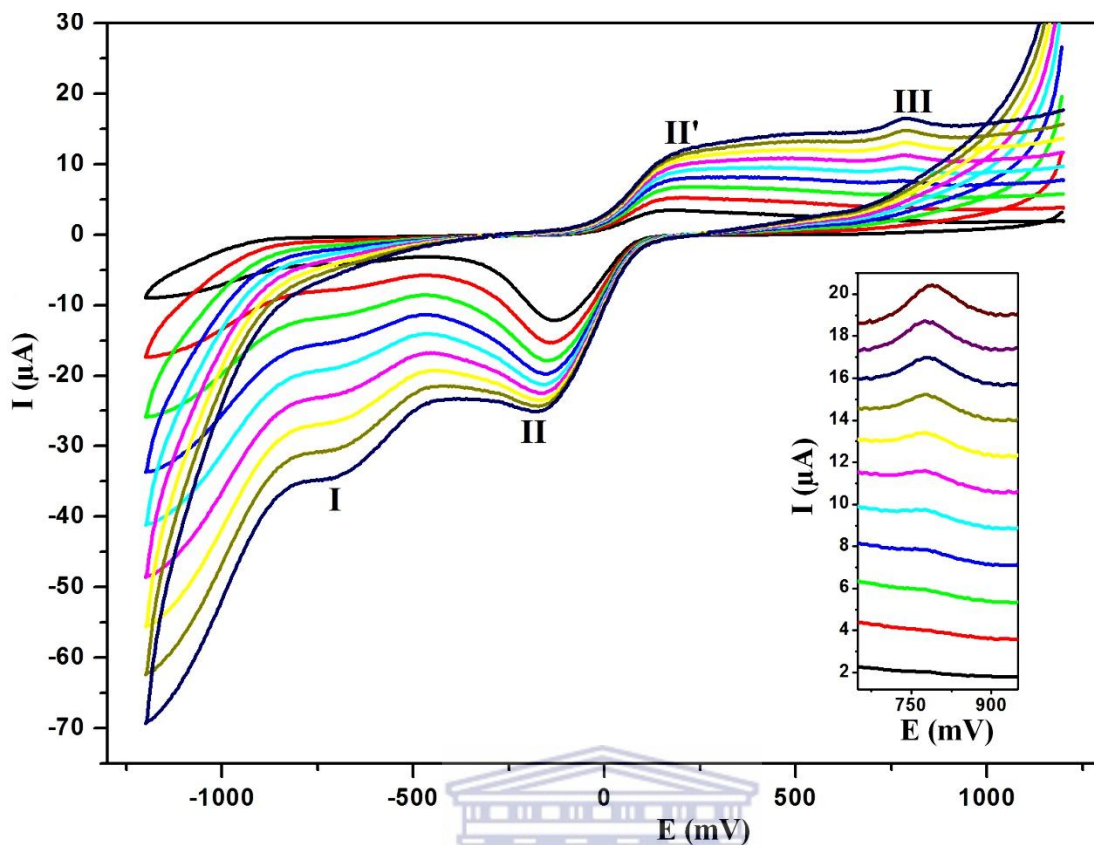
Figure 6.5: CV of the nanobiosensor to increasing PZA concentrations at 50 mV/s. Insert is a magnified view of the process at peak III, assigned to the oxidation process of BPA.

The SW was also used to confirm the behaviour observed when using CV. The SW also reveals two oxidation peaks and an increase in peak currents with increasing BPA concentrations. According to literature, the peak current is proportional to the concentration of the analyte. A calibration curve for the PZA detection was plotted and used to estimate the limit of detection and sensitivity of the nanobiosensor towards BPA. These values were calculated to be 0.12 nM and 0.3 µA/nM. The biosensor has a DLR of 0.2 nM – 1.2 nM.
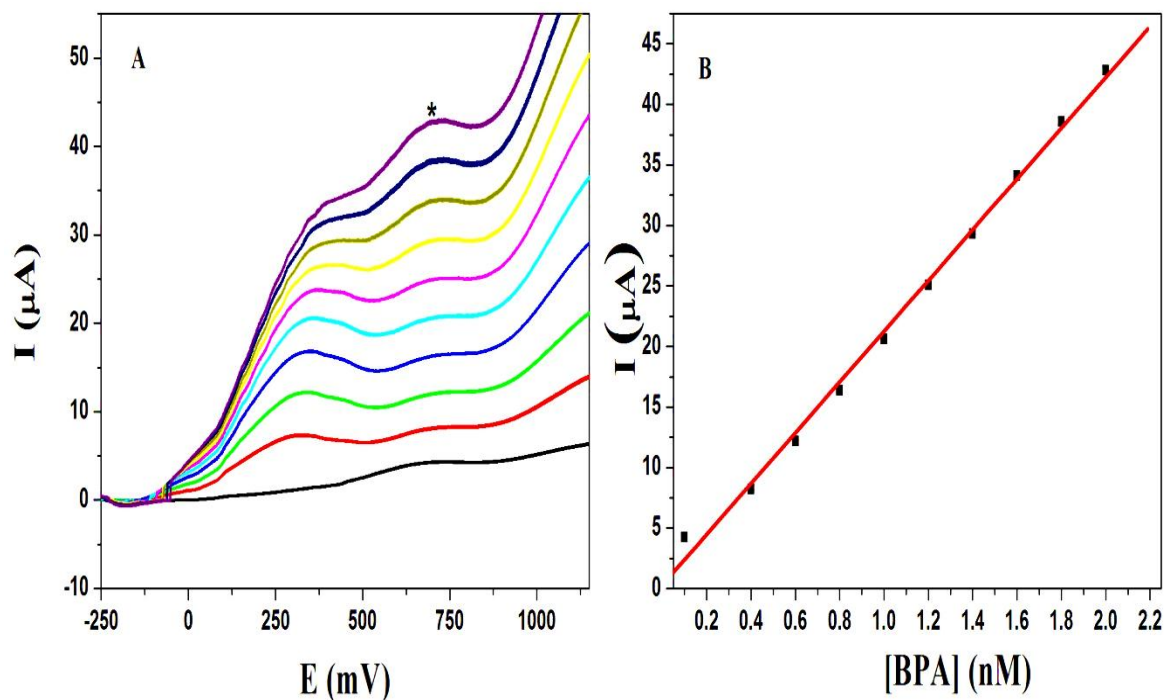
Figure 6.6: (A) SW of the nanobiosensor response to increasing PZA concentrations at 50 mV/s. The peak assigned to oxidation of BPA is marked by a star. (B) The calibration curve for the catalytic oxidation of BPA by the biosensor.

6.3 The mechanism of BPA oxidation

The mechanism proceeds via the binding of BPA into the active site of MnP. An electron donated by BPA to MnP reduces the enzyme Mn(III) to Mn(II), while an electron shuttled from the electrode through the conductive nanocomposite reduces the ferric enzyme state to ferrous state of the active site. The formed hydroxylated BPA is sequentially oxidized into a quinone metabolite.
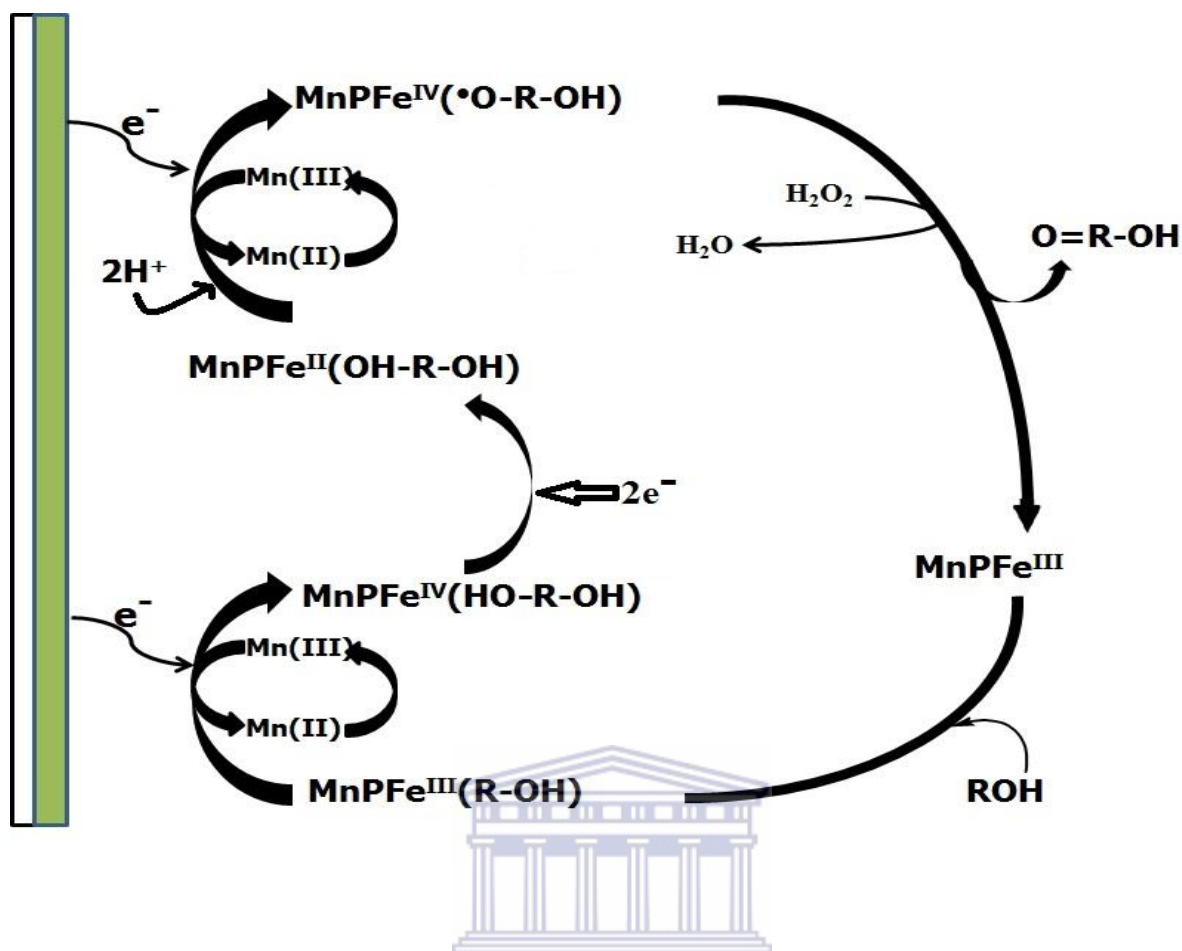
Scheme 3: The proposed mechanism for the oxidation of BPA.

Bisphenol A

5-hydroxybisphenol

bisphenol-O-quinone
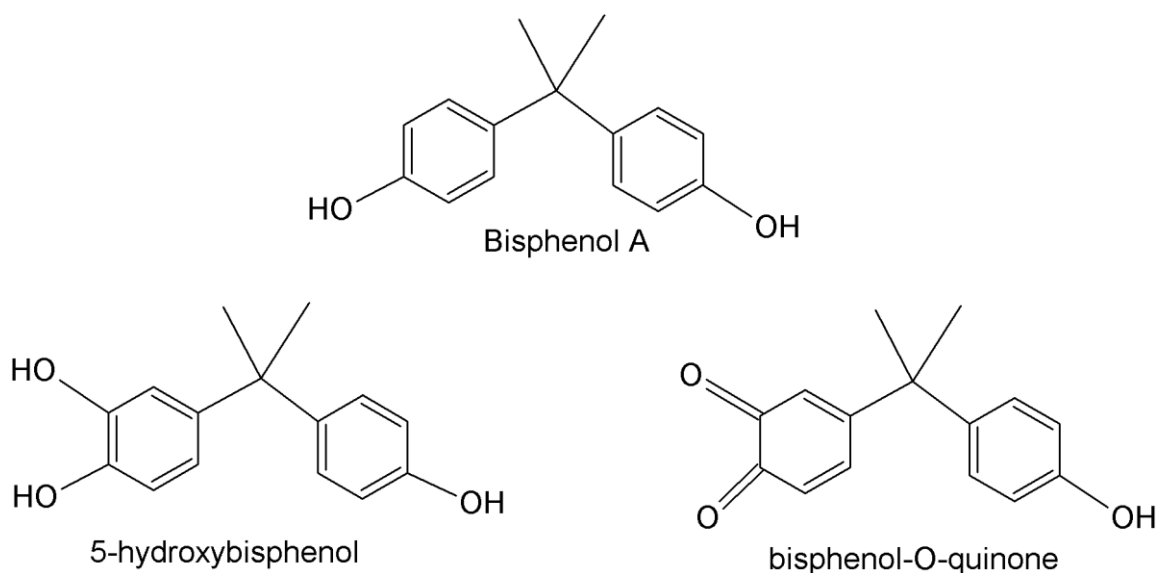
Figure 6.7: The structures of BPA and its main metabolites.

The detection limit obtained for BPA using the MnP based nanobiosensor was compared with recent studies in which different methods of detection were used. Table 1 gives the relevant information obtained.

Table 1: Detection limits for BPA by different detection methods.

Technique of detection	Detection limit	Reference
A SWNT-based DNA sensor the quantification of BPA in leachates from plastic baby bottles.	5.0 nM	[113]
Biosensor based on fullerene-C_{60} for detection of BPA from wastewater samples	3.7 nM	[114]
A biosensor comprising enzyme MnP immobilized onto a nanocomposite made of polyaniline, TiO_2 and polymethyl methacrylate	0.12 nM	This study
BPA detection in bottled drinking water using gas chromatography/mass spectrometer	4.03-7.5 ng/L	[115]
ELISA for detecting BPA in serum	1.44 ng/ml	[116]

The nanobiosensor system was characterized to exhibit a peak after the initial introduction of BPA into the system. This peak was assigned to the oxidation of BPA. The detection limit of the nanobiosensor falls within the range of the tolerable daily intake of BPA recommended by the regulatory bodies. Therefore, the novel MnP nanobiosensor can detect even very low levels of BPA.

CHPATER 7

CONCLUSIONS

Summary

This chapter covers the various aspects (success and challenges) towards the achievement of the main aims of the study. Where necessary, the chapter also entails future investigations and related studies.

7.1. Conclusions

This study has been conducted to develop nanobiosensors for detection of an anti-tuberculosis drug (pyrazinamide) and an endocrine disrupting compound (bisphenol A). The biosensors employed heme enzymes CYP2E1 and MnP respectively. With reference to the CYP2E1 based biosensor, the XRD, AFM and FTIR studies showed successful incorporation of the incorporation of multiwalled carbon nanotubes into PANI backbone with characteristic peaks assigned to the interactions between PANI and MWCNTs. The AFM images which revealed a decreased roughness after the immobilization of CYP 2E1 also confirmed successful fabrication of the biosensor. The introduction of MWCNTs improved the electroactivity of PANI, which was observed to be attained even in a neutral medium. This behaviour was investigated using CV and SW. After the immobilization of the enzyme, the electroactivity of the PANI composite was retained. The CV results after addition of PZA confirmed that the GC/PANI/MWCNTs/CYP2E1 nanobiosensor successfully catalysed the reduction of PZA into the main metabolite pyrazinoic acid, well-known to destroy the TB bacteria. A calibration plot from the increasing PZA concentrations plotted against increasing currents was used to determine the sensitivity and detection limits of the biosensor. These values were found to be 0.959 µA/µM and 0.00916 µM respectively.

The MnP based nanobiosensor employed the combined properties of the conductive PANI, biocompatible PMMA and the high surface area characterized TiO_2 nanoparticles to form a nanocomposite of enhanced properties. The SEM images of the novel hydrogellic nanocomposite revealed the structures of the individual components. Further, the FTIR and UV-Vis studies showed successful incorporation of the PMMA and TiO_2 into PANI, yielding a nanocomposite with properties in between those of the individual components. The nanocomposite also has promising properties for use in lithium ion batteries and fuel cells. Due to its biocompatibility, it can form bonds with various biomolecules such as DNA so it

can be applied in immunosensors. Also, based on its properties, the hydrogellic nanocomposite can be applied in photovoltaic cells and LEDs. Electrochemically, the nanobiosensor and the nanocomposite exhibited high electro-activity, which was shown by increasing peak currents with increasing scan rates. This behaviour showed effective electron transfer between the electrode and the active site of MnP. The biosensor proved to catalytically oxidize bisphenol A with a sensitivity and detection limit of 0.3 µA/nM and 0.12 nM respectively. This detection limit falls within the allowable daily intake of BPA recommended by the FDA.

Overall, the developed novel nanobiosensors for anti-tuberculosis drug, PZA, and endocrine disrupting compound, BPA, showed catalytic response towards detection of the two compounds. The crucial point is the detection limits of the nanobiosensors which fall within the C_{max} and allowed DTI values of PZA and BPA, respectively. therefore, these copounds are very detectable using these nanobiosensors.
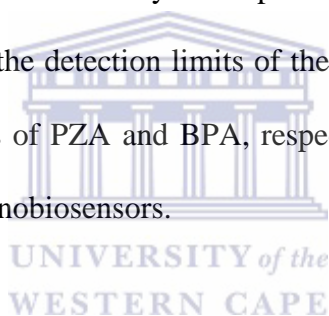
CHPATER 8

REFERENCES

Summary

This chapter gives a list of the consulted and quoted sources used throughout during reviewing of the study.

8.1 References.

[1] Bleibel W., Kim S., D'Silva K. Drug-Induced Liver Injury: Review Article. *Science*. 52 (2007) 2463-2471.[2] Department of Health: South Africa. *Annual Performance Plan 2012/13-2014/15*. (2012) 1-98.

[3] Zimic M, Fuentes P., Gilman R.H. Gutiérrez A.H. , Kirwan D, Sheen P. Pyrazinoic Acid Efflux Rate in Mycobacterium Tuberculosis is a better proxy of Pyrazinamide Resistance. *Tuberculosis (Edinb)*. 92(1) (2012) 84–91.

[4] Patkar, D., Narang, J., Yanamandala, R., Lawande, M., Shah, G.V. Central Nervous System Tuberculosis: Pathophysiology and Imaging Findings. *Neuroimaging Clinics of North America.* 22(4) (2012) 677-705.

[5] Sahota T., Pasqua, O.D. Feasibility of a Fixed-Dose Regimen of Pyrazinamide and its Impact on Systemic Drug Exposure and Liver Safety in Patients with Tuberculosis. *Antimicrobial Agents and Chemotherapy*. 56(11) (2012) 5442-5449.

[6] Zhang Y., Scorpio A., Nikaido H., Sun Z. Role of Acid pH and Defficient Efflux of Pyrazinoic Acid in Unique Susceptibility of Mycobacterium tuberculosis to Pyrazinamide. *Journal of Bacteriology*. 181 (7) (1999) 2044-2049.

[7] Salfinger M., Heifets L.B., Determination of Pyrazinamide MICs for mycobacterium tuberculosis at Different pHs by the Radiometric Method. *Antimicrobial Agents and Chemotherapy*.32(7) (1988) 1002-1004.

[8] Zhang Y., Mitchison D. The Curious characteristics of pyrazinamide: a review. *International Journal of Tuberculosis and Lung Diseases*. 7(1) 2003 6-21.

[9] Zhang Y., Wade M.W., Scorpio A., Zhang H., Sun Z. Mode of Action of Pyrazinamide: disruption of Mycobacterium tuberculosis membrane transport and energetics by pyrazinoic acid. *Journal of Antimicrobial Chemotherapy*. 52 (2003) 790-795.

[10] Lu P., Haagsma A.C., pham H., Maaksant J.J., Mol S., Lill H, Bald D. Pyrazinoic Acid Decreases the Proton Motive Force, Respiratory ATP Synthesis Activity, and Cellular ATP Levels. *Antimicrobial Agents and Chemotherapy*. 55(11) (2011) 5354-5357.

[11] Gumbo T., Dona C.S.W.S., Meek C., Leff R. Pharmacokinetics-Pharmacodynamics of Pyrazinamide in a Novel In Vitro Model of Tuberculosis for Sterilizing Effect: a Paradigm for Faster Assessment of New Antituberculosis Drugs. *Antimicrobial Agents and Chemotherapy*. 53(8) (2009) 3197-3204.

[12] Shi W., Zhang X., Jiang X., Vuan H., lee J.S., Barry 3rd C.E., Wang H., Zhang W., Zhang Y. Pyrazinamide Inhibits Trans-Translation in Mycobacterium tuberculosis. *Science*. 333 (2011) 1630-1632.

[13] Cole S.T. pyrazinamide- Old TB Drug Finds New Target. *Science*. 333 (2011) 1583-1584.

[14] Department of Health: South Africa. *Annual Performance Plan 2012/13-2014/15*. (2012) 1-98.

[15] Wang C.N., Hu O.Y. Shih T., Pai C.,, Yang P., Wen-Liang. Hepatotoxicity of Pyrazinamide. *Antimicrobial Agents and Chemotherapy*. 57(4): (2013) 685–1690.

[16] Wargo, J. Plastics that may be harmful to children and the reproductive health. *Environment & Human Health, Inc*. 2008 1-80.

[17] Bailin P.D., Byrne M., Lewis S., Liroff R. Public awareness drives market for safer alternatives: Bisphenol A market analysis report. *Investor Environmental Health Network*. (2008) 1-27.

[18] Mei Z., Chu H., Chen W., Xue F., Liu J., Xu H., Zhang R., Zheng L. Ultrasensitive one-step rapid visual detection of bisphenol A in water samples by label-free aptasensor. *Biosensors and Bioelectronics*. 39(2013) 26–30.

[19] U.S. Environmental Protection Agency. Bishenol A Action Plan. 3(29) 2010.

[20] Wetherill, Y.B., Akingembi, B.T., Kanno, J., Mclachlan, J.A., Nadal, A., Sonnenschein, C., Watson, C.S., Zoeller, R.T., Belcher, S.M. In vitro molecular mechanisms of bisphenol A action. *Reproduction Toxicology*. 24(2) (2007) 178-198.

[21] Kunza, N., Camm, E.J., Somm, E., Lodygensky, G., Darbre, S., Aubert, L.M., Hüppi, P.S., Sizonenko, S.V., Gruettera, R. Developmental and metabolic brain alterations in rats exposed to bisphenol A during gestation and lactation. *International Journal of Developmental Neuroscience*. 29 (2011) 37–43.

[22] Snyder, R.W., Maness, S. C., Gaido, K.W., Welsch, F., Sumner S.C.J., Fennell, T.R. Metabolism and Disposition of Bisphenol A in Female Rats. *Toxicology and Applied Pharmacology*. 168 (2000) 225–234.

[23] Sugiur-Ogasawara, M., Ozaki, Y., Sonta, S., Makino, T., Suzumori, K. Exposure to BPA is associated with recurrent miscarriage. *Human Reproduction*. 20 (2005) 2325-2329.

[24] Dekant, W., Vólkel, W. Human exposure to bisphenol A by biomonitoring: methods, results and assessment of environmental exposures. *Toxicology and Applied pharmacology*. 228 (2008) 114-134.

[25] Takeuchi, T., Tsutsumi, O., Ikezuki, Y., Takai, Y., Yaketani, Y. Positive relationship between androgen and endocrine disruptor, bisphenol A, in normal women and women with ovarian dysfunction. *Journal of Endocrinology*. 51 (2004) 165-169.

[26] Zhang, J., Li, Q., Chen, M., Li, H., Xu, Z. Electrochemically monitoring the removal of bisphenol A based on its anodic deposition at an ITO electrode. *Sensors and Actuators B*. 160 (2011) 784-790.

[27] Takahashi O, Oishi S. Disposition of orally administered 2,2-bis(4-hydroxyphenyl)propane (bisphenol A) in pregnant rats and the placental transfer to fetuses. *Environmental Health Perspectives*. 108 (2000) 931-935.

[28] Hu, J.Y., Aizawa, T., Ookubo, S. Products of aqueous chlorination of bisphenol A and their estrogenic activity. *Environmental Science and Technology*. 36 (2002) 1980-1987.

[29] Dairkee, S.H., Seok, J., Champion, S. Bisphenol A induces a profile of tumor aggressiveness in high-risk cells from breast cancer patients. *The Journal of Cancer Research*. 68(7) (2008) 2076-2080.

[30] Newbold, R.R., Jefferson, W.N., Padilla-Banks, E. Prenatal Exposure to Bisphenol A at Environmentally Relevant Doses Adversely Affects the Murine Female Reproductive Tract Later in Life. *Environmental Health Perspectives*. 117(6) (2009) 879-885.

[31] Crain, D.A., Eriksen, M., Iguchi, T., Jobling, S., Laufer, H., LeBlanc, G.A,. Guillette Jr L.J. An ecological assessment of bisphenol-A: Evidence from comparative biology. *Reproductive Toxicology*. 24 (2007) 225–239.

[32] Sutiakova, I., Kovalcovicova, N., Tulenkova, M., Sutiak, V. Bisphenol A and its potential toxic effects on living organisms. *Journal of Microbiology, Biotechnology and Food Sciences*. 2(2) (2012) 526-535.

[33] Donald, P.R. Antituberculosis drug-induced hepatotoxicity in children. *Paediatric Reports*. 3(e16) (2011) 51-63.

[34] Sajiki, J., Yonekubo, J. Leaching of bisphenol A (BPA) to seawater from polycarbonate plastic and its degradation by reactive oxygen species. *Chemosphere*. 51 (2003) 55–62.

[35] Fernandez, M.F., Arrebola, J.P., Taoufiki, J., Navalon, A., Ballesteros, O., Pulgar, R., Vilchez, J.L., Olean, L. Bisphenol A and chlorinated derivatives in adipose tissue of women. *Reproduction Toxicology*. 24 (2007) 259-264.

[36] CANSA, Fact Sheet on Bisphenol A. (2011) 1-10.

[37] Markey, C.M., Wadia, P.R., Rubin, B.S., Sonnenschein, C., Soto, A.M. Long-term effects of fetal exposure to low doses of the xenoestrogen bisphenol-A in the female mouse genital tract. *Biological Reproduction*. 72(6) (2005) 1344–1351.

[38] Le, H. H., Carlson, E.M., Chua, J.P., Belcher, S.M. Bisphenol A is released from polycarbonate drinking bottles and mimics the neurotoxic actions of estrogens in developing cerebellar neurons. *Toxicology Letters*. 176 (2008) 149-156.

[39] Kuramitz, H., Nakata, Y., Kawasaki, M., Tanaka, S. Electrochemical detection of bisphenol A. Application to the removal of bisphenol A using a carbon fiber electrode. *Chemosphere*. 45 (2001) 37-43.

[40] Cao, X.L., Corriveau, J., Popovic, S. Sources of low concentrations of bisphenol A in canned beverage products. *Journal of Food Protection*. 73(8) (2010) 1548-1551.

[41] Ballesteros-Gomez, A., Rubio, S., Perez-Bendito, D. Analytical methods for the determination of bisphenol A in food. *Journal of Chromatography A*. 1216 (2009) 449–469.

[42] Koichi, I., Megumi, W., Tae, H., Shigeru, O., Takashi U., Yoshihiro Y., Hiroyuki, N.

Application of liquid chromatography–mass spectrometry to the quantification of Bisphenol A in human semen. *Journal of Chromatography B*. 773 (2002) 97–102.

[43] Zhao, M., Li, Y., Guo, Z., Zhang, X., Chang, W. A new competitive enzyme-linked immunosorbent assay (ELISA) for determination of estrogenic bisphenols. *Talanta*. 57 (2002) 1205–1210.

[44] Rather, J.A, De Wael, K. Fullerene-C_{60} sensor for ultra-high sensitive detection of bisphenol A and its treatment by green technology. *Sensors and Actuators B*. 176 (2013) 110-117.

[45] Yina, H., Zhoua, Y., Xua, J., Aia, S., Cuia, L., Zhub, L. Amperometric biosensor based on tyrosinase immobilized onto multiwalled carbon nanotubes-cobalt phthalocyanine-silk fibroin film and its application to determine bisphenol A. *Analytica Chimica Acta*. 659 (2010) 144-150.

[46] Crean, C. Lahiff, E., Gilmartin, N., Diamond, B., O'Kennedy, R. Polyaniline nanofibres as templates for the covalent immobilisation of Biomolecules. *Synthetic Metals*. 161 (2011) 285–292.

[47] Horfrichter, M., Scheibner, K., Schneega, I., Fritsche, W. Enzymatic Combustion of Aromatic and Aliphatic Compounds by Manganese Peroxidase from *Nematoloma frowardii*. *Applied and Environmental Microbiology*. 64(2) (1998) 399-404.

[48] Perez, J.P.H., Lopez-Cabarcos, E., Lopez-Ruiz, B. The application of methacrylate-based polymers to enzyme biosensors. *Biomolecular Engineering*. 23 (2006) 233-245.

[49] Arshak, K., Velusamy, V., Korostynska, O., Oliwa-Stasiak, K., Adley, C. Conductive Polymers and Their Applications to Biosensors: Emphasizing on Foodborne Pathogen Detection. *IEEE Sensors Journal*. 9 (12) 92009) 1942-1958.

[50] Iwuoha, E.I., Smyth, M.R. Reactivities of organic phase biosensors: 6. Square-wave and differential pulse studies of genetically engineered cytochrome P450$_{cam}$ (CYP101) bioelectrodes in selected solvents. *Biosensors and Bioelectronics*. 18 (2003) 237-244.

[51] Guiseppi-Elie, A. Electroconductive hydrogels: Synthesis, characterization and biomedical applications. *Biomaterials*. 31 (2010) 2701-2716.

[52] Owino, J.H.O., Arotiba, O.A. Baker, P.G.L., Guiseppi-Elie, A. Synthesis and characterization of poly(2-hydroxyethyl methacrylate)-polyaniline based hydrogel composites. *Reactive and Functional Polymers*. 68 (2008) 1239-1244.

[53] Gunaydin, O., Yilmaz, F. Copolymers of Glycidyl Methacrylate with 3-Methylthienyl Methacrylate: Synthesis, Characterization and Reactivity Ratios. *Polymer Journal*. 39(6) (2007) 579-588.

[54] Ozoner, S.K, Yilmaz, F., Celik, A., Erhan, E. A novel poly(glycidyl methactylate-co-3-thienylmethyl methacrylate)-polypyrrole-carbon nanotube-horseradish peroxidase composite film electrode for the detection of phenolic compounds. *Current Applied Physics*. 11 (2011) 402-408.

[55] Kwon, O., McKee, M.L. Calculations of Band Gaps in Polyaniline from Theoretical Studies of Oligomers. *Journal of Physical Chemistry B*. 104 (2000) 1686-1694.

[56] Iwuoha, E.I., Mavundla, S.E., Somerset, V.S., Petrik, L.F., Klink, M.J., Sekota, M., Baker, P. Electrochemical and Spectroscopic Properties of Fly Ash-Polyaniline Matrix Nanorod Composites. *Michrochimica Act*. 155 (2006) 453-458.

[57] Santos, L., Martin, P., Ghilane, J., Lacaze, P., Randriamahazaka, H., Abrantes, L.M., Lacroix, J. Electrosynthesis of well-organized nanoporous poly(3,4-ethylenedioxythiophene) by nanosphere lithography. *Electrochemistry Communications*. 12 (2010) 872-875.

[58] Mickova, I., prusi, A., Grcev, T., Arsov, L. Eelectrochemical polymerization of aniline in the presence of TiO2 nanoparticles. *Bulletin of the Chemists of Macedonia*. 25(1) (2006 45-50.

[59] Pawar, S.G., Patil, S.L., Chougule, M.A., Mane, A.T., Jundale, D.M., Patil, V.B. Synthesis and Characterization of Polyaniline:TiO2 Nanocomposites. *International Journal of Polymeric Materials and Polymeric biomaterials.* 59 (2010) 777-785.

[60] Ramelow, U.S., Pingili, S. Synthesis of Ethylene Glycol Dimethacrylate-Methyl Methacrylate Copolymers, Determination of their Reactivity Ratios, and a Study of Dopant and Temperature Effects on their Conductivities. *Polymers.* 2 (2010) 265-285.

[61] Ostrovskii, D., Torell, L.M., Appetecchi, G.B., Scrosati, B. An electrochemical and Ramn spectroscopical study of gel polymer electrolytes for lithium batteries. *Solid State Ionics.* 106 (1998) 19-24.

[62] Martins, T.D., Weiss, R.G., Atvars, T.D. Synthesis and Photophysical Properties of a poly(Methyl Methacrylate) Polymer with Carbazolyl Side Groups. *Journal of the Brazilian Chemical Society.* 19(8) (2008) 1450-1461.

[62] Cui, W., Tang, D., Gong, Z. Electrospun poly(vinylidene fluoride)/poly(methyl methacrylate) grafted TiO2 composite nanofibrous membrane as polymer electrolyte for lithium-ion batteries. *Journal of Power Sources.* 233(2013) 206-213.

[63] Lahiff, E., Lynam, C., Gilmartin, N., O'Kennedy, R., Diamond, D. The increasing importance of carbon nanotubes and nanostructured conductive polymers in biosensors. *Analytical and Bioanalytical Chemistry.* 398 (2010) 1575-1589.

[64] Yadav, S., Devi, R., Kumar, A., Pundir, C.S. Trie-enzyme functionalized ZnO-NPs/CHIT/c-MWCNT/PANI composite film for amperometric determination of creatinine. *Biosensors and Bioelectronics.* 28 (2011) 64-70.

[65] Zhang, J., Kong, L., Wang, B., Luo, y., Kang, L. In-situ electrochemical polymerization of multi-walled carbon nanotubes/polyaniline composite films for electrochemical supercapacitors. *Synthetic Materials.* 159 (2009) 260-266.

[66] De Riccardis, M.F., Martina, V. New method to obtain hybrid conducting nanocomposites based on polyaniline and carbon nanotubes. *Energia, Ambiente e Innovazione.* 6 (2011) 86-95.

[67] Huang, J., Li, X., Xu, J., Li, H. Well-dispersed single-walled carbon nanotubes/polyaniline composite films. *Carbon.* 41 (2003) 2731-2736.

[68] Abdiriym, T., Ubul, A., Jamal, R., Rahman, A. Solid-State Synthesis of Polyaniline/Single-Walled Carbon Nanotubes: A Comparative Study with Polyaniline/Multi-Walled Carbon Nanotubes. *Materials.* 5 (2012) 1219-1231.

[69] Lyons, M.E.G., Keeley, G.P. Carbon Nanotube Based Modified Electrode Biosensors. Part 1. Electrochemical Studies of the flavin Group Redox Kinetics at SWCNT/Glucose Oxidase Composite Modified Electrodes. *International Journal of Electrochemical Society.* 3 (2008) 819-853.

[70] Kumar, A.S., Lo, P., Chen, S. Electrochemical synthesis of TiO_2 nanoparticles and their use as a platform for flavin adenine dinucleotide immobilization and efficient electrocatalysis. *Nanotechnology.* 19(25) (2008) 1-7.

[71] Daniel, D., Gutz, I.G.R. Microfluidic cell with TiO_2-modified gold electrode irradiated by an UV-LED for *in situ* photocatalytic decomposition of organic matter and its potentiality

for voltammetric analysis of metal ions. *Electrochemistry Communications*. 9 (2007) 522-528.

[72] Sarmah, S., Kumar, A. Photocatalytic activity of polyaniline-TiO$_2$ nanocomposites. *Indian Journal of Phycics*. 85(5) (2011) 713-726.

[73] Choudhury, B., Dey, m., Choudhury, A. Defect generation, d-d transition, and band gap reduction in Cu-doped TiO$_2$ nanoparticles. *International Nano Letters*. 3925) (2013) 1-8

[74] Vijayalakshmi, R., Rajendran, V. Synthesis and characterization of nano-TiO$_2$ via different methods. *Archives of Applied Science Research*. 4(2) (2012) 1183-1190.

[75] Mickova, I., Prusi, A., Grcev, T., Arsov, L. Electrochemical polymerization of aniline in presence of TiO$_2$ nanoparticles. *Bulletin of the Chemists and Technologists of Macedonia*. 25(1) (2006) 45-50.

[76] Zhang, L., Liu, P., Su, Z. Preparation of PANI-TiO$_2$ nanocomposites and their solid-phase photocatalytic degradation. *Polymer Degradation and Stability*. 91 (2006) 2213-2219.

[77] Rathod, R.C., Umare, S.S., Didolkar, V.K., Shambharkar, B.H., Patil, A.P. Production and Characterization of PANI/TiO$_2$ Nanocomposites: Anticorrosion Applications on 316LN SS. *Trans Indian Institution of Metals*. 66(2) (2013) 97-104.

[78] Yang, H., Zhu, Y., Chen, D., Li, C., Chen, S., Ge, Z. Electrochemical biosensing platforms using poly-cyclodextrin and carbon nanotube composite. *Biosensors and Bioelectronics*. 26(1) (2010) 295-298.

[79] Norouzian, D. Enzyme Immobilization: The State of Art in Biotechnology. *Iranian Journal of Biotechnology*. 1(4) 2003 197-206.

[80] Ozoner, S.K, Yilmaz, F., Celik, A., Erhan, E. A novel poly(glycidyl methactylate-co-3-thienylmethyl methacrylate)-polypyrrole-carbon nanotube-horseradish peroxidase composite film electrode for the detection of phenolic compounds. *Current Applied Physics*. 11 (2011) 402-408 .

[81] Wang, J., Myung, N.V., Yun, M., Monbouquette, H.G. Glucose oxidase entrapped in polypyrrole on high-surface-area Pt electrodes: a model platform for sensitive electroenzymatic biosensors. *Journal of Electroanalytical Chemistry*. 572 (2005) 139-146.

[82] Iwuoha, E.I., de Villaverde, D.S., Garcia, N.P., Smyth, M.R., Pingarron, J.M. Reactivities of organic phase biosensors. 2. The amperometric behaviour of horseradish peroxidase immobilised on a platinum electrode modified with an electrosynthetic polyaniline film. *Biosensors and Bioelectronics*. 12 (8) (1997) 749-761.

[83] Schneider, E., Clark, D.S. Cytochrome P450 (CYP) enzymes and the development of CYP biosensors. *Biosensors and Bioelectronics*. 39 (2013) 1-13.

[84] Saxena, A., Singh, P., Yadav, D.K., Sharma, P., Alam, S., Khan, F., Thul, S.T., Shukla, R.K., Gupta, V., Sangwan, N.S. Identification of cytochrome P450 heme motif in plants proteome. *Plant Omics Journal*. 6(1) (2012) 1-12.

[85] Heinzkil, m., Bech, L., Halkier, T., Schneider, P., Anke, T. Characterization of Laccase and Peroxidases from Wood-Rotting Fungi (Family *Coprinaceae*). *Applied and Environmental Microbiology*. 64(5) (1998) 1601-1606.

[86] Jarvinen, J., Taskila, S., Isomaki, R., Ojamo, H. Screening of white-rot fungi manganese peroxidases: a comparison between the specific activities of the enzyme from different native producers. *AMB Express*. 2(62) 92012) 1-9.

[87] Shin, K., Kim, Y.H., Lim, J. Purification and Characterization of Manganese Peroxidase of White-Rot Fungus *Irpex lacteus*. *The Journal of Microbilogy*. 43(6) (2005) 503-509.

[88] Petruccioli, M., Frasconi, M., Quaratino, D., Covino, S., Favero, G., Mazzei, F., Federici, F., D'Annibale, A. Kinetic and redox properties of MnP II, a major manganese peroxidase isoenzyme from *Panus tigrinus* CBS 577.79. *Journal of Biological and Inorganic Chemistry.* 14 (2009) 1153-1163.

[89] van den Boogaard, J., Kibiki, G.S., Kisanga, E.R., Boeree, M.J., Aarnoutse, R.E. New Drugs against Tuberculosis: Problems, progress and Evaluation of Agents in Clinical Development. *Antimicrobial Agents and Chemotherapy*. 53(3) (2009) 849-862.

[90] Shi, T., Pai, C., Yang, P., Chang, W., Wang, N., Hu, O.Y. A novel Mechanism Underlies the Hepatotoxicity of Pyrazinamide. *Antimicrobial Agents and Chemotherapy*. 57(4) (2013) 1685-1690.

[91] Hudson, S.A., McLean, K.J., Munro, A.W., Abell, C. *Mycobacterium tuberculosis* cytochrome P450 enzymes: a cohort of novel TB drug targets. *Biochemical Society Transactions.* 40 (2012) 573-579.

[92] Zhang, Y., Wade, M.W., Scorpio, A., Zhang, H., Sun, Z. Mode of action of pyrazinamide: disruption of Mycobacterium tuberculosis membrane transport and energetics by pyrazinoic acid. *Journal of Antimicrobial Chemotherapy*. 52 (2003) 790-795.

[93] Swart, A., Harris, V. Drug Interactions with tuberculosis therapy. *CME*. 23(2) (2005) 56-60.

[94] Cole S.T. Pyrazinamide −Old TB Drug Finds New Target. *Science.* 333 (2011) 1583-1584.

[95] Wolfgang, D., Wolfgang, V. Human exposure to bisphenol A by biomonitoring: Methods and assessment of environmental exposures. Toxicology and Applied Pharmacology. 228 (2008) 114-134.

[96] Wei, X., Huang, Y., Wong, M.H., Giesy, J.P., Wong, C.K.C. Assessment of risk to humans of bisphenol A in marine and freshwater fish from Pearl River, China. Chemosphere. 85 (2011) 122-128.

[97]Katoch, A., Burkhart, M., Hwang, T., Kim, S.S. Synthesis of polyaniline/TiO2 hybrid nanoplates via a sol–gel chemical method. *Chemical Engineering Journal*. 192 (2012) 262-268.

[98] Das, M., Sumana, G., Malhotra, B.D. Application of nanostructured ZnO films for electrochemical DNA biosensor. *Applied Physical Letters*. 99 (2011) 1-8.

[99] Joshi, M., Bhattacharyya, A., Ali, S.W. Characterization techniques for nanotechnology applications in textiles. *Indian Journal of Fibre and Textile Research*. 33 (2008) 304-317.

[100] Guo, H., Zhu, H., Lin, H., Zhang, J. Synthesis of polyaniline/multi-walled carbon nanotube nanocomposites in water/oil microemulsion. *Materials Letters*. 62 (2008) 3919–3921.

[101] Liu, A., Sun, K., Yang, J., Zhao, D. toxicological effects of multi-wall carbon nanotubes in rats. Journal of Nanoparticles and Respiration. 10 (2008) 1303-1307.

[102] Ji, L., Zhou, L., Bai, X., Shao, Y., Zhao, G., Qu, Y., Wang, C., Li, Y. Facile synthesis of multiwall carbon nanotubes/iron oxides for removal of tetrabromobisphenol A and Pb(II). Journal of Materials Chemistry. 22 (2012) 15853-15862.

[103] Kandawar, S.B., Deshpande, M.D., Agrawal, S.P. Transport properties of conductive polyaniline nanocomposites based on carbon nanotubes. International Journal of Composite Materials. 2 (2012) 32-36.

[104] Nie, G., Zhang, L., Cui, Y. Preparation of Pd nanoparticles deposited on a polyaniline/multiwall carbon nanotubes nanocomposite and their application in the Heck reaction. *Reaction Kinetics, Mechanism and Catalysis*. 108(1). (2013) 193-204.

[105] Zhang, Q., Wang, W., Li, J., Zhu, J., Wang, L., Zhu, M., Jiang, W. Preparation of thermoelectric properties of multi-walled carbon nanotube/polyaniline hybrid nanocomposites. *Journal of Materials Chemistry A*. 1 (2013) 12109-12114.

[106] Tapia, A.K.G., Rosario, E.J., Basilia, B., Sarmago, R.V. FTIR and XPS analysis of thermally aged polyaniline emeraldine films: relationship to morphological and electrical properties after doping. *Journal of Nuclear and Related Technologies.* 6(2) (2009) 27-40.

[107] Molapo, K.M., Ndangili, P.M., Ajayi, R.F., Mbambisa, G., Mailu, S.M., njomo, N., Masikini, M. Electronics of conjugated polymers (I): polyaniline. International Journal of Electrochemical Science. 7 (2012) 11859-11875.

[108] Muchindu, M., Iwuoha, E., Pool, E., West, N., Jahed, N., Baker, P., Waryo, T., Williams, A. Electrochemical ochratoxin A immunosensors system developed on sulphonated polyaniline. Electrolysis. 23 (2011) 122-128.

[109] Guascito M. R.; Malitesta C.; Manno D.; Turco A., 'A new amperometric nanostructured sensor for the analytical determination of hydrogen peroxide' *Biosensors and Bioelectronics* **24** (2008) 1057-1058.

[110] Mulaudzi, T., Ludidi, N., Ruzvidzo, O., Morse, M., Hendricks, N., Iwuoha, E., Gehring, C. Identification of a novel Arabidopsis thaliana nitric oxide/binding molecule with guanylate cyclase activity in vitro. *FEBS Letters*. 585 (2011) 2693-2697.

[111] Khuhawar, M.Y., Rind, F.M. Liquid chromatographic determination of isoniazid, pyrazinamide and rifampicin from pharmaceutical preparations and blood. Journal of Chromatography B. Analytical, Technological, Biomedical Life Sciences. 766 (2002) 357-363.

[112] McIlleron, h., Wash, P., Burger, A., Norman, J., Folb, P.I., Smith, P. Determinants of rifampicin, isoniazid, pyrazinamide and ethambutol pharmacokinetics in a cohort of tuberculosis patients. Antimicrobial Agents and Chemotherapy. 50 (2006) 1170-1177.

[113] Jiang, X., Ding, W., Luan, C., Ma, Q., Guo, Z. Biosensor for bisphenol A leaching from baby bottles using a glassy carbon electrode modified with DNA and single walled carbon nanotubes. *Microchimica Acta.* 180 (11-12) (2013) 1021-1028.

[114] Rather, J.A., De Wael, D. Fullerene-C_{60} sensor for ultra-high sensitive detection of bisphenol-A and its treatment by green technology. *Sensors and Actuators B*. 176 (2013) 110-117.

[115] Mai A E., Zainab M A., Promy V., Zeinab K H., Sawsan A. O., Maha E., Maha H.D., Ebtisam M.A., Bisphenol A Detection in Various Brands of Drinking Bottled Water in Riyadh, Saudi Arabia Using Gas Chromatography/Mass Spectrometer. *Tropical Journal of Pharmaceutical Research*. 11(3) (2012) 455-459.

[116] Kim, D.H., Oh, C.H., Hwang, Y., Jeong, I., Ahn, K.J., Chung, H., Chang, J. Serum Bisphenol A Concentration in Postmenopausal Women with Osteoporosis. *Journal of Bone Metabolism*. 19(2) (2012) 87-93.

UNIVERSITY *of the*
WESTERN CAPE